BIOPHYSICAL INVESTIGATIONS OF THE Aβ AGGREGATION PROCESS

by

Saketh Chemuru Muni

Bachelor of Technology, Anna University, 2006

Submitted to the Graduate Faculty of

School of Medicine in partial fulfillment

of the requirements for the degree of

Doctor of Philosophy

University of Pittsburgh

2014

UNIVERSITY OF PITTSBURGH

SCHOOL OF MEDICINE

This thesis was presented

by

Saketh Chemuru Muni

It was defended on

December 8, 2014

and approved by

Seth Horne, Ph.D., Department of Chemisty

Patrick H. Thibodeau, Ph.D., Department of Cell Biology and Physiology

Patrick van der Wel, Ph.D., Department of Structural Biology

Dissertation Advisor: Ronald Wetzel, Ph.D., Department of Structural Biology

To my mom and dad,
for holding me close to their heart,
yet setting me free to follow my own.

BIOPHYSICAL INVESTIGATIONS OF THE Aβ AGGREGATION PROCESS

Saketh Chemuru Muni

University of Pittsburgh, 2014

The presence in patient's brain tissues of neuritic plaques containing Aβ aggregates is one of the pathological hallmarks of Alzheimer's disease (AD), and Aβ aggregates have been implicated in the disease mechanism. These facts have inspired a large number of biophysical and structural studies on Aβ behavior over the last 25 years. Much remains to be learned, but there are a number of barriers to progress, including the challenges of making and manipulating these peptides and understanding their aggregation behavior. This thesis describes an improved method for the chemical synthesis of highly aggregation prone peptides like Aβ, insights into some previously unrealized limitations of a widely used "disaggregation" procedure for making high quality monomer solutions, and two fundamental studies on aspects of Aβ self-assembly. The improved synthesis method involves reversible addition of Lys residues to the C-terminus of the peptide during solid phase synthesis, which we show improves the synthetic yield and also improves the chromatographic behavior of the peptide during purification. The new knowledge about disaggregation reveals that a method involving sequential treatment of peptides with trifluoroacetic acid (TFA) and hexafluoroisopropanol (HFIP), while very effective with $A\beta_{40}$, can alter the self-assembly of $A\beta_{42}$, compared with an alternative protocol, and introduce highly stable oligomers that may possess substantial toxicity. In one fundamental study, we show that the minor brain form, $A\beta_{43}$, aggregates more slowly than $A\beta_{42}$ to make amyloid fibrils that are highly inefficient at seeding $A\beta_{42}$ monomers. In another study, we describe the surprising result

that amyloid fibrils of D-Aβ_{40} can seed L-Aβ_{40} monomers, and vice versa, suggesting a curious lack of structural discrimination to the prion-like propagation of Aβ amyloid in vitro. The results add to our knowledge of Aβ amyloid assembly and how it can best be studied in the laboratory.

TABLE OF CONTENTS

LIST OF TABLES

LIST OF FIGURES

ABBREVIATIONS

AD	Alzheimer's disease
CD	Circular Dichroism
TEM	Transmission Electron Microscopy
ThT	Thioflavin T
FTIR	Fourier Transform Infra-red spectroscopy
TFA	2,2,2-Trifluoroacetic acid
HFIP	1,1,1,3,3,3-Hexafluoro-2-propanol
Fmoc	Fluorenylmethyloxycarbonyl
t-Boc	tert-Butylocycarbonyl
RP-HPLC	Reverse-Phase High performance liquid chromatography
UV	Ultra Violet
DLS	Dynamic Light Scattering
PBS	Phosphate Buffered Saline
HX-MS	Hydrogen-deuterium Exchange Mass Spectrometry
PMSF	Phenylmethanesulfonyl fluoride
HATU	1-[Bis(dimethylamino)methylene]-1H-1,2,3-triazolo[4,5-b]pyridinium 3-oxid hexafluorophosphate
HBTU	1-[Bis(dimethylamino)methylene]-1H-1,2,3-benzotriazolium

	Hexafluorophosphate
COMU	(1-cyano-2-ethoxy-2-oxoethylidenaminooxy)dimethylamino-morpholino-carbedium hexafluorophosphate

CONTRIBUTOR NAMES

R.K.	Ravindra B. Kodali
I.B.	In-Ja L. Byeon
I.K.	Indu Kheterpal
D.K.	David Kaleta
K.K.	Karunakar Kar

ACKNOWLEDGEMENTS

"Guru Brahma Guru Vishnu Guru Devo Maheshwaraha Guru Saakshat Para Brahma Tasmai Sree Gurave Namaha."

In India, since the Vedic ages, schools are referred to as *Gurukuls*, where students are considered as the *extended family* (kula) of their *teachers* (gurus). I am humbled to have Dr. Ronald Wetzel as my *guru*, and be a part of his academic family. His passion, dedication, and energy never cease to amaze me, and I hope that I gained a fraction of those over the course of my graduate studies. I am deeply indebted to him for making my stay at University of Pittsburgh as comfortable as it could have *ever* been.

I would like to thank my thesis committee members, Prof. Seth Horne, Prof. Patrick H. Thibodeau and Prof. Patrick van der Wel for their time and effort in helping me bring this dissertation to life. I have enjoyed the few committee meetings that I have had with them and their view of the big picture and academic rigor. I would also like to thank them for their help during my postdoc search. I must also acknowledge all the past and the present members of the Wetzel lab for their support over the years. I have to thank Murali and Ashwani for helping me with the initial baby steps in the lab. Special thanks are due to Banka, Kar, Smita, Elizabeth, Rakesh, Pinaki, Irene, Kenny with whom I spent most of my fun-filled lab time. In particular, a special thanks is dedicated to Ravi for all his help and guidance in making me understand the

projects and helping me obtain the EM and FTIR data. A big deal of my work has been with his support, guidance and ideas.

Thanks to fellow MBSB students and other members of the Structural Biology department for making my stay memorable. Special thanks are due to Jen walker and Susanna Godwin at the graduate school office for reminding me of course registrations and forms to be submitted and also all the faculty in the MBSB graduate program with whom I interacted during the courses. Special thanks to Dr. Gordon Rule for his help in my admission into the program.

My stay in Pittsburgh would be largely routine had it not been for the lost list of friends and roommates I have had over the years. Karthik, Siva, Prashanth, Arjun, Nisha, Vamshi, Pooja, Melanie, Shantanu, Basha, Tumul, Vignesh, Madhu, Dhishan, Anu, Vishnu, Uday, Priyanka and many others have breathed life into my stay and made me happy in tough times. They have shared many of my laughs and wonderful memories over the past few years.

Finally, I would like to thank my wonderful family. My dad Mr. C. Krishna Reddy is a great inspiration for me and will always be the source of my courage. My mom Mrs. Nirmala has been as caring and concerned as one could ever hope for. They never complained or questioned my ability during tough times in graduate school and were always present to vent out my frustration and happiness.

PUBLICATIONS

1. **Chemuru, S**., Kodali, R. and Wetzel, R. "C-terminal threonine reduces $A\beta_{43}$ amyloidogenicity compared with $A\beta_{42}$". Manuscript submitted.

2. **Chemuru, S**., Kodali, R. and Wetzel, R. "Facile chiral cross-seeding of $A\beta_{40}$ amyloid fibrils". Manuscript under preparation.

3. **Chemuru, S**., Kodali, R. and Wetzel, R. "Improved chemical synthesis of hydrophobic Aβ peptides using addition of C-terminal lysines later removed by carboxypeptidase B", *Biopolymers.* 2014. **102** (2) 2014; p 206-221.

4. Kodali, R., Williams AD, **Chemuru, S**. and Wetzel R., "Abeta(1-40) Forms Five Distinct Amyloid Structures whose beta-Sheet Contents and Fibril Stabilities Are Correlated". *J Mol Biol*, 2010. **401**(3): p. 503-517.

1.0 INTRODUCTION

1.1 ALZHEIMER'S DISEASE AND AMYLOID- β (Aβ) PEPTIDES

1.1.1 Overview of Alzheimer's Disease (AD)

Alzheimer's disease (AD) is the most common form of dementia in humans and is an irreversible, progressive neurodegenerative disease that gradually leads to the loss of memory, thinking skills, and the ability to carry out daily activities. Eventually the destruction of brain functions leads to death of the individual. According to recent estimates, as many as 5.3 million people in the U.S., and 26.6 million people worldwide, have developed AD and these numbers are expected to quadruple by 2050 [1]. It is currently the sixth leading cause of death in the U.S.

AD was first described in 1906 based on the autopsy of a woman who died of an unusual mental illness [2]. On analysis of the brain tissue, many abnormal clumps and tangled bundles of fibers were found, which were later termed amyloid/senile plaques and neurofibrillary tangles, respectively. Since then, these two classical brain lesions have become the major neuropathological features of AD. In the 1960s, the use of electron microscopy allowed the ultra-structures of these plaques and tangles to be studied, revealing the fine fibrillar structures of these brain lesions long before the proteins that are the source of these deposits were identified [3-6]. With advances in biochemical pathology, the compositions of the plaques and tangles were

identified in the 1980s. It was found through biochemical analysis that the amyloid plaques mainly contain extracellular deposits of a previously unknown 4-kDa amyloid-β (Aβ) protein [7-10]. The neurofibrillary tangles were found to be mainly composed of hyperphosphorylated versions of a microtubule-associated protein, tau, found predominantly in neurons [11-14]. Tau was previously discovered as a protein binding to microtubules and assisting in their formation and stabilization [15]. However, upon phosphorylation, it loses its ability to bind to microtubules and the unbound tau clumps together in neurofibrillary tangles [16]. Both Aβ and tau proteins are present in a highly ordered and aggregated form known as 'amyloid fibrils' in the plaques and tangles.

Due to the fact that amyloid plaques and neurofibrillary tangles can occur independently of each other, and that neurofibrillary tangles are also present in many less common neurodegenerative diseases in the absence of Aβ deposition [17, 18], it has been suggested that the tangles are likely to occur as a secondary response to the injury of neuronal cells [19, 20]. Therefore, AD studies have primarily focused on Aβ peptides. Indeed, with extensive research on Aβ peptides over the years, more evidence was gained in support of their direct involvement in AD. Some of the key evidence for the importance of Aβ in AD pathology include: (a) increased amounts of soluble Aβ in individuals with Down syndrome who eventually develop AD over time and whose duplicated chromosome is home to the gene for the amyloid precursor protein, APP, whose breakdown generates Aβ peptides [21, 22]; (b) genetic studies of the familial forms of early-onset AD have implicated several point mutations in the Aβ peptide sequence as the critical mutations, e.g. Arctic (E22G), Dutch (E22Q), Flemish (A21G), and Iowa (D23N) mutant peptides [23-27]. It has been shown that these peptides have greater propensity for oligomerization and aggregation in vitro, and are directly linked to the genetically inherited

forms of the disease [23, 28-30]. Other FAD (familial AD) mutations have been discovered near the γ-secretase cleavage site on APP which lead to increased production of Aβ [31]; (c) Other genetic studies uncovered several FAD mutations in the enzymes that process APP, such as presenilin-1, in such a way to generate higher concentrations of more pathogenic forms of Aβ [32, 33]. The presenilins are components of a proteolytic complex involved in APP processing and degradation; (d) The direct incubation of Aβ peptides with neuronal cells, or the overexpression of amyloid precursor proteins (APP, whose proteolysis generates Aβ peptides (see below)), results in cell death [34-36]; (e) The direct injection of Aβ peptides into mice, or the overexpression of amyloid precursor protein (APP), results in significant neurodegeneration and cognitive deficits in mice [37, 38].

Thus, it is clear that Aβ peptides play a critical role in the development of AD and is quite likely that their toxicity involves some sort of aggregation step.

1.1.2 Origin of Aβ peptides and presence of proteolytic variants

Aβ is a small (~4 kDa), an intrinsically disordered peptide, which is normally present in both cerebrospinal fluid and blood at extremely low physiological concentrations (nanomolar or less) [39]. It is formed by the sequential cleavage of an integral transmembrane protein, amyloid precursor protein (APP). Although the primary physiological function of this precursor protein remains unknown, the protein is found in many tissues including in the synapses of neurons. APP undergoes post translational processing involving its cleavage by various secretases and proteases [40]. In the major non-amyloidogenic pathway (~90% of APP is processed in this pathway), APP is sequentially cleaved by α-secretase and γ-secretase yielding in two relatively benign membrane associated C-terminal fragments, p3 and AICD (Amyloid Precursor Protein

Intracellular Domain). The α-cleavage site is located in the middle of the Aβ sequence and produces a large extracelluar domain called sAPP-α. In the other amyloidogenic pathway, APP is acted upon initially by β-secretase forming a membrane bound C-terminal fragment (C99) that can no longer be efficiently cleaved by α-secretase. γ-secretase then acts on C99 to release AICD and Aβ peptides [41] (**Figure 1-1 a**). The Aβ peptide portion of the cleaved amyloid precursor protein is then released extracellularly.

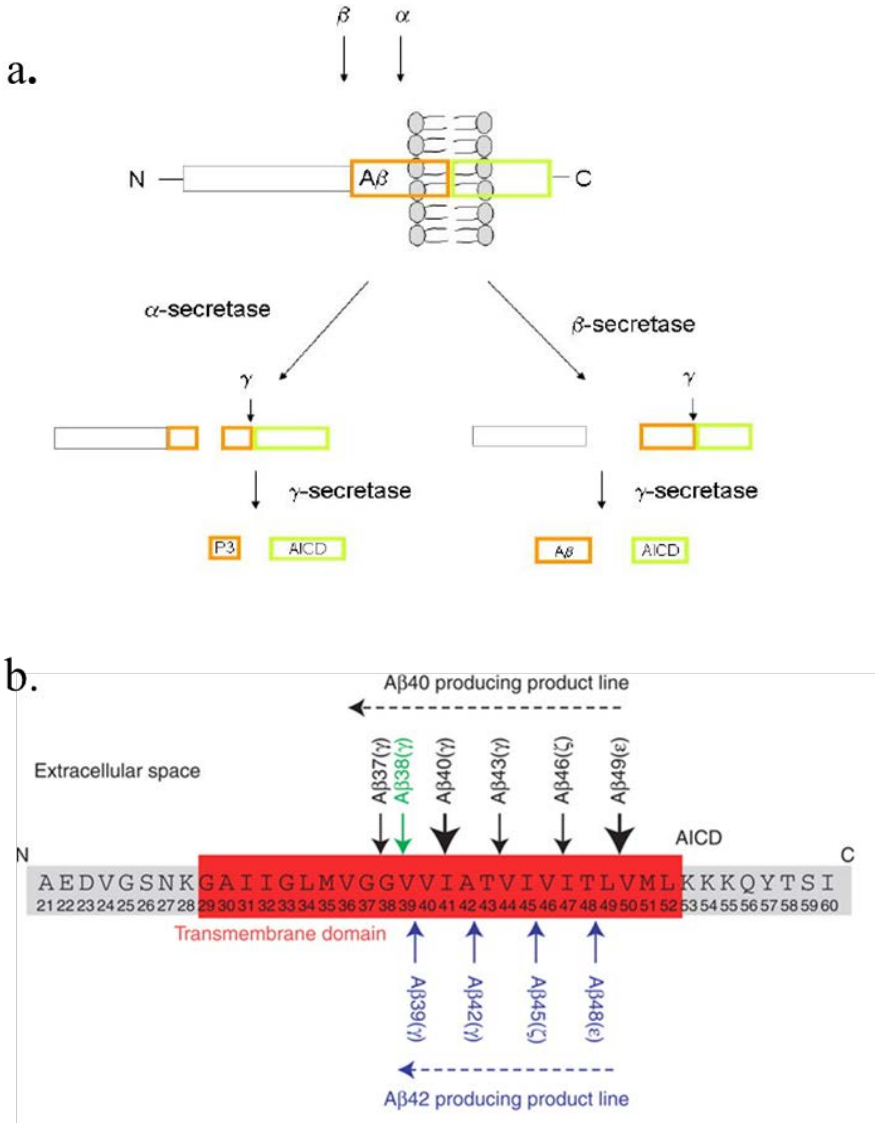

Figure 1-1: Proteolytic processing of amyloid precursor protein (APP) by secretases.
a. The cleavage of amyloid precursor protein by α-secretase followed by γ-secretase cleavage yields the benign P3 and AICD fragments, whereas the cleavage by β-secretase followed by γ-secretase yields Aβ peptides and AICD.
b. Sequential processing of APP by γ-secretase enzyme resulting in the two predominant product lines. From [42].

Variability in the cleavage site of γ-secretase creates several Aβ peptide forms, with lengths of the major products varying from 39 to 43 amino acids. The variability in the C-terminal cleavage site occurs due to the fact that γ-secretase has multiple cleavage sites within the transmembrane domain of APP. It has been postulated that the enzyme sequentially cleaves APP multiple times at 3-4 amino acid intervals along the transmembrane α-helix domain starting with the initial cleavage products of $A\beta_{49}$ and $A\beta_{48}$ [43-45] (**Figure 1-1 b**). Longer Aβ species, for example, $A\beta_{49}$, $A\beta_{48}$, $A\beta_{46}$, $A\beta_{45}$ and $A\beta_{43}$ have been found in cell lysates and also in homogenates of APP-transgenic mouse brains by using SDS-PAGE gel analysis [44, 46, 47].

Among the Aβ peptides that have been detected, the 40 residue peptide $A\beta_{40}$ and the 42 residue $A\beta_{42}$ are the most common forms present in disease brain (see **Figure 1-2** for their sequences). The aggregates formed from these peptides deposit outside the neurons in dense formations known as senile plaques or neuritic plaques, in less dense aggregates as diffuse plaques and also sometimes in the walls of small blood vessels in the brain in a process known as amyloid angiopathy. The diffuse plaques are composed of non-fibrillar amorphous aggregates that are not associated with degenerative changes, whereas the neuritic plaques contain Aβ fibrils that are associated with pathological changes [48]. While $A\beta_{40}$ is much more abundant, $A\beta_{42}$ is much more amyloidogenic [49], which means it can oligomerize and fibrilize (see below) much more rapidly than $A\beta_{40}$.

β-amyloid(1-40): DAEFRHDSGYEVHHQKLVFFAEDVGSNKGAIIGLMVGGVV
β-amyloid(1-42): DAEFRHDSGYEVHHQKLVFFAEDVGSNKGAIIGLMVGGVVIA

Figure 1-2: Sequences of $A\beta_{40}$ and $A\beta_{42}$.

Evidence has been reported for the presence of small oligomers of longer Aβ species in the brains of individuals with AD [50]. Especially, the presence of $A\beta_{43}$ is seen in plaque cores obtained from occipital and frontal cortex in both sporadic and familial AD cases and also in the case of diffuse plaques [51]. Longer Aβ species have also been detected in the case of transgenic mice models and in cell cultures expressing APP [44]. There has been no comprehensive biophysical study so far conducted on Aβ variants which are longer than 42 amino acids. Recent data indicate that $A\beta_{43}$ showed higher propensity to aggregate and higher levels of neurotoxicity [52]. These recent findings indicate that $A\beta_{43}$ - a neglected species in AD research - may have an impact on AD, and shows the potential importance of studying the aggregation properties of longer Aβ species, like $A\beta_{43,}$ both alone and in association with the more common Aβ species.

In **Chapter 5**, we studied the in vitro aggregation properties of $A\beta_{43}$ peptide and the results obtained indicate that the $A\beta_{43}$ peptide has differing fibril formation properties when compared to its close homolog $A\beta_{42}$. In **Chapter 3**, we demonstrate an improved way to make difficult-to-synthesize $A\beta_{46}$ and provide preliminary data that it forms amyloid considerably faster than $A\beta_{42.}$

1.1.3 β-amyloid neurotoxicity hypothesis

Although it has been shown that Aβ peptides are neurotoxic, and are directly linked to AD, the underlying mechanism remains unclear. Over the years, different hypotheses for β-amyloid neurotoxicity have been developed.

In the original amyloid hypothesis, it was proposed that the amyloid fibrils that make up the neuritic plaques first observed by Alzheimer are the fundamental cause of the disease [53,

54]. However, recent studies do not fully support this hypothesis. For example, it has been found that, in transgenic animals that over-express APP, neuronal abnormalities and cognitive deficits start to appear well before amyloid plaques can be detected [55-57]. Furthermore, little correlation between overall amyloid plaque density and clinical severity of dementia has been found [58, 59]. In some cases, a significant amount of amyloid plaques were found in the brain tissues from patients without AD, whereas in other cases, few amyloid plaques were detected in the brain tissues from patients with severe AD. One hypothesis to explain these observations consistent with the original amyloid hypothesis is that fibril deposition in particular parts of the brain and at particular times (long before autopsy) might be critical [60]. Another hypothesis that stands in distinction to the amyloid hypothesis, is that small oligomeric species of Aβ peptides formed prior to mature amyloid fibrils may be the real toxic species [61], while the amyloid fibrils might play a protective role by scavenging the smaller forms of toxic Aβ.

A central question in AD field is: by what mechanism might extracellular amyloid aggregates formed by Aβ harm the cells? One hypothesis suggests that metastable oligomeric structures that have been described in the formation of many amyloid-forming peptides, when produced extra-cellularly, can cause potentially toxic alterations of cell membranes [62]. In line with this, studies have indicated that Aβ oligomers are the origin of neurotoxicity, potentially through membrane permeabilization [63-67]. It is thought that the oligomers induce neurotoxicity by forming pores/channels in the cell membranes and that these pores allow a rapid, uncontrolled influx of ions, particularly calcium ions, into the neuronal cells, which may directly lead to the cell death, or trigger the apoptosis signaling pathway [68]. In another study, the toxicity mechanism was suggested to be associated with the exposure of toxic surfaces formed by the oligomers and their interactions with other molecules. For example, recently

cellular prion protein PrP^c emerged as a specific receptor of toxic Aβ oligomers which then mediates synaptic dysfunction [69]. In other study, synaptic binding of Aβ oligomers to putative receptor proteins is reported to inhibit long term potentiation, leading to impaired cognitive performance and AD.

However, the exact meaning of the term 'toxic Aβ oligomer' has been loosely used in the field and is confusing. In fact, the Aβ aggregation pathway is highly complex leading to heterogeneous populations of intermediate species with differing structures and toxicities as summarized below and as illustrated in **Chapter 5**.

1.2 MECHANISM OF Aβ AGGREGATE FORMATION

1.2.1 Introduction to aggregation

Proteins are fundamental components of living organisms and they participate in most cellular processes. Each protein molecule acquires its unique structure by folding, which depends on the primary amino acid sequence of the molecule [70]. This unique structure gives the protein a unique function. This fully functional state of the proteins is called its native or folded state. However, some protein molecules undergo misfolding or even aggregation, thereby losing their functionality. Often these misfolded structures, through mechanisms that are as yet poorly worked out, can be toxic to the living cells. Sometimes these misfolded and conformationally unstable protein monomers can lead to the formation of insoluble protein aggregates, such as amyloid fibrils, which are characterized by specific structural features. These aggregates are predominantly β-sheet rich, long thread-like structures with a typical diameter of 6-12 nm and a

length >100 nm. Such structures are classified as “amyloid fibrils” and the phenomenon is termed as “amyloid aggregation”. The classic histopathological definition of an amyloid is an extracellular, proteinaceous deposit that exhibits apple-green birefringence when viewed under a microscope under polarized light after staining with Congo red [71]. Recently, amyloid species have been observed in distinct intracellular locations as well [72]. A biophysical definition of an amyloid species is a broader classification which includes any polypeptide chain that polymerizes to form a ‘cross-β’ structure, in vivo or in vitro (**Figure 1-3**) [73]. Presence of such amyloid cross-β structures can be identified using fluorescent dyes, stain polarimetry and CD or FTIR; but the predominant test to see if a structure contains cross-β fibers is by placing the sample in an X-ray diffraction beam. The term ‘cross-β’ was based on the observation of two sets of diffraction lines, one longitudinal and one transverse, that form a characteristic ‘cross’ pattern. The two characteristic scattering diffraction signals produced at 4.7 and 10 Å, corresponding to inter-strand and stacking distances in β-sheets.

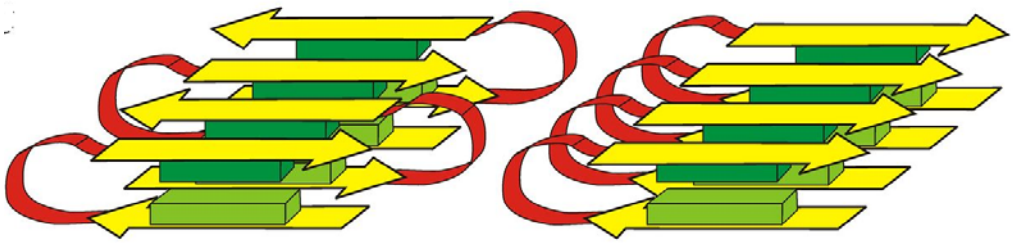

Figure 1-3: Schematic representation of a double layered anti-parallel (left) and parallel (right) cross-β motif [74], the fundamental building block of amyloid structure

Amyloid aggregation of the specific disease related proteins occurs in several age-related neurodegenerative diseases, including Alzheimer’s, Parkinson’s and Huntington’s diseases [75-78]. Many proteins which aggregate in vivo have been found to aggregate in a similar fashion under physiological conditions in vitro. Autopsies of deceased patient’s brains show deposits of

amyloid fibrils [79-83], and in the pathway towards amyloid aggregation, some of these proteins also form quasi-stable soluble intermediate structures [55, 84-86]. Recent research suggests that these smaller soluble (i.e., diffusible) protein aggregates are principally responsible for the corresponding pathology in the case of neurodegerative diseases. For Aβ protein, these structures are classified as monomers (4 kDa); multimers (such as dimers, trimers, tetramers, hexamers, etc.) [87-89]; large oligomers (few nm diameter) [90], amyloid spheroids (2-30 nm) [91], and large soluble aggregates or protofibrils (~10's of nm in length) [92]. Although much work remains to be done to characterize their mechanistic inter-relationships, the aggregation process is often modeled as the sequential progression of the peptide population through the following species.

a. Monomers

b. Misfolded monomers

c. Dimers/tetramers and small oligomers

d. Large diffusible non-β aggregates

e. Protofibrils and large β aggregates

f. Amyloid fibrils

These species have been depicted as a cartoon in the **Figure 1-4**. For disease-causing proteins, one or a few of these species are believed to be responsible for the dysfunction of neurons in diseased brains. Since recent reports suggest that the soluble aggregates (species c and d) might be the most toxic species, destabilizing these intermediates with respect to their precursors and/or their products has been proposed to be a potential way to ameliorate toxicity and disease. It is not clear which of these species is ‘on-pathway’ to fibril formation and which of these, if any, are ‘off pathway’ of fibril formation.

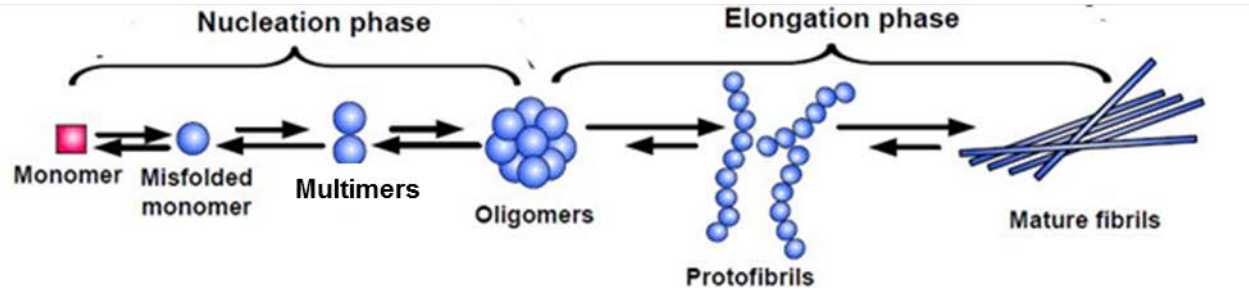

Figure 1-4: Cartoon representation of Aβ aggregation pathway (Adapted from [93])

1.2.2 Oligomerization of Aβ amyloid peptides

The small intermediates formed in the aggregation process of Aβ peptides are commonly called oligomers. However, some ambiguity of this terminology exists in the amyloid field. To date, many types of Aβ oligomers have been documented and described in the literature, e.g. protofibrils [94-97], annular structures [87, 98], and Aβ-derived diffusible ligands (ADDLs) [61, 99]. In general, Aβ oligomers tend to remain in suspension in aqueous solution after low speed centrifugation; however this is not an iron-clad criterion. The heterogeneity of Aβ oligomers has been demonstrated by various structural and biochemical techniques [100]. One investigation of Aβ oligomers suggested that they are heterogeneous, and exist in equilibrium with each other and also with the monomers and with the final aggregates (in the case of 'on-pathway aggregates') [87].

Oligomers are referred to as spherical species by EM or other biophysical techniques. Although they are generally considered to be smaller in size in comparison with fibrils, this size definition is usually based on how soluble they are under centrifugation conditions. The dimensions of the oligomers confirm to a high molecular weight of the oligomeric states and to the presence of a large number of peptide chains (in the order of hundreds to 1000s of

monomers). Hence, sometimes the large soluble oligomers are referred to as “non-fibrillar aggregates”, and the smaller oligomers can denote multimeric assemblies. Current literature, however, does not show these differences and often just denotes them as ‘low-molecular-weight’ and ‘high-molecular-weight’ oligomers.

Oligomeric structures also typically represent the earliest kinetic intermediates of the amyloid formation reaction and they occur as metastable states that appear and disappear over the time before which fibrils begin to form. Structural studies on oligomers require them to be stable for the period of analyses, and techniques have been devised to trap these intermediates species through appropriate methods, including ligand binding, covalent modification, etc.

There are several other features that discriminate oligomers from fibrils apart from size and shape differences. The characteristic feature of amyloid aggregates is the presence of a generic ‘cross-β-structure’. Some oligomers do have β-sheet structure and have the ability to bind to ThT and are termed as “β-oligomers” [101]. Other oligomers which do not have such generic structures are classified as “non-β oligomers” [102]. The oligomer field in the case of Aβ is diverse and confusing. The secondary structural characteristics of oligomers can vary substantially from high β-sheet content to random-coil-like conformations and even α-helical structures [103] depending on the methods used to prepare them. In some studies, the similarity of the structures between β-sheet rich oligomers and fibrils have been shown [101], whereas in other cases significant differences in the CD and FTIR spectra or antibody binding properties of certain oligomers and fibrils have been shown [102].

These data are testament to the idea that oligomers are present in highly polymorphic states; that is, a single polypeptide chain can make multiple types of oligomers based on growth conditions or at different times in an assembly reaction. Such variations can occur, between

different samples, where they result from such sources as different preparation protocols and where differences are recognizable through discrete antibody binding interactions. On the other hand, polymorphism may arise even within the same sample, apparently as the result of stochastic fluctuations. Such intra-sample heterogeneity can be demonstrated by single-particle techniques, such as EM or fluorescence correlation spectroscopy (FCS) [104-106].

1.2.3 Are oligomers on or off pathway?

One of the important questions in the amyloid field is whether the oligomers and protofibrils, which are typically seen during the aggregation reaction, lie on or off the pathway of amyloid formation. It is very difficult to study amyloid aggregation mechanism in vitro to obtain data to make kinetic arguments to support or disprove a hypothesis on precursor-product relationships. In some cases, spherical intermediate oligomeric structures have been proposed to serve a key, on-pathway role in both the nucleation and elongation steps of the formation of amyloid fibrils. In one such model, nucleation takes place by 'conformational conversion' of oligomers to form 'nucleus' which can then be converted to fibrils by elongation process [107]. According to this model, fibril growth can then happen either by subsequent additional conformational conversions of oligomer docked on the ends of the fibril, or by monomer addition. In the case of $A\beta_{40}$ protofibrils, the β-sheet regions have been shown to provide the core for the β-sheets in the corresponding mature fibrils [108], consistent with protofibrils being on-pathway intermediates.

By contrast, many other data are inconsistent with the hypothesis that oligomeric forms are on the amyloid assembly pathway [109, 110]. For example, in the case of Aβ, amyloid fibrils have been shown to grow in low concentrations of denaturant where no oligomer formation was seen [110]. Under certain conditions, stable oligomers and protofibrils were seen without the

conversion to mature amyloid as detected by ESI-MS [111]. Often times, the presence of an off-pathway stable intermediate depends on the reaction conditions. As shown in **Chapter 4**, the presence of stable off-pathway intermediates can complicate the study of amyloid fibrils.

1.2.4 Structure of protofibril intermediates

Protofibrillar intermediates represent the species that are structurally the closest to the final end-stage fibrils. They represent the late-stage intermediates of the amyloid pathway and can be distinguished from oligomers by their elongated, linear shape. Protofibrils lack the tertiary structure features and periodic symmetry of the mature fibrils. They are typically composed of one filament of the fibril (diameters of usually less than 6 nm) (however sometimes fatter protofibrils have been seen), shorter in length (usually below 100 nm) and are also more curvilinear or wigly in shape. The interaction of Aβ protofibrils to amyloid-staining dyes, such as CR and ThT are typically weaker than those observed for mature fibrils [112]. CD, IR and X-ray diffraction demonstrate that these filaments in the case of Aβ peptide, consists of high levels of β-sheet structure [113, 114]. Previous work from our lab and others have shown that, for some stable Aβ protofibrils, there is a difference in the extent of β-sheet protection between protofibrils and fibrils with protofibrils exhibiting lower level of β-sheet elements as measured by hydrogen-deuterium exchange [115]. In some cases, solid-state NMR has been used to study the secondary structures of protofibrils at a residue-specific basis sometimes showing a simpler β-hairpin conformation [116] and other times more complex hexameric barrel conformation [117].

1.2.5 Structure and stability of mature Aβ fibrils

Mature amyloid fibrils are the end stage reaction products of the fibrillogenic pathway. They typically possess a long, linear, sometimes twisted and highly regular morphology that is visible by TEM and other microscopic techniques. The generic 'cross-β' structure (**Figure 1-3**) that produce spacings at 4.7 and ~ 10 Å is a property of various amyloid fibrils, irrespective of their sequence [73]. Mature Aβ amyloid fibrils can extend several microns in length, while the fibril width can vary between 5 - 15 nm, but different fibril polymorphs can present significantly different values [118]. Most Aβ amyloid fibrils are twisted when viewed under TEM which are termed 'crossover' points [119]. Mature amyloid fibrils are usually characterized by a high affinity for amyloidogenic dyes, such as CR and ThT. In the case of various Aβ peptides, detailed structural data of the fibrils are now available, including residue-specific assignments of the secondary structural elements of different fibril polymorphs using ssNMR and HX-MS studies [120, 121] and electron density maps obtained with cryo-microscopy at sub-nanometer resolutions [122].

As in globular proteins, the net individual interactions within the structure of the folded fibril, balanced against destabilizing forces, determines fibril stability. This stability is high but not infinitely so, and a thermodynamic equilibrium is typically reached where some amount of monomer exists [123, 124]. Thus, fibril growth is generally a reversible process, i.e., fibrils can revert back to soluble oligomeric species or monomers upon dilution of the fibril into buffer. This equilibrium value, termed critical concentration (C_r) is a reproducible property of a particular amyloid form grown in a specific set of conditions [125]. This dynamic equilibrium value can be approached both from the soluble monomer side (forward reaction) and from the aggregate side (reverse reaction) [124, 126] (**Figure 1-5**). These values can be converted to free

energy values for fibril assembly reactions, similar to a protein folding curve [127], or they can simply be compared qualitatively, with the understanding that the lower the C_r, the more stable the fibril.

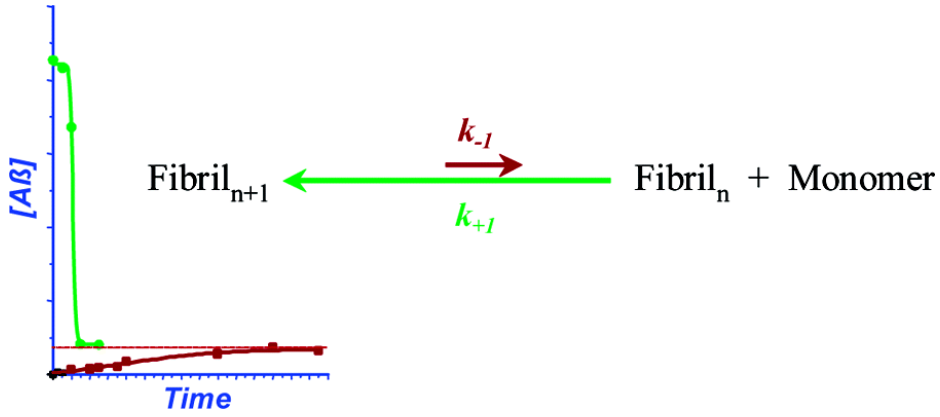

Figure 1-5: Thermodynamic equilibrium between fibrils and monomers [124]

Both X-ray diffraction and NMR studies have revealed the highly ordered, β-sheet rich structure of Aβ amyloid fibrils [28, 121, 128]. The structure contains a unique quaternary, intermolecular cross β-sheet that spans across more than one molecule (**Figure 1-6**) [129]. However, one complexity in studying amyloid aggregates arises from the fact that structural polymorphism exists, i.e., one polypeptide chain can grow into more than one stable structure [130] (see below) and hence the high-resolution structures of Aβ aggregates known to date could be biased by the conditions used for aggregation.

A diverse set of peptides and proteins with the capability to form fibrillar structures has been identified. Surprisingly, little sequence homology has been found. Furthermore, several proteins not associated with amyloid disease have also been shown to be able to form fibrils under certain conditions [131]. Therefore, the amyloid motif has been suggested to be a rather fundamental motif of the polypeptide backbone [131, 132].

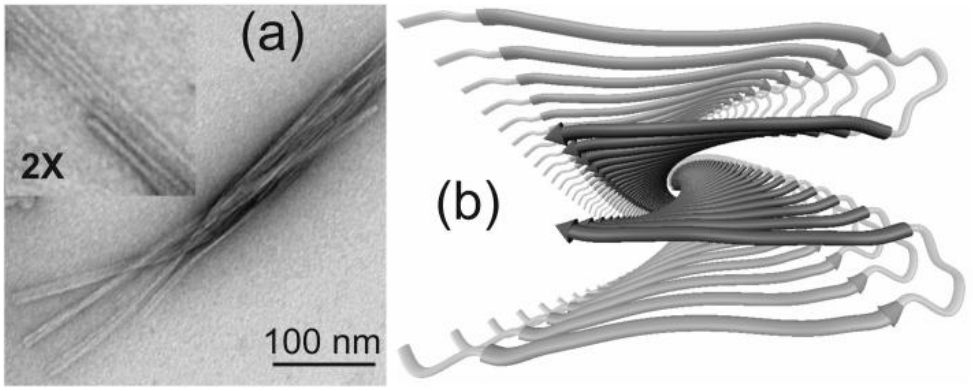

Figure 1-6: ss-NMR model of $A\beta_{40}$ fibrils.
TEM morphology (a) and fibrillar structural model (b) for $A\beta_{40}$ fibril based on ss-NMR and EM data for fibrils grown at 25 ºC under no salt and agitation conditions showing a parallel arrangement of in-register intermolecular β-sheets. (Figure from [133])

1.2.6 Presence of structural polymorphism

The cross-β sheet structure constructs the core of amyloid protofilaments. These protofilaments represent the filamentous substructures of mature fibrils. The helical twist of the protofilaments can give rise to a discernible overall helicity that can be seen in many, but not all, amyloid fibrils. Although the basic structural arrangement of the cross-β structure is conserved for different fibrils, there are different possibilities how they can pack into the 3-D fibril structure. Such variable protofilament arrangements can be one of the reasons for several distinct amyloid fibril morphologies. These fibrils can differ in several structural properties, such as the extent of residues in β-sheet formation, cross-sectional thickness of the fibril, the helical pitch, etc.

The interior of the protofilament can vary from one fibril to another resulting in difference in the extent of β-sheet protection in the fibril [125]. For example, in the case of $A\beta_{40}$ peptide our lab has previously shown that it can produce a broad variety of differently structured amyloid fibrils in vitro that differ in the extents and locations of hydrogen bonded β-sheet

structure within the fibril [125]. These polymorphs have also be shown to vary in their thermodynamic parameters (C_r), ThT binding and EM morphology. Structural polymorphism of amyloid fibrils has been reported for numerous other polypeptide systems as well, for example amylin [134], glucagon [135], the SH3 domain of phosphatidylinositol-3′-kinase [136], insulin [137] and lysozyme [132] .

1.3 CURRENT ISSUES IN Aβ STUDIES

Much has been learned in the last 25 years of research on the self-assembly of Aβ peptides, but much remains to be done. We need to come to a better understanding of how many non-fibrillar intermediates there are in amyloid assembly reactions, their structures, which ones are on-pathway and/or can interconvert, and which ones are especially cytotoxic. We also need to know more about the roles, if any, of some of the minor Aβ species that are generated in the brain. These themes are brought together in **Chapter 5**, where we describe how the self-assembly of the relatively rare $A\beta_{43}$, while following the same pathway as $A\beta_{42}$, proceeds much more slowly. The slow progression through various stages gives us an opportunity to better characterize some of these intermediates. We also found some very surprising features of the interaction of $A\beta_{43}$ with $A\beta_{42}$ in self-assembly and in fibril structure that may have some general implications.

There has been considerable speculation in recent years about the possible prion-like nature of aggregation-associated neurodegenerative diseases like AD. The idea is that disease might progress via the spread of aggregates from one neuron to the next, and be amplified in the new neuron via seeded elongation – all aspects of prion phenomena in human brains and in yeasts [138-140]. This makes it particularly important to continue to understand the process of

seeded elongation of amyloid fibrils, and in particular how universally seed structure is propagated into product fibril structure. In **Chapter 6**, in our studies of cross-seeding between D- and L-Aβ_{40}, we describe an extreme example in which amyloid fibrils dramatically increase amyloid assembly via seeding while at the same time failing to replicate the structure of the seed fibrils. Whether this disconnect between rate acceleration and structural replication will be observed more commonly, and in more biologically relevant examples, remains to be seen.

It is quite simple these days to generate data in amyloid studies, but it is a continuing challenge to do it right, and there is always room for improvements which sometimes can make a difference as to whether or not the data obtained represents the reality of the disease process. In **Chapter 4** we describe how the all-important disaggregation protocol has got to be matched to the peptide being studied, and how failing to do this can lead to flawed data that may not even be recognized as being flawed. Peptide impurities can affect aggregation properties modestly (**Chapter 3**) to severely (**Appendix A**), and it is important to work to understand purity levels and improve on them to optimize results. In **Chapter 3** we describe a very convenient modification of standard solid phase synthesis of peptides that seems capable of being generally useful in improving the quality of highly hydrophobic amyloid peptides. Methodology for characterizing amyloid can also be improved. While the ThT assay is standardly done in almost all amyloid labs, we show in **Chapter 5** that there is much more information content in ThT data than is normally appreciated, and this has helped to provide us with new insights into Aβ oligomer structures.

2.0 EXPERIMENTAL METHODS

2.1 MATERIALS AND REACTION PROTOCOLS

2.1.1 Peptide synthesis and purification

Most of the Aβ peptides used in the various studies in this thesis were synthesized chemically by solid-phase Fmoc synthesis and obtained in crude partially purified versions. In most cases, the peptides were obtained from the Keck Biotechnology Center at Yale University in synthesis scales of 25-100 µmoles. All the crude peptides were stored at -80 $^{\circ}$C. In some cases, purified wildtype $A\beta_{42}$ and $A\beta_{40}$ peptides were obtained via large-scale custom t-Boc synthesis also from the Keck Center. Pure recombinant Aβ peptides used in the thesis were obtained from rPeptide.

Crude peptides were purified using a reverse phase Agilent Zorbax SB-C3 preparative column (9.4 * 250 mm; 5 µm particle size) using the protocol described below. The peptides were dissolved in 100% formic acid (Sigma Aldrich) and sonicated in a bath sonicator for ~5 minutes. Prior to injection into the reverse phase column, the peptides were diluted to ~50% formic acid using milliQ water. Peptides were purified in a Biorad Biologic Dual Flow system by gradient elution. The buffer systems used for purification were water (Fisher Scientific, HPLC grade) + 0.05% TFA (Sigma Aldrich) (solvent A) and acetonitrile (Fisher Scientific, HPLC grade) + 0.05% TFA (solvent B). Each purification run was preceded by at

least a couple of blank runs where only formic acid was injected, in order to eliminate the presence of any residual peptide bound to the column from previous runs. During the purification run, the solvents were run at a flow rate of 4 ml/min with a gradient system that was specific to the peptide type. In the case of Aβ peptides, the fraction collection gradient was either 20-50% solvent B in the case of $A\beta_{40}$ peptides or 30-60% solvent B in the case of longer C-terminal Aβ peptides. This was done to ensure that the peptides with the highest purity elute in the middle of the shallow phase of gradient selected. Purifications were carried out either at room temperature or at 65 °C using a column heater (Sidewinder LC column heater, Restek Corp.). Fractions were collected using a Biorad fraction collector with a collection volume of 0.8 ml/fraction. Based on the absorbance signals at 214 nm, fractions corresponding to the major peak were identified and analyzed for purity by mass spectrometry. Pure fractions corresponding to the correct molecular weights were then pooled, lyophilized overnight and stored at -20 $^{\circ}$C for future use.

2.1.2 Purity analysis by Mass spectrometry

An Agilent electrospray 1100 mass spectrometer was used to determine the masses of the peptides during purification. All the fractions were first run through an analytical reverse phase column (Agilent SB Aq column, 4.6 * 50 mm; 1.8 µm particle size). The masses were determined by using the in-built analysis module present in the software. Typically, fractions with > 90% purity were pooled, lyophilized overnight and stored at -20 °C until they were disaggregated in preparation for aggregation reactions.

In some cases, the purity of Aβ preparations before the disaggregation process was more carefully assessed (**See Chapter 3**). Raw data of ion current versus mass/z was transferred to an excel sheet and plotted. A baseline was drawn in a region of mass/z spectra not occupied by significant peaks. Purity was then calculated by using the peak cluster with the highest charge state (e.g., for $A\beta_{42}$ we used the +5 state) and the ion current values normalized to 100% for the highest peak (in all cases which corresponded to the desired peptide). All the other peaks in the cluster with a normalized amplitude of >1% were included in the analysis of purity. All peaks were integrated and their areas summed and used as the denominator in the % purity calculation. Peaks corresponding to the sodium complexes of the desired Aβ were added to the pure Aβ peak to obtain the total peak area associated with desired product.

2.1.3 Chemical disaggregation protocol

It is well known that most amyloid peptides contain some amount of pre-existing aggregates which are capable of acting as seeds to accelerate the aggregation of the monomeric peptides, or as inhibitors to slow down spontaneous aggregation reaction [141, 142]. Hence detailed disaggregation methods have been developed by various groups over the years to completely remove preformed aggregates and also to achieve some degree of control and reproducibility of in vitro studies. In our group, we never attempt to save disaggregated samples for later use in experiments; rather, we always freshly disaggregated material on the day of the desired experiment. This leads to very good reproducibility and, we believe, results that best represent the behavior of monomeric peptide.

For many applications (but see **Chapter 4**), we use a detailed chemical disaggregation protocol to obtain monomers of Aβ. The method has been described previously [44, 123].

Briefly, about 1 mg lyophilized pure peptide powder was suspended in 1 ml TFA in a small glass vial. The vial was capped and sonicated in a water bath sonicator for 15 min. In a chemical fume hood, the peptide solution was dried under a gentle stream of nitrogen gas to generate a thin film on the walls of the vial. Then, the peptide was dissolved in 1 ml HFIP and incubated at 37 °C for 1 hr. A small, measured aliquot of the HFIP solution was transferred into 1% TFA in water and chromatographed on HPLC to determine the approximate concentration of peptide in the HFIP solution; and hence the amount of peptide in the vial. Again the peptide solution was dried under a stream of nitrogen gas. Then, the residue was dissolved in 2 ml HFIP. This step is done to ensure that all of the TFA will be removed from the sample when the HFIP is removed. Based on the HPLC determination of the amount of peptide in the sample, aliquots were taken into glass tubes at 0.25 mg per tube. HFIP solution in the tubes was evaporated under a stream of nitrogen again. Immediately, the peptide was dried under vacuum using a lyophilizer for 60 min to ensure that all of the TFA and HFIP had been removed from the peptide. Slowly, 0.5 ml fresh 2 mM NaOH was added per tube and was allowed to stand for 5 min undisturbed before mixing it gently to dissolve the film and then 0.5 ml 2× PBS with 0.1% sodium azide was added per tube. The peptide was centrifuged at 436,000 x *g* overnight at 4 °C in an ultracentrifuge in the case of $A\beta_{40}$ peptide and for only 1 hr in the case of all other longer Aβ peptides. The peptide solution supernatant (~60-70%) was carefully removed from the centrifuge tubes. The solutions were kept at 4 °C while determining the Aβ concentrations using the HPLC assay (see below), before adjusting the concentrations to the start the experiment. The use of azide in the PBS is to discourage bacterial growth during the sometimes very long aggregation reaction time courses. However, the azide is left out when preparing aggregates for FTIR analysis.

2.1.4 Peptide disaggregation through Size exclusion chromatography

We found that the chemical disaggregation protocol which our lab has been using for $A\beta_{40}$ peptides was not ideal for longer Aβ lengths, since the method used sometimes influenced the reaction kinetics and the final morphology of the aggregates (**Chapter 4**). To obtain disaggregated peptide that behaved more ideally, we used a recently developed approach of isolating fresh monomer by size exclusion chromatography (SEC) from peptide freshly dissolved in a strong denaturing solvent like guanidine hydrochloride (Gdn-HCl) solution [143]. SEC was carried out on a Superdex 200 10/300 column (GE Health Sciences) equilibrated in PBS on an Agilent 1200 isocratic HPLC system with a flow rate of 0.5 mL/min and elution monitored at 215 nm. Purified, lyophilized peptides were dissolved in 8M Gdn-HCl, sonicated briefly (bath sonicator), injected into the SEC column, and the fractions collected. Generally, separate peaks were observed eluting at the positions of oligomers and monomers. The monomer fractions were immediately analyzed for Aβ concentration, pooled, adjusted to the desired concentration by adding 1X PBS, and immediately used in the desired experiment.

2.1.5 Determination of starting monomer concentrations

Peptide concentrations were determined using an Agilent analytical RP-HPLC system. Peptides were injected by the auto-sampler onto an analytical Agilent C8 column and eluted using an acetonitrile buffer similar to the purification buffer B. The elution profile was monitored by absorbance at the A_{215nm} detector channel and the area of the elution peak was determined using Agilent ChemStation software. The area under the curve was converted to peptide concentration using a standard curve that relates peptide masses to HPLC areas.

This curve is determined by using the extinction coefficient at 215 nm (calculated using the method described in [144]) to calculate peptide concentration for 4-5 samples using an absorbance spectrophotometer (Beckman Coulter DU800). These calibrated samples were then individually injected into RP-HPLC to obtain A_{215} peak area which was then plotted against the corresponding concentration determined by the absorbance value to form the standard curve. Although Aβ peptides exhibit very similar standard curves, they are generally reproducibly different from each other. We therefore normally generate and use specific, separately determined standard curves for each chemically different peptide being studied.

2.2 KINETIC ANALYSIS OF AGGREGATION

2.2.1 Sedimentation assay

The sedimentation assay was the predominant method of choice used to study the aggregation kinetics and other thermodynamic properties of the peptides studied in this work [123]. The advantage of this method is that it gives a completely unbiased report on the aggregation of a peptide, regardless of the kind of aggregates being formed. Briefly, the method consisted of taking aliquots from an ongoing reaction of Aβ at any particular time and centrifuging each at 436,000 x g on a table top ultracentrifuge (Beckman Coulter Optima TLX) for 30 minutes and then carefully isolating 70% of the supernatant. The concentration of peptide in the supernatant is then determined by injection into the RP-HPLC (as described above). The area under the curve at 215 nm gives the exact amount of monomer present in the sample at that time point.

This is carried out typically in duplicates till the end of aggregation when there is no apparent change in monomer concentrations of aliquots taken ~ 24 hrs apart. This final monomer concentration represents the equilibrium concentration of the peptide in the forward reaction.

2.2.2 Thioflavin T binding measurements

One of the unique and characteristic features of amyloid aggregates is their ability to bind ThioflavinT (ThT), a dye which binds to most amyloid structures. The mechanism of binding of the aggregates to the dye is not understood structurally in great detail, however, it is generally accepted that ThT behaves as a molecular rotor and amyloid fibrils provide the 'lock' site for inhibiting the dye's rotation when it is bound to the fibrils [145, 146]. This binding of the aggregates to the dye can be studied as a kinetic assay along with HPLC sedimentation assay to provide additional information on the properties of the aggregates along the aggregation pathway and also as a means to compare the structures of the final aggregates formed from various peptides. For example, as shown in **Chapter 5**, the detection of aggregates seen in the sedimentation assay, by measuring the amounts of monomer drop, which at the same time do not bind ThT, can point to the presence of non-β oligomers [147].

To perform the time course ThT binding experiment, an aliquot of an ongoing reaction was taken at any particular time, mixed with a standard excess of ThT (4 µl of 1.5 mM stock to give final concentration of 15 µM) and the fluorescence measured using a Jobin Spectrofluorimeter. Typically, aliquots of the reaction were chosen such that 1 µg of total Aβ peptide is present in the cuvette for ThT binding. The total volume during the measurement was adjusted to 400 µl using 1x PBS. The instrumental parameters are as follows (λex = 445 nm; excitation slit width = 2 nm; λ_{em} = 489 nm; slit width = 4 nm).

The ThT binding can be quantified using the following method. First, the ThT fluorescence of a blank solution was determined. This was done by replacing the volume of aggregates taken with PBS solution. Next, this value was subtracted from the raw fluorescence values obtained from ThT binding per μg of Aβ at each time point. Next, the resulting ThT value was weight normalized to the amount of aggregates present at each time point. This was done by using the % aggregate (total Aβ - % monomers) obtained from the HPLC sedimentation assay. The resulting values were plotted as ThT absorbance units vs time similar to HPLC sedimentation curve.

The ThT reading can also be used to detect the presence of oligomer present during the early part of the reaction. This can be done in at least two ways. The first way is to simply compare the progress curves of the aggregation reaction as monitored by sedimentation and by ThT, plotted on the same graph. If the ThT curve is not a simple mirror image of the plot of loss of monomer over time by sedimentation, it is an indication that there are intermediates with different ThT sensitivities. The other way is to normalize both the time-dependent ThT data and the sedimentation data to 100%, then plot one versus the other for the reaction. If this plot deviates from a straight line with a slope of 1, it is an indication of the presence of intermediates with different ThT binding/fluorescence along the reaction profile [147] (**See Chapter 5**).

2.2.3 Dissociation reactions

Dissociation reactions were initiated with end stage fibril reaction mixtures to look for the true equilibrium concentration value between monomers and fibrils [148]. This value known as critical concentration (C_r) is an important thermodynamic parameter of the aggregates [149]. To undergo dissociation reactions, an aliquot was removed from the completed reaction mixture (at the end of sedimentation kinetics curve), and diluted in 1x PBS. (It is important to

use a reaction mixture and not a sample of isolated fibrils, since manipulating and storing fibrils can sometimes compromise their reversibility). The dilution was done such that the remaining monomer concentration was sufficiently below the apparent C_r value (based on the end-stage plateau monomer concentration from the forward reaction) to allow observation of an increase in monomer concentration as aggregates dissociate when the mixture returns to equilibrium. At the same time, the total amount of peptide in the diluted reaction must be substantially greater than the C_r, sufficient to ensure that some fibrils will still be present at equilibrium. For example, if a forward reaction had a starting concentration of 10 μM, and appears to equilibrate at 1 μM of monomer in the fibril assembly reaction, a 5-fold dilution of a late time point will bring the monomer concentration to 0.2 μM (well below the expected C_r), while maintaining a total peptide concentration of 2 μM in the reaction mixture, ensuring a clear store of aggregates at equilibrium. The diluted sample was incubated at 37 °C and aliquots were taken for concentration of monomers using HPLC sedimentation assay as described previously.

2.2.4 Seeding experiments

Seeded fibril elongation reaction can be used as an assay to explore amyloid fibril structure by looking at the compatibility of one amyloidogenic peptide with another in a "cross-seeding" reaction. For this assay, the final fibrils acting as seeds were isolated from spontaneous growth reactions by centrifugation at 436,000 x g for 30 min, and washed with one or more cycles of suspension of the pellet in the eventual elongation buffer (PBS, pH 7.4) followed by isolation by centrifugation. Fibrils were then sonicated in suspension using a microprobe sonicator [Sonic

Dismembrator Model 500; Fisher Scientific (20 kHz)], and the fibril weight concentrations were determined by dissolving an aliquot of the fibril suspension in formic acid followed by an HPLC assay as described previously. Aβ monomer was disaggregated, dissolved in PBS, and sonicated fibrils of the different polymorphic seeds added to an exact final concentration in the range of 5-10% (w/w). Reactions were carried out at 37 °C without agitation in PBS and followed by the sedimentation assay. In some cases, ThT measurements were also carried out.

2.3 AGGREGATE SIZE AND SHAPE STUDIES

2.3.1 Dynamic Light Scattering

Dynamic light scattering measurements (DLS) were done using the DynaPro plate reader (Wyatt technology) equipped with a temperature control. DLS was mainly used to follow the time-course of aggregation and to detect for the presence of oligomers followed by their size characterization. Aliquots at specific time-intervals were taken (~80 µl) and were transferred into a fresh well of a 384-well microplate and the scattering data was recorded. Typically, the measurements were performed at 37 $^{\circ}$C with an acquisition time of 5 secs/scan and 10 acquisitions/sample. In each of the experiments, the software displays the average of 10 acquisitions and this representative data is selected for analysis. In most cases, only acquisitions which have good correlation and decay were averaged for analysis and other acquisitions were neglected.

2.3.2 Aggregate morphologies by Electron microscopy

Aggregate morphologies at different stages of aggregation were studied by transmission electron microscopy. 10 µl of an on-going reaction of any particular peptide of interest was taken at defined time-intervals and transferred onto a freshly glow-discharged carbon-coated grid, adsorbed for 2 minutes, washed twice by adding 10 µl of deionized water followed by blotting, then 10 µl of 1% (w/v) uranyl acetate was added. In order for optimal staining, the uranyl acetate was removed by blotting within 30 secs and the grid was washed with deionized water again. The grids thus prepared were either imaged immediately or were stored for visualization later at room temperature. Grids were imaged on a Tecnai T12 microscope (FEI) operating at 120kV and a magnification of 30,000X. The microscope was equipped with an Ultrascan 1000 CCD camera (Gatan) with a post-column magnification of 1.4X.

2.4 SECONDARY STRUCTURE ANALYSIS OF AGGREGATES

2.4.1 Hydrogen Deuterium exchange Mass spectrometry

Significant insights into fibril structure could be derived from knowledge of the pattern and extent of hydrogen bonding within the fibril [150]. Recently HX-MS and HX-NMR studies have been described for amyloid systems like, β-2 microglobulin [151], transthyretin [152], Aβ [115, 153] and prion proteins [154, 155]. Our lab has developed the application of HX-MS technique to the analysis of amyloid fibrils of full length $A\beta_{40}$ to reveal those residues which are involved in highly protected H-bonded structure [108, 115, 125, 150, 153, 156].

2.4.1.1 In line analysis for global protection values

The detailed description of the global HX-MS experiment has been described previously [156]. The brief methodology is presented here:

Mature amyloid fibrils are isolated by centrifugation at *20,800* x *g* for 30 min in a bench-top centrifuge. Check for good amount of pellet formation. The resulting fibril pellet is decanted and washed with 200 µl D_2O solution, followed by centrifugation at *20,800* x *g* for 30 min. Centrifugation at very high *g*-forces is not a viable option because ultra-centrifuged pellets are difficult to quickly re-suspend for the H/D exchange measurement. Use gel loading tips to remove final traces of any protonated solvent without disturbing the pellet. Again, the aggregates are re-suspended in 60-70 µl of D_2O solution and left at RT. This marks the start of the exchange reaction. The solution was kept overnight and the HX exchange was analyzed after 16-20 hrs of D_2O incubation. After this, the aliquots from the exchanging suspension can be infused into one arm of the mixing T-tube using a syringe pump (**Figure 2-1**). The exchange reaction of deuterium into fibrils reaches completion after about 20 hrs; hence, this time of exchange is typically selected for the samples analyzed in this thesis.

H-X exchange measurements require identification of a processing solvent that quickly dissolves fibrils within the mixing T, quenches exchange, and is MS-compatible for efficient ionization [156]. Using this set of constraints (some of which may be instrument dependent), we used a processing solvent that is a mixture of 1:1 water: acetonitrile with 0.5% formic acid, with pH ~2.5 which is optimal to dissolve the highest possible concentration of fibrils in the mixing T and in the capillary prior to ESI. The flow rates used for infusing sample (0.5 µl/min) and solvent (9 µl/min) into the mixing T serve to dilute the sample by a factor of ~20 and establish a ~10sec

dwell time from mixing to spray. Reduced dissolution temperatures can also be explored to minimize exchange further (see below).

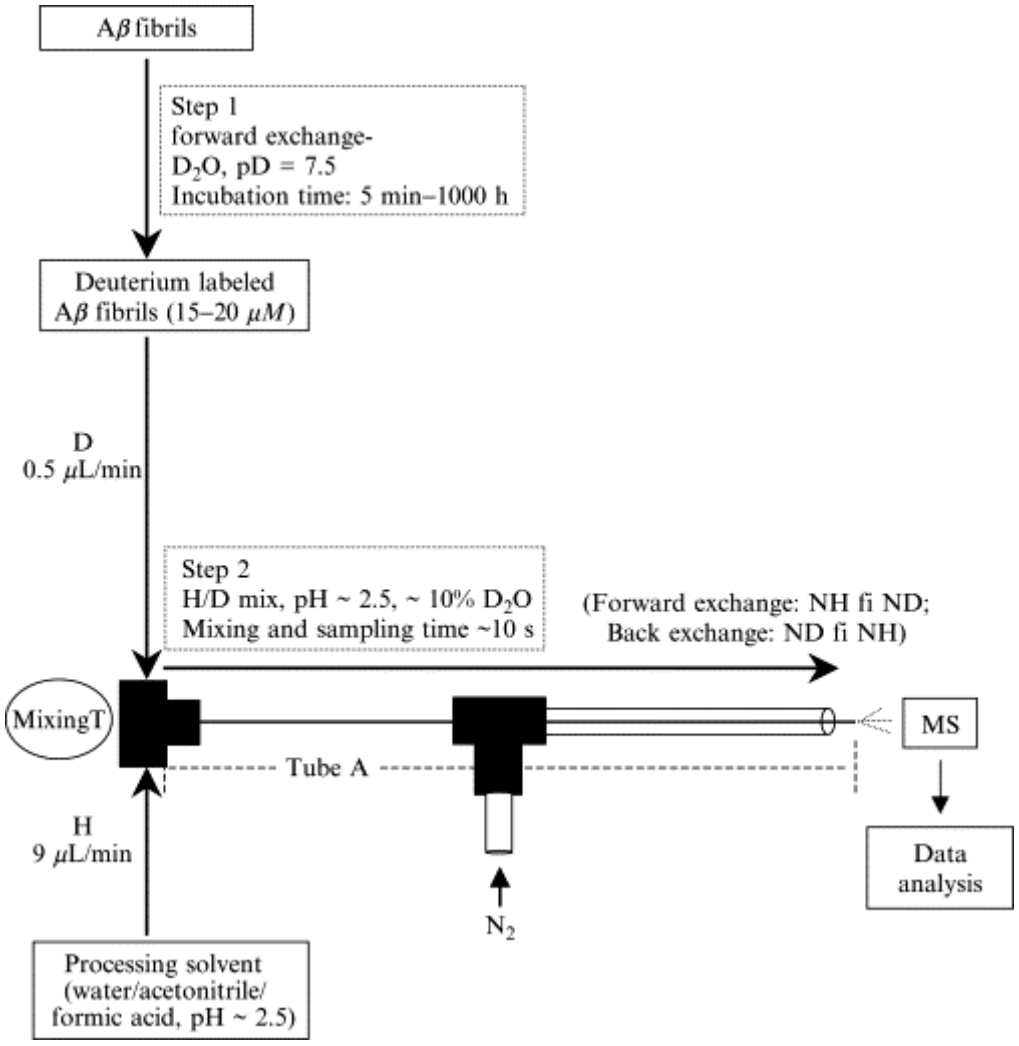

Figure 2-1: Schematic of the experimental setup of the hydrogen/deuterium exchange-mass spectrometry (MS) [156]

2.4.1.2 Inline pepsin digestion

Segmental analysis was done two different ways. First, as shown previously with the help of on-line pepsinolysis approach using the T-tube system shown earlier [125]. The fibrils in D_2O were loaded onto one arm of the T-tube just like during global exchange experiment and the other arm contains quenching solution along with pepsin (0.5 mg/ml in 0.5% formic acid; 9 µl/min) and passed directly into the MS instrument.

2.4.1.3 Offline pepsin digestion using pepsin agarose beads

In the second approach to segmental analysis, electrospray ionization HX-MS data of the C-terminal pepsin fragment was obtained using a modified solubilization protocol using Gdn-HCl and a modified digestion protocol using pepsin-agarose beads (Sigma Aldrich) [155]. Briefly, the aggregates were suspended in D_2O for 16-20 hrs just like in the case of global exchange analysis. Then the aggregates in D_2O were spun down (*20,800* x *g*, 30 min) and the pellet was dissolved in 20 µl of ice cold solution of 8M Gdn-HCl + 0.1% formic acid for 10 secs to undergo rapid dissolution. The dissolution and digestion were carried out at 4 °C to slow down artifactual exchange. The sample was quickly vortexed and 100 µl of pepsin agarose in 0.1% cold formic acid was added for 10 secs. The sample was spun down quickly (14,000 *rpm*, 30 secs) and the supernatant was analyzed by LC-MS at 4 °C to obtain the ESI-MS pattern for the aggregates. As controls, we also performed the C-terminal digestions of fully protonated and fully deuterated monomers.

2.4.2 FTIR spectroscopy

FTIR of the aggregates were performed by taking a large volume of aliquots of the final aggregates (~500 µl) and spinning down at *20,800* x *g* for 30 mins. Aggregates were isolated, washed with PBS and then re-dissolved in ~5 µl 1x PBS to get a highly concentrated sludge. Spectra were acquired by then placing this aggregate sludge between two polished CaF_2 windows on an ABB Bomem FTIR instrument by using the in-built data acquisition module, BioCell (BioTools, Inc.). The data were acquired by averaging over 400 scans, at a scan rate of 4 cm^{-1}, at room temperature. The data were also corrected for residual buffer absorption. The resulting spectra was deconvoluted to a second derivative spectrum and analyzed for the presence of various secondary structures.

2.4.3 Circular dichroism Spectroscopy

Circular dichroism spectroscopy was used to determine the secondary structure of some aggregates used in this study (**See Chapter 5**). The aggregates obtained were typically in PBS buffer (pH 7.4). Far-UV CD spectra were recorded using a Jasco J-810 spectropolarimeter. Spectra were collected in a 0.1 mm cuvette with a resolution of 0.5 nm using at a spectral rate of 100 nm min^{-1}. Spectra were collected and averaged over five scans and corrected for the appropriate buffer.

3.0 IMPROVED CHEMICAL SYNTHESIS OF Aβ PEPTIDES USING FLANKING C-TERMINAL CHARGED RESIDUES

[This chapter has text, figures and tables reprinted/adapted with permission from the following published journal paper [157]: **Chemuru, S**., Kodali, R. and Wetzel, R. "Improved chemical synthesis of hydrophobic Aβ peptides using addition of C-terminal lysines later removed by carboxypeptidase B", *Biopolymers.* 2014. **102** (2) 2014; p 206-221. In this chapter, I had help from R.K. in the collection of TEM and FTIR data and I.B. in the collection of proton-NMR data used in some purity analysis]

3.1 OVERVIEW

Owing to the high hydrophobicity of Aβ and many other amyloidogenic peptides, they introduce significant challenges to obtain good yield and purity during solid phase chemical synthesis. This is mainly due to significant aggregation during synthesis and purification. Chemical synthesis of $A\beta_{40}$ is not very challenging, but addition of C-terminal hydrophobic residues to generate Aβ molecules of longer lengths create a much more difficult synthesis resulting in low yields and purities of the resulting peptides. In this chapter, we describe a new method of reversible addition of C-terminal flanking charged residues to Aβ peptides to significantly improve their

synthetic quality, yield and purity. We linked 2-6 Lys residues to the Aβ peptide's C-terminus through peptide bonds during the synthesis. These extra charged residues are then removed post-purification using an immobilized carboxypeptidase B (CPB) column. With this method, we obtained both $A\beta_{42}$ and $A\beta_{46}$ peptides of much higher purity than those obtained without Lys addition. This approach of reversible Lys addition is applicable as a generally useful method for making difficult hydrophobic peptides which otherwise cause problems during synthesis.

3.2 INTRODUCTION

3.2.1 Background

Our lab has historically looked at the aggregation kinetics and biophysical properties of aggregates formed from $A\beta_{40}$ peptides and their mutants which were synthesized using solid phase peptide synthesis obtained in small scale crude form from Keck Biotechnology Center. But, when we started working with chemically synthesized crude Fmoc synthesis of $A\beta_{42}$, we experienced difficulties during purification of the crude peptide using analytical HPLC column. The purification using the analytical C-3 resin yielded low yields and very low purities (**Figure 3-1**). The HPLC chromatogram showed a broad profile with no obvious peak for the desired pure product. MS analysis of the purest fraction only yielded ~65% purity and significant amount of other deletion impurities. These impurities were not separated even after repeated purification runs and with narrower gradients. Hence, it was not possible to work with this material for our studies and we started exploring options to improve the synthesis and purity of $A\beta_{42}$ and other longer biologically relevant variants of Aβ. One of the reasons for this low purity of longer Aβ

derivatives was due to their higher hydrophobicity and β-branched amino acid content at the end of the sequence which leads to problems during synthesis and also during their purification.

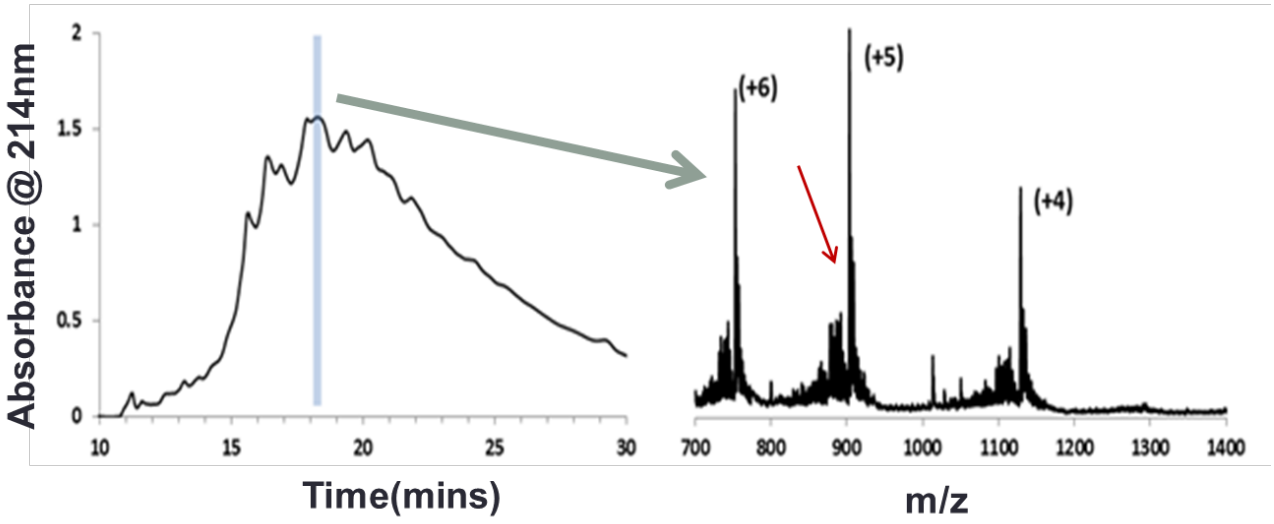

Figure 3-1: RP-HPLC purification and LC-MS profile of crude $A\beta_{42}$.
RP-HPLC purificatation of Fmoc synthesis of crude $A\beta_{42}$ using a preparative column (Agilent SB-C3) and 30-60% gradient of acetonitrile in water. LC-MS spectra of the purest fraction (blue bar) is shown here which shows significant amount of impurity peaks (red arrow).

3.2.2 Problems due to aggregation during synthesis

Most of the amyloidogenic peptides fall under the category of 'difficult sequence' containing peptides and solid-phase peptide synthesis of these 'difficult sequence'-containing peptides is very problematic and challenging for a synthetic chemist [158-160]. Due to the highly hydrophobic nature of these peptides, they often result in low yields during synthesis and also in very low purities [159, 161-163]. Some examples of these difficult-to-synthesize proteins are amyloid forming peptides like amyloid-β (Aβ) [159], α-synuclein [164, 165], and acyl carrier protein $(ACP)_{65-74}$ and also other hydrophobic trans-membrane segments of proteins, like glycophorin A, epidermal growth factor (EGFR) and M2 ion channel [166]. The hydrophobic

stretches present in these peptides appear to promote aggregation during synthesis and purification.

In the case of AD research, it is imperative to obtain high quality Aβ peptides and their analogs for in vitro research for performing biophysical, structural and toxicity studies. Because of the synthetic challenges present in making longer versions of Aβ, longer than $A\beta_{42}$, even though these peptides are known to be present in the AD brain and affect the disease pathology, their biophysical properties have not been well-characterized. This is mainly due to the synthetic challenges associated in working with highly pure versions of these peptide analogs.

The difficulty in solid-phase synthesis of amyloidogenic peptides is attributed to intermolecular hydrophobic interactions between resin-bound peptide chains and between the peptide and the resin itself resulting in poor solvation and formation of extended structures during synthesis [167, 168]. This aggregation of the growing peptide chain on the resin results in steric hindrance of the growing N-terminus leading to a decrease in the extents of de-protection in each cycle and hence to incomplete repetitive coupling reactions [169]. The aggregation of these hydrophobic peptides has been characterized directly on resin-bound peptides by various techniques, such as ssNMR [167, 170], FTIR [171] and Raman spectroscopy [172]. This aggregation is clearly a serious problem in solid-phase synthesis since it leads to lower yields and difficulties in purifying the peptides present in low amounts. Impure amino acid deletion sequences of varying lengths but with similar properties accumulate during the synthesis and are difficult to separate from the target peptide. The resulting decrease in the purity of the crude peptide, as well as the intrinsically poor solubility of these hydrophobic sequences, also often results in subsequent difficulties in purification [163]. These sometimes hidden impurities can have consequences for the properties of the synthetic product that are significantly amplified

compared to the purity level. For example, it has been shown previously that even small amounts of certain impurities in synthetic Aβ peptide can radically reduce Aβ aggregation and neurotoxicity [173].

3.2.3 Methods to improve chemical synthesis

Several attempts have been made to improve the Fmoc solid phase synthesis of such hydrophobic peptides. Some of the approaches include the use of solvent additives to provide optimal coupling agents, like anisole to prevent aggregation [174-176]; improved de-protection agents to aid in C-terminal synthesis [177]; the use of better coupling reagents developed recently, like HATU [175, 178]; and other organic solvent additives which prevent aggregation during synthesis [176, 179, 180]. Other techniques that have been explored include microwave assisted synthesis [181, 182] and the use of a more hydrophilic PEG based copolymer resin [183]. Some approaches specifically target the peptide backbone. These include photo-triggered interruption of amide bond formation with ester bonds (o-acyl isopeptide) [184-186], introduction of pseudoproline [187], which acts as a β-sheet breaker to prevent aggregation during coupling, and the use of other chemical moieties to act as backbone protecting intermediates [188, 189]. Most of these techniques are useful in producing much higher yields of hydrophobic peptides but are also, to varying degrees, cumbersome and expensive to undertake on a routine basis.

Another approach to improve synthesis is to alter side chains that improve solubility on the resin and during purification, in such a way that the modification can be reversed after purification. For example, oxidation of Met_{35} was employed to suppress aggregation of resin bound $A\beta_{42}$ during synthesis, followed by reduction after purification [190]. Reversible

solubilization has also been accomplished by adding, during the synthesis, a cationic C-terminus separated from the peptide of interest by a labile non-peptide bond, which can either be removed to directly generate the peptide of interest [191], or can be incorporated into a fragment condensation approach to make longer polypeptides [192-194]. Data on the efficiencies of cationic tail removal are generally not reported, however. In fact, in some cases, the reversible cationic tail approach was determined to not be beneficial due to relatively low yields [195].

In this Chapter, we introduce an alternative strategy for the reversible cationic tail approach in an effort to improve the synthesis of sequence variants of Aβ peptide. The method involves direct addition of C-terminal Lys residues during solid phase synthesis through only normal peptide bonds, and subsequent removal of the Lys tail using carboxypeptidase B enzyme (CPB) immobilized onto agarose beads. CPB is an exopeptidase and cleaves one residue at a time from the C-terminus and is highly specific for basic amino acids. We show that the method provides superior yields and purities of the human brain peptides $A\beta_{42}$ and $A\beta_{46}$.

3.3 METHODS

3.3.1 Peptides used

Wild type $A\beta_{42}$ and $A\beta_{46}$ peptides used in this study, without and with C-terminal lysines (**Table 3-1**), were synthesized at the Keck Biotechnology Resource Laboratory using standard Fmoc solid phase synthesis methodology using a PTI Symphony peptide synthesizer. All the amino acids during synthesis were double coupled with a four-fold amino acid excess using HBTU activator in DMF solution. The resins used were Life Technologies Peg-PS pre-loaded low load

resins carrying the appropriate C-terminal amino acid. Recombinant $A\beta_{42}$ used in the study for comparison was purchased from rPeptide.

Table 3-1: Peptide sequences described in this work

Peptide	Sequence
$A\beta_{42}$	DAEFRHDSGY EVHHQKLVFF AEDVGSNKGA IIGLMVGGVV IA
$A\beta_{42}K_2$	DAEFRHDSGY EVHHQKLVFF AEDVGSNKGA IIGLMVGGVV IAKK
$A\beta_{42}K_3$	DAEFRHDSGY EVHHQKLVFF AEDVGSNKGA IIGLMVGGVV IAKKK
$A\beta_{46}$	DAEFRHDSGY EVHHQKLVFF AEDVGSNKGA IIGLMVGGVV IATVIV
$A\beta_{46}K_3$	DAEFRHDSGY EVHHQKLVFF AEDVGSNKGA IIGLMVGGVV IATVIVKKK
$A\beta_{46}K_6$	DAEFRHDSGY EVHHQKLVFF AEDVGSNKGA IIGLMVGGVV IATVIVKKKK KK

3.3.2 Preparation of CPB-agarose column

CPB enzyme, pre-treated with PMSF to remove any contaminating serine protease activity, was purchased from Worthington Biochemicals (Catalog No: LS001724). Very High Density Glyoxal Beads (6BCL), containing 6% agarose beads conjugated with aldehyde groups reactive with protein primary amino groups, were obtained from Agarose Bead Technologies. Crosslinking of CPB to the glyoxal beads was performed according to the modification of the procedure previously described by Blanco et al [196]. The aldehyde groups in the resin react with the exposed primary amines in the enzyme. This results, after reduction with a reducing agent, in a stable and reusable resin for our studies. The various steps involved during cross-linking are briefly described below.

Approximately, 10 mg CPB was dissolved in 10 ml of 0.1 M sodium bicarbonate buffer at pH 10.0. The ligand solution was then mixed with 2 ml Glyoxal Agarose Beads and stirred gently for 5-6 hrs at 4 °C until the enzyme activity bound to the beads remained constant, as monitored using the Hippuryl-L-Arginine (Hip-L-Arg) assay. Hip-L-Arg is a well-known CPB substrate and we measured its hydrolysis by determining the increase in absorbance at 254 nm upon addition of the enzyme. Aliquots of the enzyme-bead mix were taken every hour for the substrate assay and absorbance at 254 nm was measured. Once there is no change in the immobilized CPB activity over the period of an hour, 20 mg of a reducing agent, sodium borohydride, was added to the suspension and stirred for 30 mins at room temperature in an open container in the chemical fume hood to allow hydrogen gas to escape. After the reaction, the CPB-agarose beads were loaded onto a Bio-rad Econo-column and washed with 10 mls of pH 7.5 phosphate buffer. The resin was further washed with Tris.HCl buffered saline (TBS), pH 9.0, then the same buffer containing 20% ethanol. The columns were stored at 4 °C until they were used for lysine cleavage. These columns were stable for over a month and were reused for 5-6 times. The enzyme activity was monitored occasionally to confirm stability by taking aliquots and performing the substrate assay.

3.3.3 Calculation of purity percent by ^{1}H-NMR

As a complementary method to analyze purity along with MS (see **Chapter 2**), in some cases purity was also assessed by integration of NMR spectra using the published procedure of Zagorski [159]. Thus, proton-NMR spectra (900 MHz) of purified pools of $A\beta_{42}$ peptides after the RP-HPLC step were obtained in TFA-d solution (0.5 ml). Peaks corresponding to the His-2H, aromatic and αH protons were integrated. Integrals were scaled to the three His-2H protons

at 8.56 ppm and the total α-H protons relative to the His-2H protons were calculated. This value was compared to the theoretical number of α-H protons to determine purity [159]. In the case of $A\beta_{42}$, the total theoretical number of α-Hs were 52 (including Gly (6), β-CH_2-Ser (4)).

3.3.4 Optimized method to remove C-terminal Lys residues

The standard protocol is summarized in **Figure 3-2**. The CPB-agarose column described above was equilibrated to room temperature and washed with at least five column volumes of TBS buffer. HPLC purification pool (adjusted to pH 7.5 in 1X PBS buffer) containing purified Aβ-Lys tail peptide (typically 2-3 mls of ~ 1 mg/ml) was flowed over the column bed at approximately 0.2 ml/min flowrate, adjusting the flow rate with the column stopcock. The column was then washed with 2 ml TBS. One ml fractions from both the peptide load and wash were collected. Fractions were analyzed by LC-MS to identify peptide-containing fractions and confirm complete removal of Lys residues. If Lys removal was found to be incomplete (this only happened with the K_6 tail peptide), the column flow-through was passed through the column again. LC-MS analysis was done to check for the presence of any contaminating enzyme activity. (Commercially available CPB sometimes has contaminating carboxypeptidase A (CPA), trypsin, chymotrypsin activity which would cleave Aβ into impure fragments). Peptide containing fractions were pooled and the pool adjusted to pH 2.0 using formic acid, loaded onto the RP-HPLC column, and re-purified using the standard gradient. Fractions were checked for purity, pooled, and lyophilized. After use, columns were washed with 20% ethanol in TBS and stored at 4 °C.

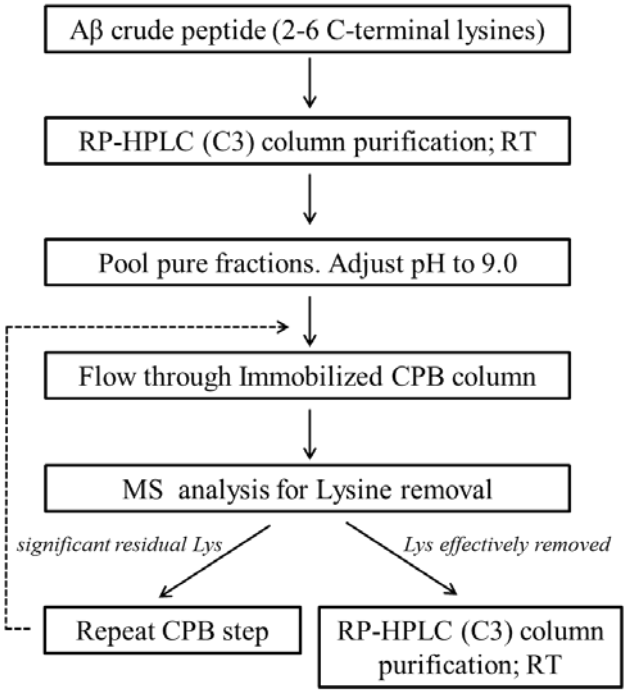

Figure 3-2: Flowchart of the general methodology of Lys removal by immobilized CPB-agarose column

3.4 RESULTS

3.4.1 Optimization of conditions for enzymatic removal of lysines

Using very high density glyoxal beads, we obtained almost 50-60 % immobilization of the CPB used. In our studies, we chose to maximize column loading efficiency, to make sure the lysine removal occurs in the quickest possible manner without any aggregation of the reduced solubility product happening on the beads. We used highly purified CPB obtained from Worthington Biochemical Corporation as we found out that this enzyme had very little activity of other contaminating enzymes (data not shown). The enzyme is pre-treated with a serine protease inhibitor (PMSF) which can inhibit the action of trypsin and chymotrypsin [197]. Immobilized

CPB made with this product was also free of any measureable CPA levels and required no further PMSF treatment over multiple uses of the same column. We also tested for low levels of any contaminating enzyme that might introduce fragmentation by running a 1.0 mg/ml solution of $A\beta_{42}K_3$ peptide onto the column prepared with 2x density of CPB per milliliter of resin, stopping flow for 5 mins, then resuming flow. Analysis of this flow through product showed no contaminating peaks due to contaminating enzymes.

During method optimization, we used the Hip-L-Arg substrate assay to characterize CPB-agarose activity over a broad pH range of 5 - 10 and also a temperature range 4 - 37 °C (data not shown), and determined the best conditions to be pH 9.0 and room temperature (RT). We also found that the covalently immobilized CPB was excellent over a period of 30 days, not exhibiting any detectible loss after storage at 4 °C. We found that CPB activity was unchanged when peptide substrates were dissolved in the HPLC elution buffer (40% acetonitrile v/v in H_2O), after adjusting pH to 9.0. This important result told us that we can remove Lys residues by directly treating the HPLC pool from purification of the Lys-tail peptide. We found that when we used the same column to treat an $A\beta_{42}$ peptide followed by an $A\beta_{46}$ peptide, we did not detect any $A\beta_{42}$ carryover into the $A\beta_{46}$ product. This suggested that even though the peptides we processed were highly hydrophobic, it is possible to use the same column for treatment of different peptides. However, since the columns are inexpensive and simple to prepare, one could eliminate any concern about possible carryover by using a new column packing for each synthesis or each different peptide. In principle, the HPLC purification of peptides after Lys-tail removal may not be required. However, it seemed possible that additional contaminants might be removed by doing this, and recoveries in the second HPLC purification were excellent (**Table**

3-2). Typically we obtained yields for the combined CPB-agarose and subsequent RP-HPLC purification steps of about 75% (**Table 3-2**).

Table 3-2: Recoveries of the peptide $A\beta_{42}$ at each step via $A\beta_{42}K_3$ lysine removal

Step	Step recovery	Cumulative
Reverse phase HPLC (25 °C) purification from crude	10.3 %	10.3 %
Lysine removal by carboxypeptidase B column	79 %	8.1 %
Repeat reverse phase HPLC (25 °C) purification	96 %	7.8 %

3.4.2 Lysine addition to $A\beta_{42}$ improves synthetic efficiency and RP-HPLC purification profile

The goal for adding C-terminal charged residues was to improve solubility of the peptide during purification. To check if Lys addition, improved the chemical synthesis of Fmoc synthesis versions of $A\beta_{42}$ peptides, we looked at the RP-HPLC purification profiles of the crude peptides (**Figure 3-3**).

First, we analyzed the RP-HPLC chromatograms of $A\beta_{42}$ synthesized without C-terminal Lys residues. The RP-HPLC chromatogram of the initial purification of Fmoc-synthesized $A\beta_{42}$ peptides made without any C-terminal Lys residues (**Figure 3-3 A, left panel**) is typical for $A\beta_{42}$ and its analogs synthesized using this method. The A_{214}-monitored chromatogram shows a broad profile with no obvious peak for the desired product.

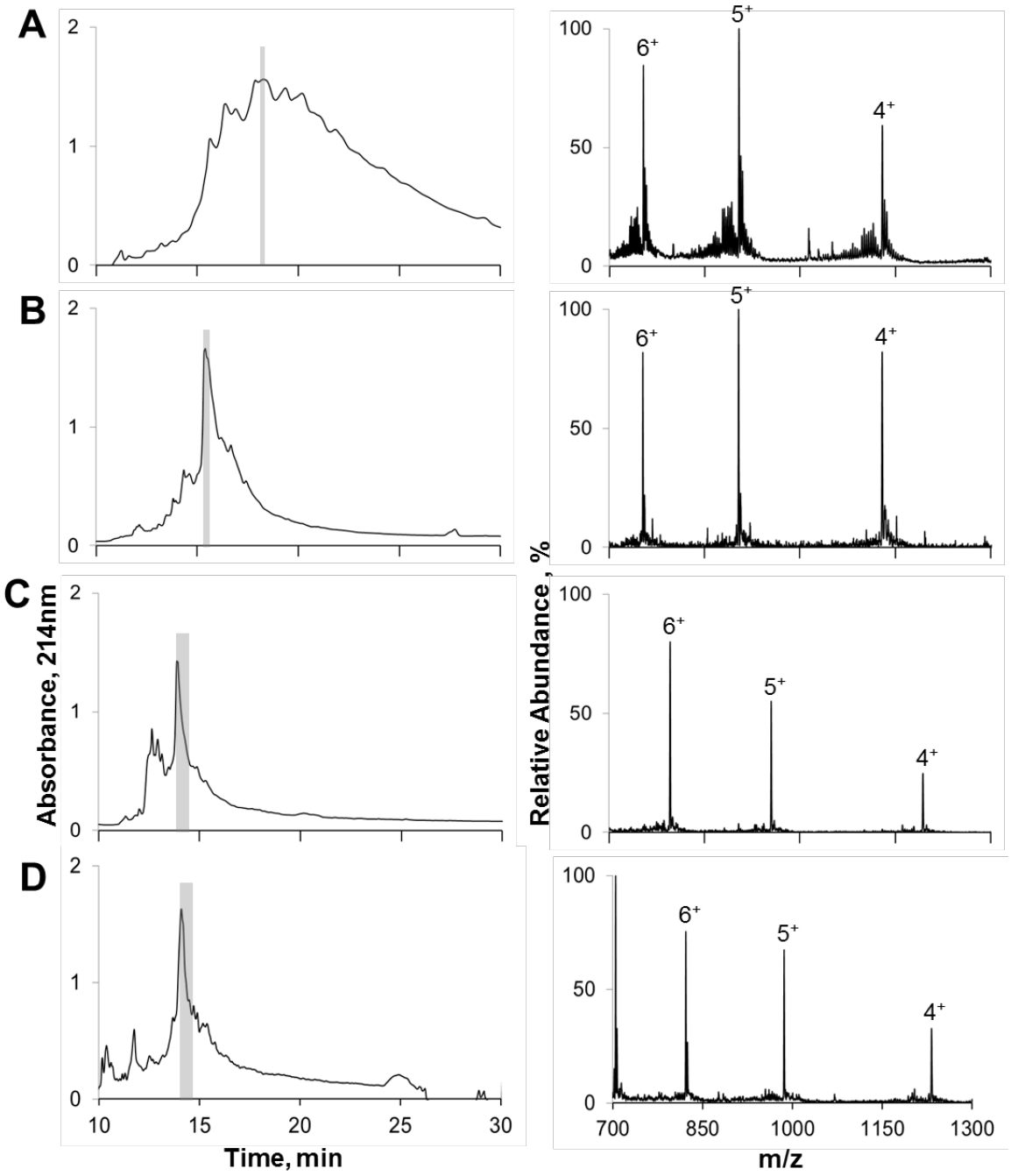

Figure 3-3: Addition of lysines to C-terminus of Aβ$_{42}$ improves reversed phase chromatography purification. RP-HPLC purification profiles of the various crude peptides synthesized using Fmoc chemistry. A) Aβ$_{42}$ at RT column temperature; B) Aβ$_{42}$ at column temperature of 65 °C; C) Aβ$_{42}$-K$_2$ at RT column; and D) Aβ$_{42}$–K$_3$ at RT column. The shaded region represents the fractions which were of highest purity and the electrospray mass spectra of each pool are shown in the corresponding right panel.

MS analysis of the purest fraction revealed a large number of significant small peaks which proves that this sample is highly impure (**Figure 3-3 A; right panel**). By closely examining the m/z peaks of the +5 charge state cluster, we determined that the purest fraction (grey bar) from this purification study was only ~ 65% pure (**Table 3-3**). Many of the major impurity peaks in this fraction correspond to Aβ deletion peptides, mainly due the expected aggregation of the peptide on the resin during synthesis.

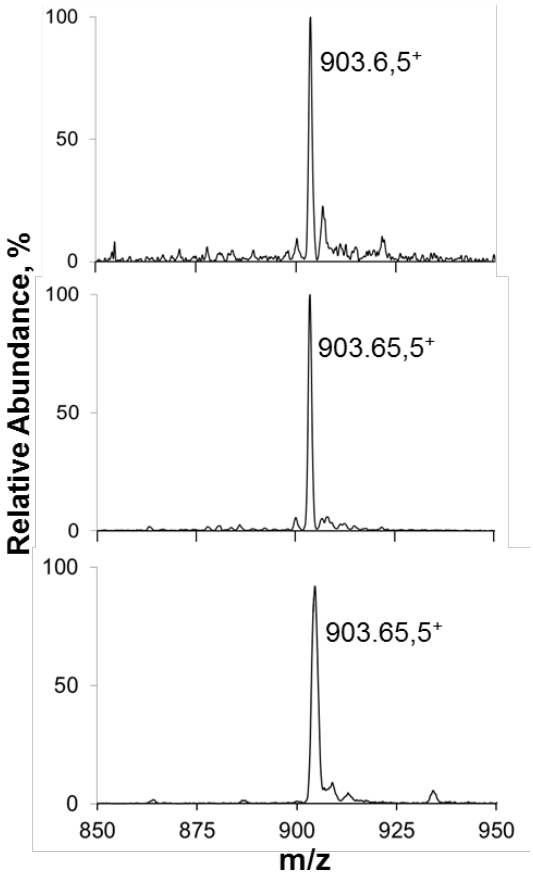

Figure 3-4: Electrospray mass spectrograms of +5 charge state of purified Aβ$_{42}$ peptides.
a) Aβ$_{42}$ synthesized using Fmoc chemistry and purified by 65°C RP-HPLC column; b) Aβ$_{42}$ obtained from Aβ$_{42}$-K$_2$ as described; c) Aβ$_{42}$ obtained by recombinant methods (rPeptide).

The major impurity peaks correspond to losses of single Ala (M_{obs} 4441.7 Da), Gly (M_{obs} 4455.9 Da) or Ser (M_{obs} 4426.5 Da) residues from the wild type Aβ$_{42}$ peptide (M_{obs} 4513.2 Da).

All these impurities co-elute with the pure $A\beta_{42}$ under our 25 °C RP-HPLC conditions. Not only is the purity of the most pure fraction quite low, the amount of authentic wild type Aβ contained in this fraction represents a synthetic yield of only 2.7% (**Table 3-3**). Presumably this yield would drop to lower levels if further purification efforts were undertaken to get the purity to an acceptable level.

In some cases it is possible to improve the purification of synthetic peptides by operating the RP-HPLC column at higher temperatures [198, 199]. Therefore, we subjected the same crude $A\beta_{42}$ peptide reaction product to RP-HPLC chromatography with the column equilibrated to 65° C. The chromatogram obtained (**Figure 3-3 B; left panel**) exhibits a dominant peak, which was confirmed to be $A\beta_{42}$ by MS. The MS spectrum of the purification pool (**Figure 3-3 B, right panel; Figure 3-4 A**) exhibits higher purity (80.6 %) than the 25 °C chromatography fraction (**Table 3-3**). We confirmed this purity level by determining purity using an alternative method, the proton NMR integration method of Zagorski ([159]) This method gave a purity of the 65 °C purified peptide of 82.3 % (**Table 3-3**), in very good agreement with the MS method. The amount of $A\beta_{42}$ in the purified pool corresponds to a synthetic yield of 5.4 %. The purity of ~ 80 % may be sufficient for some studies, but it is not optimal and clearly not as high as the purities of 90-97 % for commercial recombinant $A\beta_{42}$ we determined using the MS (**Figure 3-4 C**) and NMR methods (**Table 3-3**).

We next investigated the degree to which Lys-tails improved the overall quality of the synthetic product, and the percent yields, in $A\beta_{42}$ syntheses. We observed a marked improvement in the chromatographic separations of both $A\beta_{42}$-K_2 (**Figure 3-3 C**) and $A\beta_{42}$-K_3 (**Figure 3-3 D**), each of which exhibited a major peak in the 25 °C HPLC purification, similar to what is observed in the 65 °C purification of the $A\beta_{42}$ product (**Figure 3-3 B**).

Table 3-3: Data summary for Aβ syntheses and aggregation reactions[a]

Final peptide	Initial peptide	Column temp, °C	% purity (MS)	% purity (NMR)	Yield (overall)	Hours to 50% agg.	C_r (μM)
$A\beta_{42}$	$A\beta_{42}$[b]	n/a	96.9	90.0	N/A	6.0	0.07
$A\beta_{42}$	$A\beta_{42}$[c]	n/a	91.5	n.d.	N/A	9.0	0.115
$A\beta_{42}$	$A\beta_{42}$	25	64.9	n.d.	2.7	26	0.24
$A\beta_{42}$	$A\beta_{42}$	65	80.6	82.3	5.4	17	0.16
$A\beta_{42}$	$A\beta_{42}K_2$	25	89.7	n.d.	6.2	n.d.	n.d.
$A\beta_{42}$	$A\beta_{42}K_3$	25	90.2	87.2	7.8	9.5	0.13
$A\beta_{46}$	$A\beta_{46}$	25	69.4	n.d.	1.0	n.d.	n.d.
$A\beta_{46}$	$A\beta_{46}$	65	74.6	n.d.	2.0	n.d.	n.d.
$A\beta_{46}$	$A\beta_{46}K_3$	25	88.4	n.d.	5.6	n.d.	n.d.
$A\beta_{46}$	$A\beta_{46}K_6$	25	91.0	n.d.	4.7	n.d.	n.d.

[a]All peptides from Keck small scale Fmoc synthesis unless otherwise indicated; [b]produced by recombinant DNA expression and purification at rPeptide; [c]from large scale t-Boc synthesis with purification at Keck; n.d. = not determined; n/a = not applicable.

Furthermore, the purities of the peptides purified at 25 °C from the crude reaction mixtures (actually determined after Lys removal; **Figure 3-4 B**) were superior to synthetic $A\beta_{42}$ purified both at 25 °C and at 65 °C (**Table 3-3**). The yields of these Lys-tail peptides in the purified pools were ~ 11 % for both $A\beta_{42}$-K_2 (not shown) and $A\beta_{42}$-K_3 (**Table 3-2**). These substantially higher yields suggest that, as expected, the Lys tails improve not only the purification of the reaction product but also the quality of the product.

3.4.3 Lysine removal using immobilized enzyme

Optimized CPB-agarose conditions (**see 3.3.4**) were used to remove the Lys tails from the $A\beta_{42}$ peptides described above. After Lys removal and re-purification by RP-HPLC, the purities of the final $A\beta_{42}$ products were in the 90% range (**Table 3-3**). This purity level is approaching that of recombinant $A\beta_{42}$ (90% vs. 97% by MS, 87% vs. 90% by NMR; **Table 3-3, Figure 3-4 C**). Furthermore, the final percent yields $A\beta_{42}$ after Lys removal and re-purification by RP-HPLC were in the 6-8 % range, significantly better than the yields obtained for $A\beta_{42}$ synthesized without C-terminal Lys tails (**Table 3-3**). Considering purity as well as synthetic yield, the approach of reversible addition of C-terminal Lys residues followed by 25 °C HPLC purification and CPB removal is even superior to direct synthesis of $A\beta_{42}$ alone followed by 65 °C chromatography (**Table 3-3**).

3.4.4 Lysine addition to the C-terminus of $A\beta_{46}$ peptide

Having validated the reversible Lys-tail method on $A\beta_{42}$, we now turned the method to the peptide $A\beta_{46}$, which is expected to be much more hydrophobic, aggregation prone, and difficult to synthesize and purify due to the added C-terminal Thr-Val-Ile-Val sequence (**Table 3-1**). In fact, we confirmed that conventional methods give very poor yields of this peptide, with poor final purities. The RP-HPLC chromatogram of the purification of the crude Fmoc synthesized $A\beta_{46}$ at 25 °C (**Figure 3-5 A**) exhibits a broad profile with a single fraction containing a small amount of partially pure peptide (**Table 3-3**). The LC-MS spectrum of the purified fraction (not shown) revealed various impurities which co-elute with the pure $A\beta_{46}$ peptide.

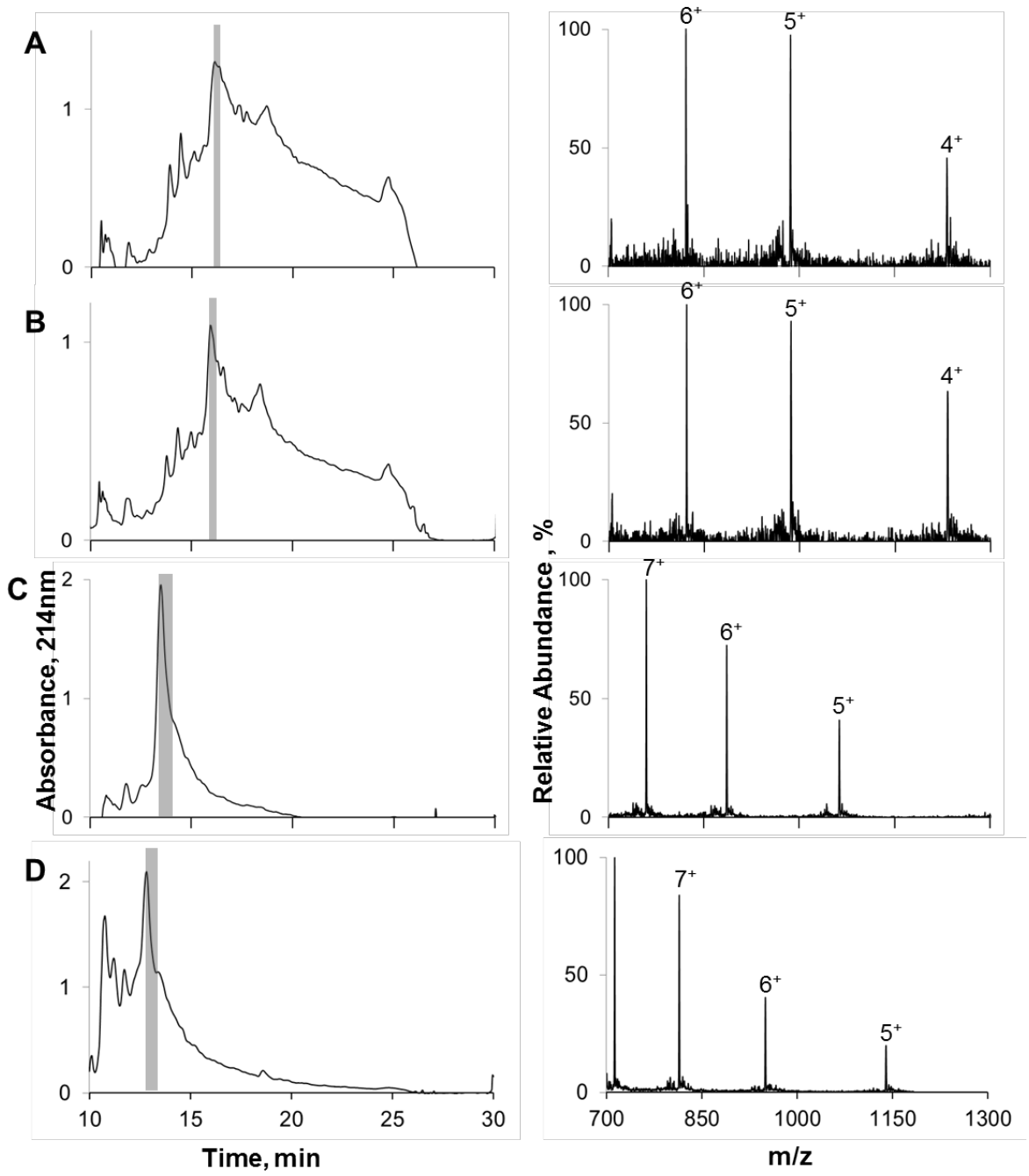

Figure 3-5: Addition of lysines to C-terminus of $A\beta_{46}$ improves synthetic purity.
RP-HPLC purification profiles of the various crude peptides synthesized using Fmoc chemistry. A) Crude $A\beta_{46}$ purified at RT column; B) Crude $A\beta_{46}$ purified at column temperature of 65 °C; C) $A\beta_{46}$-K_3 purified at RT column; and D) $A\beta_{46}$–K_6 purified at RT column. The shaded region represents the fractions which were of highest purity and the electrospray mass spectra of each pool are shown in the corresponding right panel.

The yield (1%) and purity (69%) of $A\beta_{46}$ obtained in this product pool were quite low (**Table 3-3**). Running the purification with a column temperature to 65 °C gave a purified pool with only modest improvements in yield (2 %) and purity (75 %) (**Table 3-3; Figure 3-5 B and Figure 3-6 A**). Hence, as expected from its sequence, the $A\beta_{46}$ peptide behaves more poorly than the $A\beta_{42}$ peptide when directly synthesized by Fmoc chemistry.

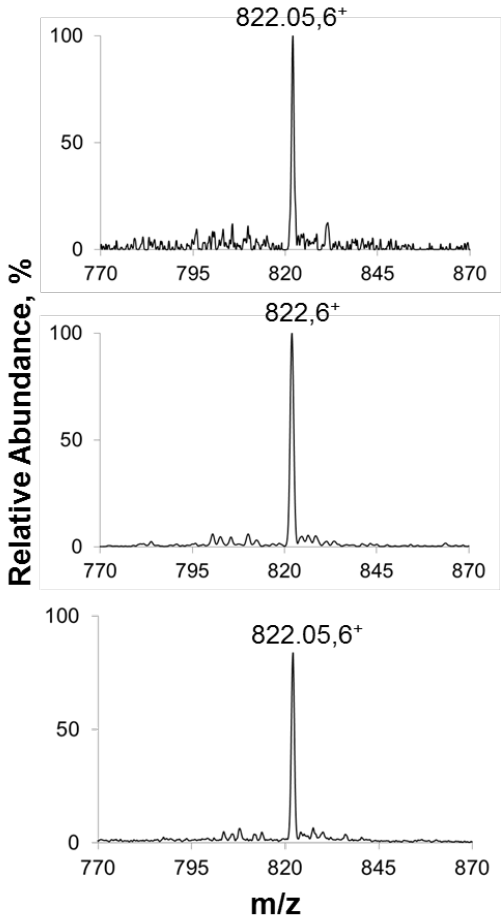

Figure 3-6: Electrospray mass spectrograms of +6 charge state of purified $A\beta_{46}$ peptides.
A) $A\beta_{46}$ synthesized using Fmoc chemistry and purified by 65 °C RP-HPLC column; B) $A\beta_{46}$ obtained from $A\beta_{46}$-K_3 and C) from $A\beta_{46}$-K_6 as described.

We found, however, that addition of C-terminal lysines to the $A\beta_{46}$ peptide afforded a marked improvement in product purity and yield of the Fmoc synthesized peptide. RP-HPLC chromatography of the crude synthetic product of both an $A\beta_{46}$-K_3 and $A\beta_{46}$-K_6 peptide

exhibited dominant product peaks in the RP-HPLC purification, in contrast with the broad, featureless profile of the peptide without added Lys residues (**Figure 3-5**). After removal of C-terminal Lys residues, the final yields of $A\beta_{46}$ were in the range of 4.6 – 5.7 %, and the MS-determined purities were in the range of 88 – 91 % (**Table 3-3**). This is in contrast to yields in the 1 – 2 % range, and purities in the 69 – 75 % range, for $A\beta_{46}$ synthesized without a Lys-tail, even using 65 °C HPLC.

3.4.5 Analysis of source of the benefits of the Lys-tail method

Although the reversible addition of Lys residues was envisioned to mainly provide the benefit of improved chromatographic behavior of the initial synthetic product, we had the impression that there might also be a significant benefit in terms of the initial total synthetic yield. To put this impression on a firm basis, we quantified the contribution of the added Lys residues to both aspects of solid-phase synthesis of $A\beta_{42}$ and $A\beta_{46}$ by carrying out small scale purifications at 65 °C and analyzing the chromatography fractions (**2.1.2**) (**Figure 3-7**). The results clearly show that the addition of C-terminal Lys residues benefits the total synthetic yield and the purification yield separately, by substantial margins in the range of 50% each. For example, while the total amount of $A\beta_{42}$ present in the crude reaction mixture represents about a 15% synthetic yield compared with theoretical, the total amount of $A\beta_{42}$-K_2 corresponds to a 23% synthetic yield. This gives an improvement of about 52% in synthetic yield (**Table 3-4**). Similarly, the added lysine residues clearly aid purification. Thus, based on the total amount of $A\beta_{42}$ generated in the synthesis, only 18.6% of that material is found in the most pure chromatographic fraction in the 65°C "mini-purification" (**Figure 3-7A, left panel**). In contrast, 31.5% of the total available $A\beta_{42}$-K_3 is found in the pool of the highest purity fractions of a similar purification (**Figure 3-7**

B; left panel). This corresponds to a benefit to the efficiency of the purification on the order of about 70% for the Lys tail method (**Table 3-4**). Together these two factors combine to produce a calculated 2.6-fold improvement in isolated yield of purified $A\beta_{42}$, with an improvement in the purity of the pool from 79% to 93%.

A similar analysis shows similar benefits in the preparation of $A\beta_{46}$ (**Figure 3-7 right panels; Table 3-4**). We determined a benefit in synthetic yield of about 63 %, and a benefit in purification yield of 42 %, for a total 2.3-fold improvement in expected yield of purified peptide. The purity of the pool also increased, from 70 % to 91 %.

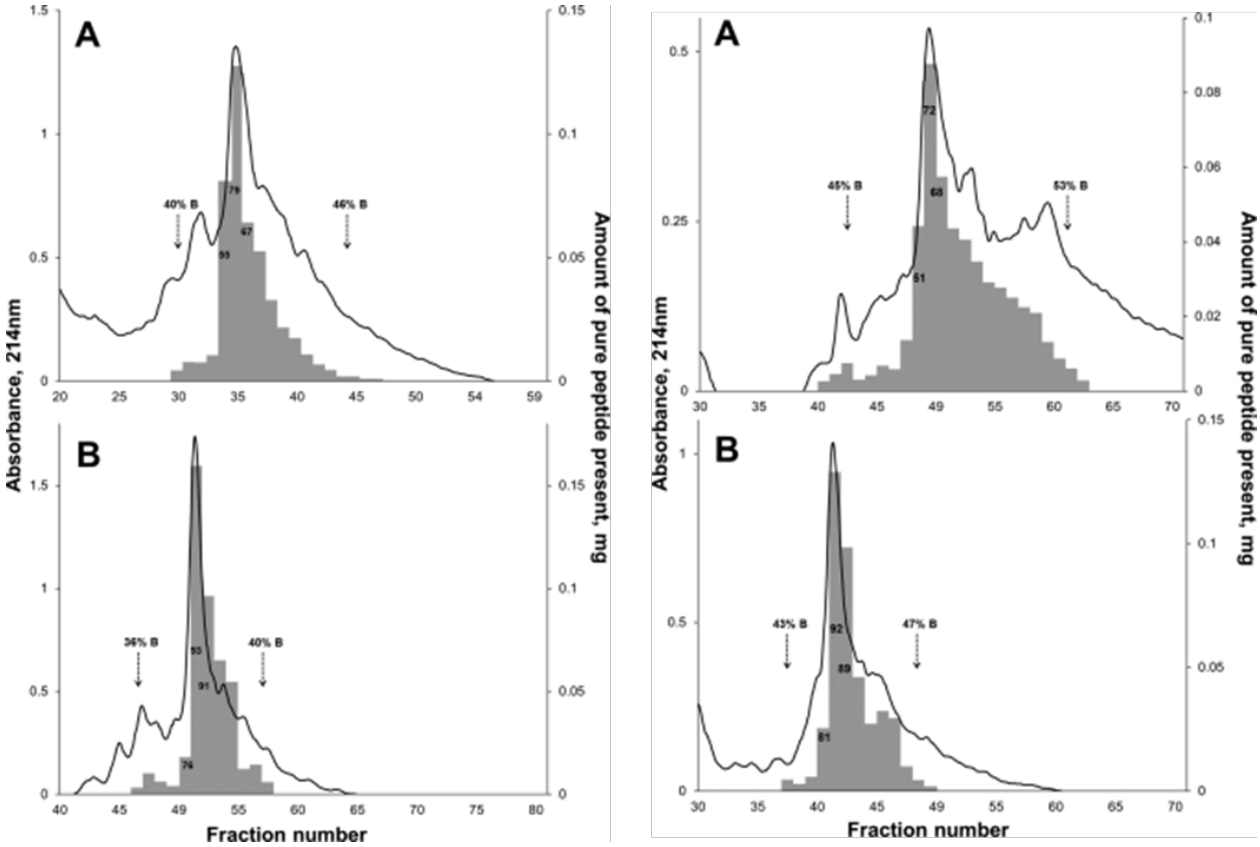

Figure 3-7: Analysis of 65 °C purifications of $A\beta_{42}$ and $A\beta_{46}$ peptides.
Several mg of crude peptides of $A\beta_{42}$ and $A\beta_{46}$ (Panel A; left and right respectively) and $A\beta_{42}$-K_2 and $A\beta_{46}$-K_3 peptides (Panel B; left and right respectively) purified were chromatographed on the preparative column. Total weight of the correct peptide in each fraction is indicated as gray bars superimposed on the A_{214} trace. % purity of the fractions are depicted by the numbers in each bar. Acetonitrile percent is also depicted.

Table 3-4: Relative contributions of approach to improved overall isolated yield of Aβ peptides

Peptide	Total synthetic yield (%)	% Benefit to synthetic yield	Purification efficiency (%)	% Benefit to efficiency	Fold Total improvement	% Purity of pool
$A\beta_{42}$	15.1	n/a	18.6	n/a	n/a	79
$A\beta_{42}$-K_2	23	52.3	31.5	69.4	2.6	93
$A\beta_{46}$	11.5	n/a	18.2	n/a	n/a	70
$A\beta_{46}$-K_3	18.7	62.6	25.9	42.3	2.3	91

3.4.6 Aggregation of $A\beta_{42}$ peptides synthesized by different methods

To assess the effects of the different purification levels of $A\beta_{42}$ peptides on their ability to form amyloid fibrils, we determined the spontaneous aggregation kinetics with disaggregated samples (**Chapter 2**) of various purified $A\beta_{42}$ peptides at 37 °C, pH 7.4. The reactions were carried out at a starting monomer concentration of 10 μM and the kinetics of aggregation were determined by measuring soluble monomer levels at various time points using HPLC. We found that recombinant $A\beta_{42}$ peptide obtained from rPeptide was the fastest aggregating peptide (**Figure 3-8 A**), exhibiting a time to 50% aggregation of 6 hrs (**Table 3-3**). The next fastest to aggregate version of $A\beta_{42}$ was a sample produced by t-Boc chemistry and purified by undisclosed methods at the Keck Center via their "large scale synthesis" option. This peptide, which exhibited 91.5% purity according to our own MS-based analysis (**Table 3-3**), had a $t_{½}$ of 9 hrs. (This peptide is shown simply for comparison; we do not know what special measures might have been taken in synthesis or in purification to achieve this product quality.) We found that the F-moc synthesized peptides described here aggregated at somewhat lower rates, with half-times of aggregation

inversely proportional to their purity levels. Thus, $A\beta_{42}$ obtained via $A\beta_{42}$-K_3, at 90% purity, exhibited a half-time of aggregation of 9.5 hrs (note the similarity in parameters to the t-Boc material). $A\beta_{42}$ synthesized directly and purified at 65 °C, which had a purity of 81%, showed a half-time of aggregation of 17 hrs, and directly synthesized $A\beta_{42}$ purified at 25 °C, with a 65 % purity, gave a half-time of aggregation of 26 hrs (**Table 3-3**).

The source of this variation in $t_{½}$ values is not totally clear. Since the reactions were set up at 10 μM by assuming the entire $A\beta_{42}$ peak to be authentic Aβ, some of the drop in aggregation rate with decreasing purity levels could be due to a lower starting concentration of authentic $A\beta_{42}$. Thus, in another study, the $t_{½}$ for 10 μM $A\beta_{42}$ was found to be 6.5 hrs, while the $t_{½}$ for 5 μM $A\beta_{42}$ was found to be 25 hrs; it is noted that the actual concentration of WT $A\beta_{42}$ in the sample purified at 25 °C from conventionally synthesized product would have been only 6.7 μM in the **Figure 3-8A** comparison. If all the increase in aggregation time were due to reduced WT $A\beta_{42}$ concentration, it would imply that the contaminating Aβ peptides are neutral in the aggregation process, neither contributing to it nor inhibiting it. If only part of the increase in aggregation time is due to lower starting $A\beta_{42}$ concentration, then one or more of the Aβ peptide impurities might be actually inhibiting aggregation.

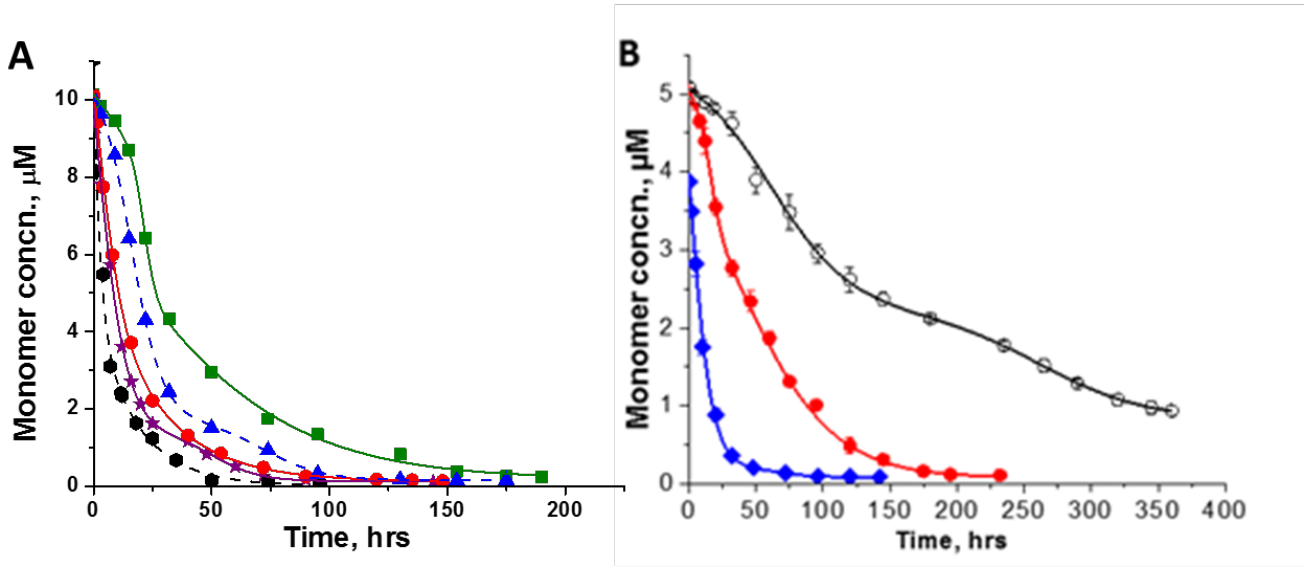

Figure 3-8: Aggregation kinetics of various Aβ derivatives.
A) $A\beta_{42}$ aggregation kinetics comparison obtained from various sources: $A\beta_{42}$ from rPeptide (♦);$A\beta_{42}$ from t-Boc synthesis (★); $A\beta_{42}$-K_3 after lysine removal $A\beta_{42}$ from $A\beta_{42}$-K_3 after lysine removal (●); $A\beta_{42}$ synthesized as $A\beta_{42}$ and purified at 65 °C (▲) or RT (■); B) Aggregation kinetics comparison of $A\beta_{46}$ (from $A\beta_{46}$–K_6) (♦); $A\beta_{42}$ (from $A\beta_{42}$–K_3) (●); and $A\beta_{40}$ (○). Fits of the actual data points were done for visual representation purposes only

Another measure of the quality of a non-covalent aggregation product, such as the $A\beta_{42}$ fibrils produced here, is the concentration of the monomer at equilibrium, which reflects the thermodynamic stability of the amyloid fibril with respect to monomer [149]. We monitored the $A\beta_{42}$ aggregation reactions until the amount of monomer in the supernatant, after centrifugation, did not change. We found that apparently the most stable amyloid is assembled from the recombinant material, giving a final monomer concentration of 0.07 μM (**Table 3-3)**. In contrast, other $A\beta_{42}$ peptides gave final monomer concentrations proportional to the purity of the starting peptide (produced *via* $A\beta_{42}$-K_3, 0.13 μM; *via* 65 °C purification of directly synthesized $A\beta_{42}$, 0.16 μM; *via* 25 °C purification of directly synthesized $A\beta_{42}$, 0.24 μM). The elevated final concentrations of amyloid assembly reactions from impure $A\beta_{42}$ could be a reflection of less stable fibrils from occasional incorporation of $A\beta_{42}$–related impurities, or due to the presence in

the monomer pool of $A\beta_{42}$–related impurities that are incapable of assembling into fibrils, or to a combination of these effects. However, it is clear that a large portion of the $A\beta_{42}$-related impurities, for example in the material that is only 65% pure, must be incorporated into amyloid fibrils along with the authentic $A\beta_{42}$, otherwise the final monomer concentration would be much higher than 0.24 μM (**Table 3-3**).

We also analyzed the samples from the various aggregation reactions of synthetic and recombinant $A\beta_{42}$ peptides by negative-stain electron microscopy. Fibrils formed from recombinant $A\beta_{42}$ (**Figure 3-9 C**) showed a more homogeneous morphology than fibrils formed from synthetic Fmoc $A\beta_{42}$ obtained after HPLC purification (**Figure 3-9 A,B**). These less homogeneous aggregates appear to have protofibrils/oligomers along with the mature fibrils in the EM images (**Figure 3-9 A,B**). These might represent the aggregates obtained from the significant amount of impurities present in these samples or the 'off-pathway' intermediates obtained by the incorporation of the impurities into authentic $A\beta_{42}$ aggregates. $A\beta_{42}$ aggregates obtained from Lys-removal do not have these dead-end intermediate products and have similar morphology to recombinant $A\beta_{42}$ (**Figure 3-9 D**).

3.4.7 Amyloid formation by different Aβ peptide variants

We compared the spontaneous aggregation of the two dominant Aβ species in the human brain, $A\beta_{40}$ and $A\beta_{42}$, with the behavior of the relatively rare variant, $A\beta_{46}$, whose synthesis is described here. All peptides were highly pure chemically synthesized material. We found that a 5 μM starting concentration of $A\beta_{46}$ monomers aggregates with a time to 50% aggregation of 9 hrs, compared with 32 hrs for a 4 μM solution of $A\beta_{42}$ (**Figure 3-8 B**). By comparison, a 10 μM

solution of $A\beta_{40}$ requires 100 hrs to reach 50% aggregation. Thus, the additional hydrophobic residues at the C-terminus of $A\beta_{46}$ appear to enhance spontaneous aggregation compared with shorter Aβ variants.

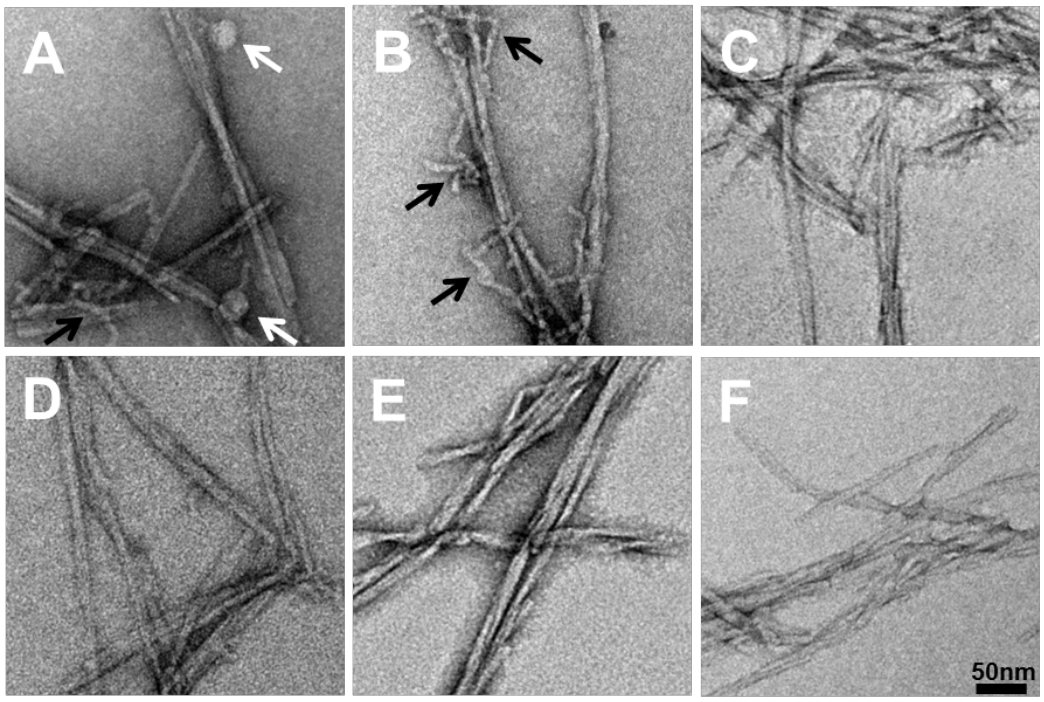

Figure 3-9: Electron microscopy analysis of various Aβ amyloid fibrils collected at the end of the aggregation reaction.

Aggregates of $A\beta_{42}$ (a) synthesized as $A\beta_{42}$ and purified at RT; (b) synthesized as $A\beta_{42}$ and purified at 65 °C; (c) synthesized by recombinant means; (d) synthesized as $A\beta_{42}$-K_3 and processed as described. Amyloid fibrils from (e) $A\beta_{40}$ obtained purified from the Keck Biotechnology Center; (f) $A\beta_{46}$ synthesized as $A\beta_{46}$-K_3 and processed as described here.

Electron micrographs of the product fibrils ($A\beta_{40}$, **Figure 3-9 E**; $A\beta_{42}$, **Figure 3-9 D**; Aβ46, **Figure 3-9 F**) show them in each case to be uniform in morphology with no non-fibrillar aggregates present. FTIR spectra show the previously described doublet in the portion of the spectrum assigned to β-sheet for $A\beta_{40}$ fibrils grown under quiescent conditions [125], while the $A\beta_{42}$ and $A\beta_{46}$ fibrils exhibit similar spectra with only a single absorption peak in this region (**Figure 3-10**).

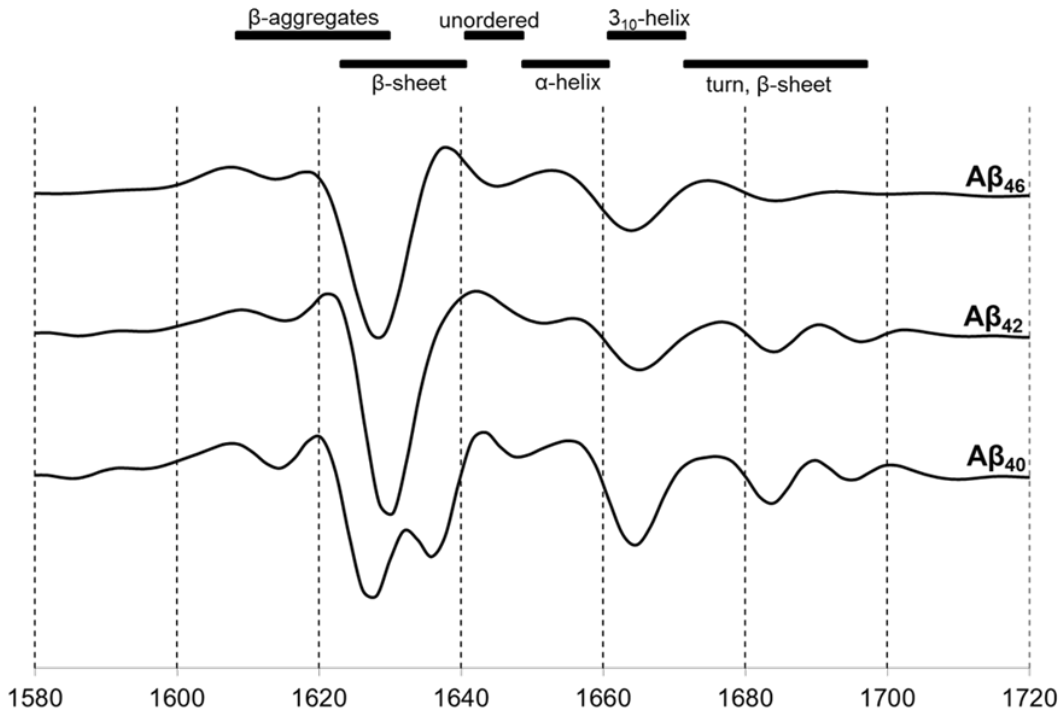

Figure 3-10: FTIR spectroscopy of the various Aβ amyloid fibrils.

3.5 DISCUSSION

One of the major problems involving in vitro Aβ research has been difficult to reproduce results on the aggregation of Aβ peptides. One of the possible explanations for this could be the difference in the general chemical purity of these synthetic peptides which are tough to synthesize and purify. Other reasons could be the presence of low but significant levels of backbone α-C-H epimerization during synthesis [173], whether or not efficient disaggregation procedures are used, and if so, which one was used, and the types of assays used to monitor aggregation kinetics and analyze aggregate morphology. Our lab had been systematically evaluating some of these variable parameters and tried to answer few questions. In this chapter,

we deal with improving the levels of purity in synthetic Aβ peptides generated from Fmoc synthesis and how to improve them.

A recent literature work on designing a synthetic strategy included inserting methionine sulfoxide into the growing Aβ chain at Met_{35} to provide improved solution properties [190]. This helps in reducing the hydrophobicity of the C-terminal part of the molecule. After purification of the synthetic product, the methionine sulfoxide was reduced back to Met. Another way to improve the solution properties of hydrophobic peptides is to append cationic tails to their N- or C-termini [200]. This general phenomenon has been exploited by our lab previously to design peptides related to HD, for example huntingtin exon 1 peptides and simple polyQ peptides by adding lysine residues to its C-termini. Here, we worked on an alternative method for reversible addition of a cationic charged residues in which only peptide bonds are used in the chemical synthesis, and this cationic tail is later removed enzymatically after synthesis. This method was inspired by recognition of the potential effectiveness of highly specific removal of cationic amino acids by the C-terminal endoproteinase CPB in a previously described robust enzyme model system for converting pro-insulin to insulin [201, 202].

In this Chapter, we show that an immobilized CPB column support is simple and inexpensive to prepare, stable over a period of multiple runs, and is simple to use in removing multiple Lys groups from the C-termini of Aβ peptides. CPB of sufficient purity is commercially available (through Worthington Biochemical Corporation) so that undesired further cleavage within the desired peptide product can be avoided. The general utility of our method remains to be seen for many other hydrophobic peptides. Some peptides may possess tertiary or self-assembled structure at the C-terminus which could impair CPB cleavage. However, in this regard the Aβ model system is a good test, since the highly hydrophobic,

oligomerization-prone Aβ is processed cleanly in our tests. Perhaps the acetonitrile component of the cleavage buffer (i.e., the HPLC elution buffer) helps prevent the formation of inhibitory structures.

We show here that the Fmoc synthetic yields and purities of Aβ peptides are improved by the reversible addition of Lys-tails during solid phase synthesis. This improvement is especially notable if 65 °C HPLC is not possible. The yield of $A\beta_{42}$ increased from 2.7 % to 7.8 %, and peptide purity increased from 65% to 90%, with the CPB-reversible addition of three C-terminal Lys residues during synthesis (**Table 3-3**). We also found that spontaneous amyloid formation kinetics trend with the purities of these $A\beta_{42}$ preparations, with the product of the synthesis *via* a Lys-tail aggregating considerably faster than the $A\beta_{42}$ synthesized directly and purified at 25 °C (**Figure 3-8A**). Interestingly, the best quality chemically synthesized $A\beta_{42}$ peptide from Lys removal aggregates nearly as fast as recombinant $A\beta_{42}$, showing that chemically synthesized and recombinant Aβ peptides are not always significantly different in their aggregation behavior if it is possible to obtain high quality synthetic material to start with.

It is well known that multiple C-termini of Aβ peptides are generated in the AD brain, some of which owe to an apparent processive action of γ-secretase on cleavage of APP [45]. One of the cleavages releases $A\beta_{46}$. It has been speculated that some presenilin FAD mutations may work by shifting the balance of Aβ peptide products to longer, more aggregation-prone versions of Aβ [203]. It has also been reported that some γ-secretase inhibitors, in blocking the formation of $A\beta_{40/42}$ peptides, result in the accumulation of intracellular $A\beta_{46}$ peptide [204]. It is therefore of considerable interest how the aggregation kinetics and morphologies of $A\beta_{46}$ and other "minor" Aβ species might differ from those of $A\beta_{42}$. A preliminary report on the aggregation of chemically synthesized $A\beta_{46}$ focused on possible cross-seeding activity, but did not

quantitatively compare individual aggregation tendencies or describe the quality of the synthetic peptides used. In the studies reported here, we focus on ensuring the purity of the $A\beta_{46}$ used, and in making direct comparisons of the aggregation kinetics and aggregate structure of $A\beta_{46}$ compared with $A\beta_{40}$ and $A\beta_{42}$.

$A\beta_{46}$ peptide has a more hydrophobic C-terminus due to the addition of the TVIV sequence to $A\beta_{42}$ (**Table 3-1**). Ile and Val are both particularly problematic for formation of β-sheet-containing aggregates (in solution and during solid phase synthesis) because of their β-branched side chains that are especially prone to β-sheet formation [205]. Hence, it was expected to behave even more poorly under standard chemical synthesis conditions than $A\beta_{42}$, as we found (**Table 3-3**). HPLC purification of $A\beta_{46}$ directly synthesized by Fmoc solid phase synthesis gave a yield of 1 % at 25 °C and 2 % at 65 °C, and purities in the 69 – 75% range (**Table 3-3**). In contrast, synthesis of $A\beta_{46}$ via the intermediate Lys-tail product gave yields in the 4.7 – 5.5% range and purities in the 88 – 91% range (**Table 3-3**). It is shown that Lys-tail addition improves the quality of the synthesis as well as the ease and effectiveness of purification. The experiments done in **Figure 3-7** and summarized in **Table 3-4** indicate that our method provides benefits for both synthetic yield and purification yield. As expected, addition of lysines narrows the elution profile of the desired product (**Figure 3-7**) and surprisingly also clearly improves the synthetic yield (**Table 3-4**).

In contrast to the experience with directly synthesized peptides, using the CPB-reversible Lys-tail method we experienced no drop-off in yield or purity attained in going from $A\beta_{42}$ to $A\beta_{46}$. This suggests that this method should be capable of making even longer Aβ peptides as well as other highly hydrophobic peptides.

Using this highly pure material, we found that $A\beta_{46}$ undergoes spontaneous amyloid formation significantly more rapidly than either $A\beta_{42}$ or $A\beta_{40}$ (**Figure 3-8 B**). The fibrils appeared similar to those of $A\beta_{42}$ in both EM morphology (**Figure 3-9**) and FTIR spectroscopy (**Figure 3-10**). We did not explore the ability of $A\beta_{46}$ to make oligomers. Our results are consistent with the possibility that $A\beta_{46}$, in spite of being present in relatively low amounts in the brain, may have a disproportionate impact on amyloid burden or other aggregation-associated events and could potentially act as a seed for other Aβ isoforms.

The use of efficient recombinant synthesis methods for preparing high quality peptides and proteins introduced a major alternative to traditional methods of peptide synthesis for producing molecules for biophysical and biological studies [206]. At the same time, chemical methods capable of producing high quality peptide material continue to have a major role to play. For example, chemical methods can generally more easily be used to prepare proteins containing unnatural amino acids and specifically isotopically labeled amino acids. At least for chemically oriented peptide labs, chemical synthesis can be a more straightforward, less labor intensive way to conduct a preliminary investigation on a new peptide sequence. We described here a general method for greatly improving the synthetic yield and quality of chemically synthesized, highly hydrophobic and amyloidogenic peptides. Using this method, we obtain purities and performance in in vitro amyloid growth assays that are quite similar to those from the recombinant version of the same molecule. We also show, however, that all chemical syntheses are not equivalent, and that rigorous methods of synthesis and analysis have important roles to generating quality molecules and quality data from those molecules.

4.0 IMPORTANCE OF DISAGGREGATION PROTOCOL IN $A\beta_{42}$ AGGREGATION

[In this chapter, I had help from R.K. in the collection of TEM, FTIR and SEC monomer-oligomer mixing experiment]

4.1 OVERVIEW

It is known that in vitro studies on amyloid peptides can be compromised if small but functionally important levels of pre-existing aggregates are present at the start of the reaction. Hence various disaggregation protocols have been developed by different groups to achieve some degree of control and reproducibility of in vitro studies. Here in this Chapter, we looked at the importance of choosing the right protocol when studying $A\beta_{42}$ peptide aggregation. Chemically synthesized $A\beta_{42}$ peptide was disaggregated *via* two procedures: a chemical disaggregation protocol of sequential treatment of TFA and HFIP; and disaggregation *via* solubilization in Gdn-HCl solution followed by monomer elution in native size exclusion chromatography. The secondary structures of $A\beta_{42}$ aggregates prepared via two different disaggregation protocols have been investigated via hydrogen-deuterium exchange mass spectrometry and compared to data obtained under similar conditions for $A\beta_{40}$. In the case of $A\beta_{42}$ aggregates prepared *via* chemical disaggregation, the structure of the final product was

dependent on the starting monomer concentration of the reaction. The reactions kept at higher concentrations never matured to form a uniform population of fibrils at the end of the reaction, as monitored by EM. This was confirmed in the HX-MS experiments where final aggregates exhibited a population with intermediate protection identical to that of protofibrils. Hence, at least with Aβ, disaggregation reaction conditions can be of critical importance in in vitro aggregation results. Conclusions drawn from experiments performed using monomer preparations obtained under different disaggregation conditions can vary significantly, not only from each other but also from the behavior of Aβ in the AD brain.

4.2 BACKGROUND

4.2.1 Summary of disaggregation protocols used on Aβ peptides

Various methods have been developed to disaggregate chemically synthesized Aβ peptides to obtain monomers, and each method has its own advantages and disadvantages. One of the first methods described was from the Lansbury lab, the first group to report on the need for disaggregation. They dissolved synthetic Aβ in DMSO, sonicated and filtered, then diluted the DMSO solution into buffer (unfortunately leaving ~ 5% DMSO as part of the buffer, with unclear consequences to the aggregation results) [94, 141]. Our group published a protocol relying on HFIP solubilization, followed by evaporation and suspension of the residue in buffer [142, 207]. Variations on these DMSO and HFIP methods continue to be used. Later, we adopted the method of Zagorski [159], in which peptide was first solubilized using TFA, and the residual TFA after evaporation was removed by HFIP evaporation [208]. The function of HFIP

was originally thought to facilitate the removal of TFA, although it was shown to have some ability to break down aggregates [207]. Other disaggregation methods introduced later include (a) brief exposure of lyophilized Aβ to strong acids or bases, followed by rapid neutralization [209]; (b) ultracentrifugation of aqueous solutions [210], (c) filtration through low-molecular weight cut off filters [211]; (c) density gradient centrifugation [212]; (d) size exclusion chromatography [95, 96, 143]. All of these techniques have been used to prepare soluble Aβ but yield preparations that vary in size and morphology. In any case, the decision to skip the disaggregation step might lead to incorrect results. The presence of any unwanted aggregate seed in the peptide solution might self-propagate and therefore influence reaction kinetics and mechanism as well as determine the final structure of the aggregated product.

In our lab, it was later found out that a 1:1 mixture of TFA and HFIP had superior disaggregation properties to TFA alone in the case of longer polyQ sequences [208]. Other parameters like incubation time and centrifugation speed can alter the properties of the starting material. A measure of the technique could be determined by measuring the lag phase of the reaction. Also when working with volatile organic solvents, it is important to completely remove the solvents before the start of the reaction. This is because buffers containing even low percentage of HFIP can radically alter the aggregation pathway of amyloidogenic peptides [113]. The protocol described in **2.1.3** gave us the best possible conditions for dissolution of chemically synthesized $A\beta_{40}$ peptides.

4.2.2 Previous unpublished results from the lab on $A\beta_{42}$ peptide aggregation

The lab has historically worked with $A\beta_{40}$ peptide and its mutants and looked at their in vitro aggregation properties. $A\beta_{40}$ is the predominant species in the AD brain, and is also one of the more well-behaved Aβ molecules to work with, so many labs, including ours, did initial work in the 1990s studying $A\beta_{40}$. However, more recently work in the field has focused on the $A\beta_{42}$ molecule based on its stronger association with disease pathology. Our lab initiated studies on $A\beta_{42}$ in the early 2000s, when I.K., fresh from her successful characterization of $A\beta_{40}$ amyloid fibrils by HX-MS, moved to $A\beta_{42}$ fibrils. Her initial studies provided confusing results, however, in that the $A\beta_{42}$ aggregation product, which appeared to be uniformly fibrillar by EM, exhibited fewer protective backbone H-bonds than $A\beta_{40}$ fibrils, in spite of $A\beta_{42}$ being faster to aggregate and giving more stable aggregates. I.K. used the lab's standard protocol (**2.1.3**) [123], used routinely and highly successfully to work with $A\beta_{40}$, to disaggregate the $A\beta_{42}$. The protocol utilizes sequential transient treatment with TFA and HFIP followed by ultracentrifugation in aqueous solution [123].

Later, post-doc D.K. took over this project, continuing to use the TFA/HFIP protocol. He found that much of the peptide was being lost in the overnight centrifugation step (after dissolving the Aβ film in aqueous buffer), so the centrifuge time was reduced to 1 hr. Even with a 1 hr spin, however, ~ 50 % of the peptide was routinely lost in the form of aggregated pellet in this protocol. Aggregates made from the disaggregated monomer at a normal starting concentration of around 10 μM exhibited the same diminished protection, compared with $A\beta_{40}$ amyloid, as seen by I.K. Interestingly, the weight-normalized ThT value of the final aggregate was also significantly lower than that of $A\beta_{40}$ fibrils. This suggested that, in spite of the absence

of visible oligomers in the EM, the $A\beta_{42}$ product might actually represent an incomplete fibril formation reaction that also contains some unusually stable intermediates with low ThT signals. D.K. began to explore this hypothesis, first by conducting $A\beta_{42}$ assembly reactions at different starting concentrations. In one experiment he compared starting concentrations of 0.8 μM and 6 μM. He found that the 6 μM reaction proceeded faster, but that the final aggregation product had a substantially lower weight-normalized ThT value than the product of the 0.8 μM reaction, consistent with the hypothesis.

To further probe the hypothesis, D.K. studied the products by HX-MS (**Figure 4-1**). He found that the resulting ESI-MS +6 spectral envelopes showed striking differences. In particular, the 6 μM product exhibited a single, very broad peak for protected $A\beta_{42}$ with a centroid for at *m/z* ~ 756.5, similar to that observed by I.K. In contrast, the 0.8 μM product showed a centroid at ~ 755.5, a lower mass indicating fewer deuteriums had exchanged into the peptide. In order to understand these data, D.K. did a curve fitting analysis by assuming there are three species of Aβ present: (a) fully exchanged peptide (at ~ 759.2; see below); (b) maximally protected peptide (at ~ 755.5; this is due to mature amyloid fibrils); and (c) peptide with intermediate protection levels (at ~ 757.5; this seemed likely to be due to some other type of aggregate with fewer backbone H-bonds). The curve fitting supported this model and showed that, in agreement with the hypothesis based on ThT data, the aggregated product from the 6 μM reaction contains essentially a 50:50 mixture of two kinds of aggregates with different numbers of protected amide protons, yielding, in the HX-MS, a very broad peak with a centroid in between that of fibrils and the other aggregates. In contrast, the 0.8 μM material contained mostly mature amyloid and little of the other aggregate.

These initial results for fibrils obtained from the 6 μM (**Figure 4-1 A**) thus clearly showed three distinct amounts of deuterium incorporation, hence three different patterns of protection showing at least two discrete aggregate conformations. The lowest *m/z* peak is attributed to the mature fibrils formed from $A\beta_{42}$. The highest *m/z* peak was also seen previously in $A\beta_{40}$ aggregates [150] which is attributed to exchange of monomers that are in equilibrium with the fibrillar aggregates and/or that dissociate, becomes fully exchanged, and reassociate with the fibrillar aggregates. The amount of protection in the intermediate *m/z* peak corresponds well with the amount of backbone amide protection found in $A\beta_{40}$ protofibrils [108]. This suggested that D.K. was observing, with $A\beta_{42}$, some kind of concentration dependent formation of a protofibrillar population that was incapable of maturing into more protected amyloid fibrils. EM analysis, however, failed to convincingly demonstrate the presence of such protofibrils. Nothing like this striking concentration dependent phenomenon had been previously reported for $A\beta_{42}$ or indeed any amyloid system. Especially given the potential importance of these protofibrillar intermediates, we decided to further characterize this effect.

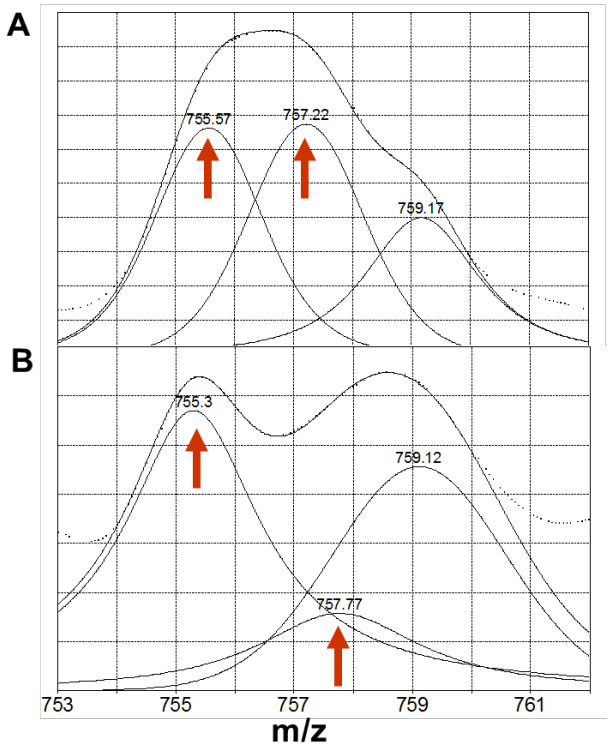

Figure 4-1: HX-MS analysis of Aβ$_{42}$ aggregates prepared from TFA-HFIP method
ESI-MS of deuterated Aβ$_{42}$ +6 charge states of mature fibrils obtained from initial monomer concentrations of A) 6.0 μM and B) 0.80 μM (D.K., unpublished data).

4.2.3 Use of size exclusion chromatography to obtain monomeric Aβ

SEC, in particular, offers several advantages for Aβ disaggregation. There are a variety of column matrices available with different separation capacities and can be used in isolation or in combination with other columns to obtain high-resolution separation and fractionation of Aβ aggregates of defined size distribution. One of other advantages of using an SEC column for disaggregation is that the columns are equipped with filters at the top that allow for the removal of insoluble (fibrillar) material from the injected sample, thus ensuring that the Aβ fractions obtained are free of any fibrillar seeds. The technique also offers the ease in accurate determination of aggregates size distribution when the SEC is coupled to a light-scattering

detector. SEC can also be used as a valuable tool to monitor early events in amyloid formation and quantification of monomer loss during the time course of fibril formation. The method also gives an inherent advantage that the Aβ peptide eluting at the position of monomer is immediately obtained in suitable solution conditions for aggregation reactions and is free of harmful or undesired substances like organic solvents, etc. SEC has also been successfully used to isolate Aβ oligomers and high-molecular-weight aggregates (including protofibrils and amorphous aggregates) from complex cell culture media or from AD brain extracts [213]. Compared with other disaggregation methods, SEC also gives the advantage of a potentially greater recovery of the injected sample which is especially useful in the Aβ research because of the inherent cost in producing chemically synthesized peptides. However, strong non-specific adsorption of hydrophobic peptides (such as Aβ) to the column matrix might result in some loss in the yield of purified material. Weaker adsorption might not prevent elution entirely but delay it, so that some aggregates might elute as apparently lower molecular weight species. This is a potential problem both in analytical analysis and in isolation of disaggregated monomers, and so care must be taken in isolating the monomers from the oligomer pool. One of the drawbacks of this technique is that the sample can become significantly diluted compared to the load. This means that significant amounts of peptide must be devoted to the disaggregation in order to obtain eluates of sufficient concentration and, furthermore, that there are difficulties in obtaining very high concentrations of monomer. In spite of the disadvantages, disaggregation by SEC [143] has a number of potentially powerful advantages and in many ways is perhaps the most rigorous disaggregation method available.

4.2.4 FTIR of HFIP films

To analyze the ordered structure of Aβ peptides present during HFIP treatment, we used a modification of the FTIR procedure described in **2.4.2** . After the $A\beta_{40}$ and $A\beta_{42}$ peptides were disaggregated by sequential treatment in TFA and HFIP (**2.1.3**), the peptide film obtained after the lyophilization step was immediately redissolved in HFIP and dried directly on the FTIR cell. FTIR experiment was done as previously described (**2.4.2**) and the primary spectra were analyzed.

4.3 RESULTS

4.3.1 Concentration dependence of $A\beta_{42}$ aggregation using TFA-HFIP disaggregation

To further investigate the preliminary results obtained in the lab on $A\beta_{42}$ aggregation (D.K.), $A\beta_{42}$ peptide was disaggregated using the chemical disaggregation method of sequential treatment with TFA and HFIP followed by resuspension in aqueous buffer and ultracentrifugation, and a series of aggregation reactions were initiated to look for the effect of initial monomer concentration on $A\beta_{42}$ aggregation behavior (Figure 4-2).

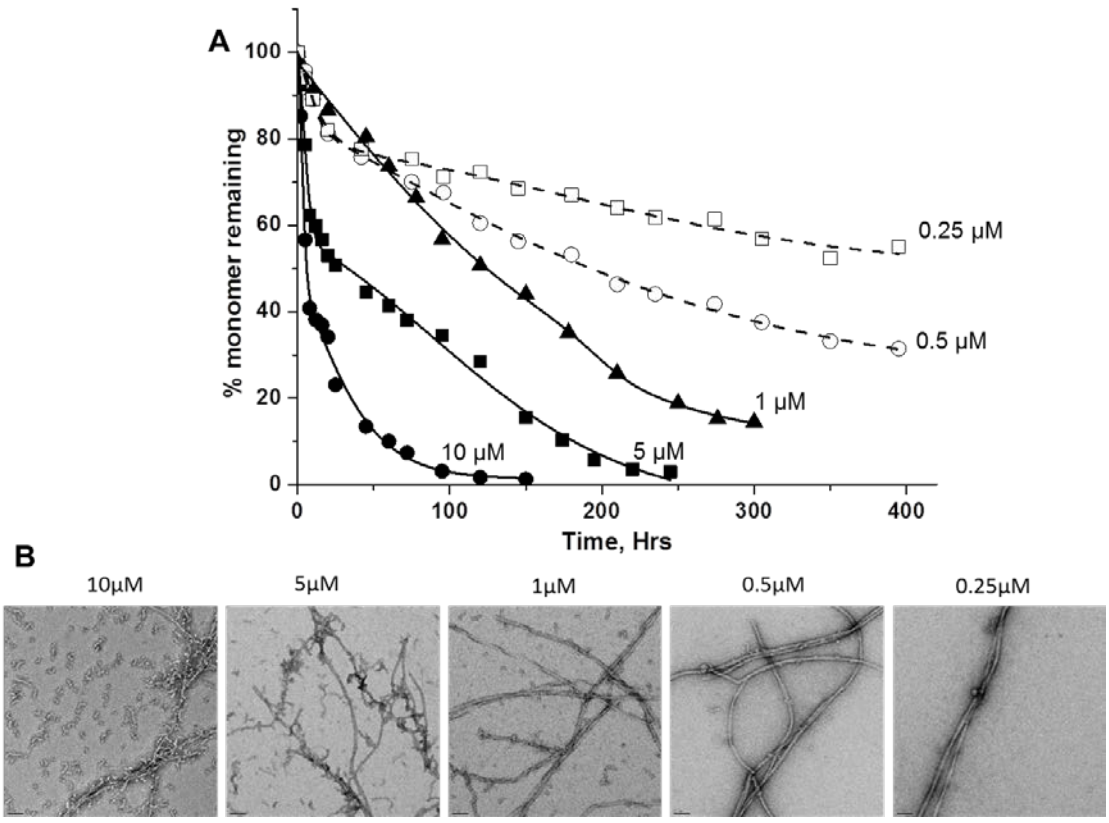

Figure 4-2: Aggregation of TFA-HFIP disaggregated Aβ$_{42}$ peptides

Aggregation kinetics (A) and final product TEM images (B) of Aβ$_{42}$ peptides disaggregated via TFA-HFIP method and kept at various starting concentrations**.** Curves are fits of the various data points obtained and are plotted for visualization purposes only.

The initial monomer concentrations analyzed were 10 μM, 5 μM, 1 μM, 0.5 μM and 0.25 μM. The aggregation proceeded in a concentration dependent manner with the higher starting concentration reaction proceeded faster (**Figure 4-2 A**). As a measure of the quality of aggregates, we measured the concentration of the monomer at the end of the reaction which is in equilibrium with aggregates (C_r). C_r values for all the reactions were not identical and showed a dependence on the starting concentration of the monomer (**Table 4-1**).

Table 4-1: C_r value measurements of various $A\beta_{42}$ aggregation reactions

$A\beta_{42}$ monomer starting concentration (μM)	C_r (μM)
10 μM, TFA-HFIP disaggregation	0.23 ± 0.02
5 μM, TFA-HFIP disaggregation	0.217 ± 0.015
1 μM, TFA-HFIP disaggregation	0.152 ± 0.007
0.5 μM, TFA-HFIP disaggregation	0.115 ± 0.01
0.25 μM, TFA-HFIP disaggregation	0.12 ± 0.004
10 μM, Gdn-HCl SEC disaggregation	0.114 ± 0.01
1 μM, Gdn-HCl SEC disaggregation	0.107 ± 0.006

The reactions kept at a higher monomer concentrations of 10 μM and 5 μM proceeded to an equilibrium value of ~0.22 μM, whereas the lower starting concentration reactions proceeded to a lower C_r value of ~ 0.12 μM. This indicates that the reactions kept at lower concentrations proceeded to form aggregates which were more stable [124, 125]. The HX-MS analysis done earlier on $A\beta_{42}$ peptide disaggregated with TFA-HFIP (**Figure 4-1**, D.K. unpublished data) showed that indeed the difference in the C_r values might be arising from the fact that the 10 μM and 5 μM reactions proceed to form a mixed populations of fibrils and protofibrils whereas the reactions at lower concentrations are forming an uniform distribution of stable amyloid fibrils. Our EM results also confirmed this result (**Figure 4-2 B**). The aggregates at the end of the reaction for 10 μM and 5 μM $A\beta_{42}$, showed the presence of significant amount of protofibril species present along with the fibrils. The 1 μM reaction also displayed the presence of protofibrils. At lower reaction concentrations, a homogeneous fibril population was seen with negligible protofibrils.

The results obtained clearly showed that the $A\beta_{42}$ peptide when kept at a higher starting concentration was not aggregating as expected and the reaction does not proceed to completion. Others have shown that $A\beta_{42}$ incubated even at relatively high concentration aggregates to form a uniform population of fibrils just like the $A\beta_{40}$ peptide. There could be multiple reasons which would result in an aberrant aggregation profile of $A\beta_{42}$. One possible reason is that the starting material might not be sufficiently pure and could be contaminated by some chemical impurities (like Aβ deletions, or epimerization products [173]). However, MS analysis of the $A\beta_{42}$ we commonly use in our experiments (large scale T-boc synthesis from the Keck Biotechnology Center) showed > 95% purity (**Table 3-3**) and almost no impure deletions were seen (data not shown). Another possibility was that the TFA/HFIP disaggregation protocol, in spite of its consistently good performance with $A\beta_{40}$, might be causing a problem with the more hydrophobic $A\beta_{42}$ peptide. We therefore carried out parallel studies with $A\beta_{42}$ disaggregated by the Gdn-HCl/SEC method of Lashuel and co-workers [143].

4.3.2 $A\beta_{42}$ aggregation through Gdn.HCl-SEC disaggregation

About 0.5 mg of pure $A\beta_{42}$ was dissolved in 0.5 mls of a 8 M aqueous solution of Gdn-HCl, sonicated for 5 minutes and injected onto the SEC column (**2.1.4**). The monomer peak obtained was pooled and the starting monomer concentrations were adjusted immediately to the desired values (**2.1.5**). Reactions were initiated at starting concentrations of 10 μM and 1 μM of $A\beta_{42}$ peptide. Interestingly, we found that the aggregation kinetics of the 10 μM reaction proceeded at a similar rate to the 10 μM reaction obtained using TFA-HFIP disaggregation. The reaction

proceeds rapidly in the first 10 hrs and then concentration drops slowly to reach equilibrium by ~100 hrs (**Figure 4-3 A**).

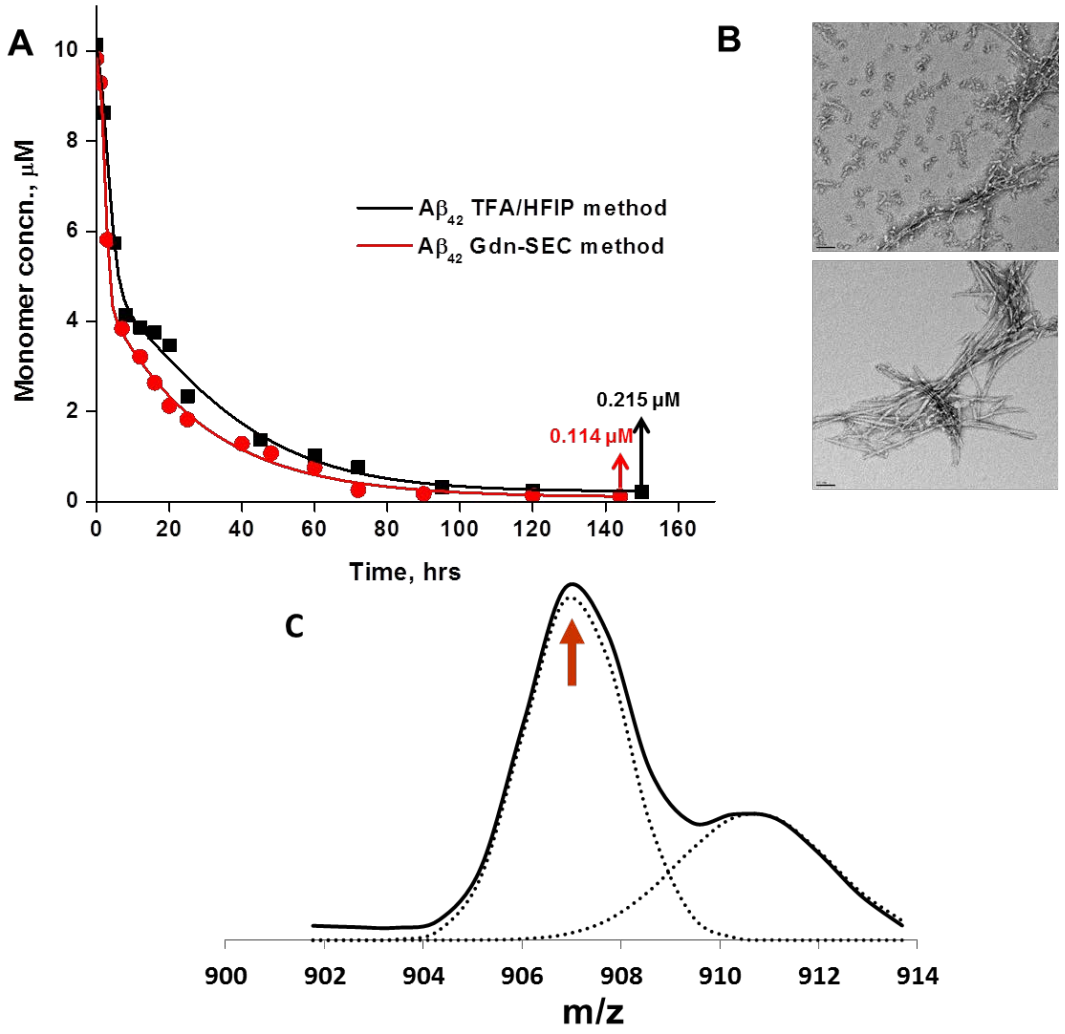

Figure 4-3: Aggregation comparison of TFA-HFIP and Gdn-SEC disaggregated Aβ$_{42}$ peptides
Aggregation kinetics (A) and TEM (B) comparison of 10 µM concentration reactions of Aβ$_{42}$ peptide disaggregated *via* TFA-HFIP or Gdn-SEC method. (C) ESI-MS spectra of the +5 charge state of aggregates formed from Aβ$_{42}$ peptide after Gdn-SEC disaggregation is employed. Fits of the data time points (A) were done for visualization purposes only.

In contrast to the 10 µM TFA-HFIP disaggregation reaction, which gives a C_r of 0.215 µM, the final C_r value of the reaction from the Gdn-HCl/SEC-disaggregated Aβ$_{42}$ is ~ 0.11 µM, indicating a more stable aggregate. EM analysis is consistent with this, showing a dramatic

difference from the TFA-HFIP monomer reaction product (**Figure 4-3 B**). While the latter shows the previously described large component of protofibrils (top panel), the Gdn-HCl/SEC material exhibits a uniform collection of amyloid fibrils (bottom panel). Finally, HX-MS analysis on the final aggregates from the Gdn-HCl/SEC monomer show the presence of only two distinct amounts of deuterium incorporation as was the case with the lower concentration aggregates formed from TFA-HFIP disaggregated material (**Figure 4-3 C and Figure 4-1 B**). The lower *m/z* peak corresponding to the secondary structure of the fibrils has similar deuterium incorporation value as was seen in the case of fibril peak obtained earlier from the lower starting concentrations of peptide disaggregated by the TFA-HFIP method (Table 4-2). In contrast to the original results of I.K., the level of protection found for these $A\beta_{42}$ fibrils now meets expectations in indicating a larger number of protected amide protons compared with $A\beta_{40}$ (see **Chapter 5**).

Table 4-2: Structural parameters from HX MS studies
Number of backbone hydrogens exchanged with deuterium, uncorrected values

Aggregates	N-H exchanged
6 μM, TFA-HFIP	12.7 (fibrils) 22.21 (protofibrils)
0.8 μM, TFA-HFIP	11.5 (fibrils)
10 μM, Gdn-HCl SEC	13.3 (fibrils)

The 1 μM Gdn-HCl SEC reaction also proceeds similarly to the 10 μM reaction, albeit much more slowly (data not shown), yielding similar values for C_r (Table 4-1). EM morphology of the final aggregates resemble the 10 μM reaction product (data not shown).

Thus, we found that the Gdn-HCl SEC method allowed us to generate a clean amyloid fibril product even when the reaction was initiated at 10 μM. These reactions were repeated many times with $A\beta_{42}$ to confirm the effect. In the case of the Gdn.HCl-SEC method, at least 10 independent experiments, including disaggregation, amyloid formation and analysis, were conducted, and results always agreed with the results presented here. The results using TFA-HFIP disaggregation were also highly reproducible, although occasionally we saw good behavior even at ~10 μM with $A\beta_{42}$ disaggregated by this method. Nonetheless, in 6 out of 9 independent experiments we saw incomplete aggregation reactions when higher concentrations of monomer were incubated.

The results are of practical importance, indicating that for Aβ molecules longer than $A\beta_{40}$, the Gdn.HCl-SEC method is a superior disaggregation protocol for obtaining well-behaved monomer. The rest of this chapter is devoted to our efforts to understand the differences between the two disaggregation protocols, which may have some fundamental significance in addition to the practical applications.

4.3.3 DLS comparison of early time points

One difference between the two disaggregation methods is the nature of the denaturing solvents used. While TFA and HFIP are both volatile solvents, both can demonstrate unusual avidity for peptides and can be difficult to completely get rid of, and this could alter the properties of the peptide [214]. In contrast, Gdn-HCl has a long history in the study of protein folding, where, in many cases with simpler globular proteins, reversible unfolding with recovery of protein properties is observed.

Another difference between the methods is the time between when monomer is generated and when it can be harvested. With our standard TFA-HFIP method, the monomer solubilized in water is centrifuged to clear any remaining aggregates. As mentioned earlier, long centrifugation times led to loss of material, presumably because of aggregation during the centrifugation time, and even a one hour centrifugation gave significant loss. So it seems quite certain that monomers are being compromised during the centrifugation step. In contrast, the time between the emergence of monomers from the SEC column in the Gdn.HCl-SEC method can be very short (~ 5 mins) before aggregation reactions are initiated.

Thus, it seems possible that one of these factors, or perhaps the two in combination, give rise to the difference in results.

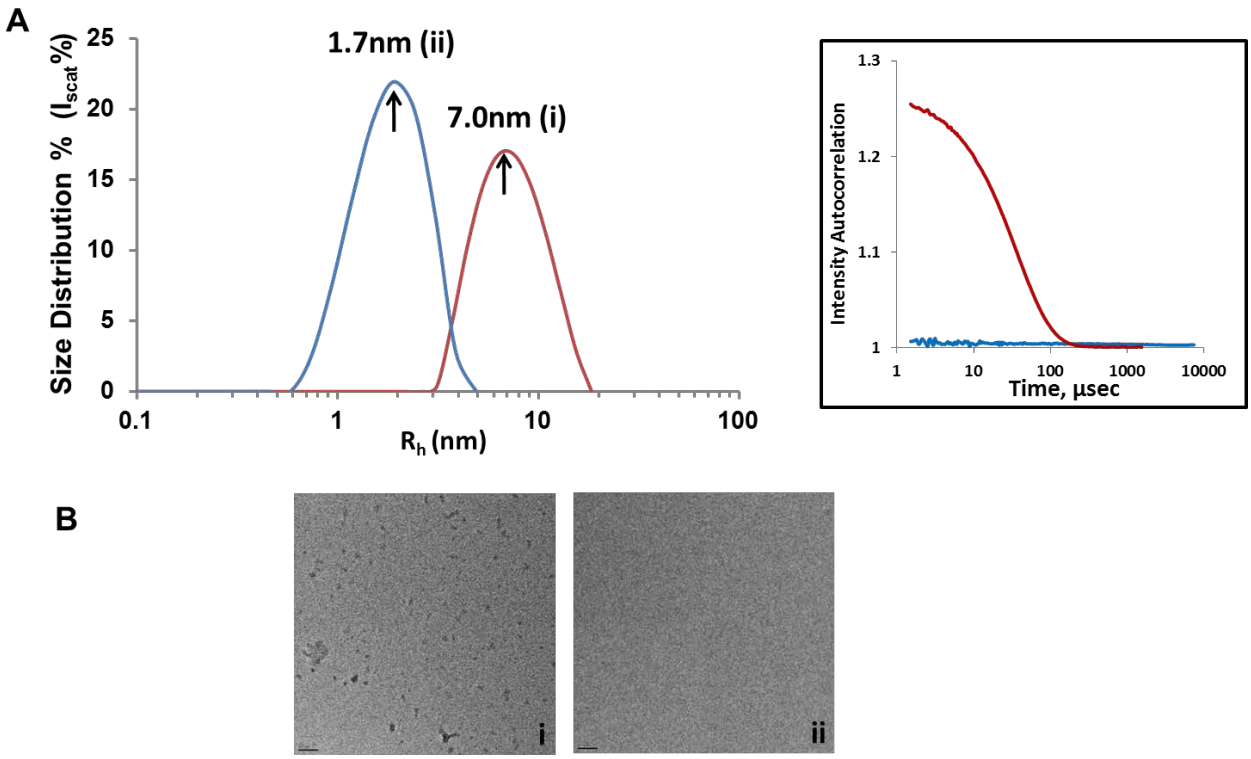

Figure 4-4: Presence of pre-formed aggregates during TFA-HFIP disaggregation of Aβ$_{42}$ peptides
A.Aβ$_{42}$ peptide obtained in 1X PBS immediately after the ultra-centrifugation step in the case of TFA-HFIP disaggregation (red) and obtained in monomer pool immediately after fractionation in SEC (blue) were analyzed via DLS to look for pre-formed aggregates. The panel on the right represents raw intensity auto correlation plots vs time. B. TEM images of the peptide at the same time point.

To see if $A\beta_{42}$ at time = 0 hrs (i.e., immediately after setting up the PBS solution) does indeed show some oligomers, we analyzed samples at this time point using DLS. In the case of $A\beta_{42}$ collected immediately after the ultra-centrifugation step of TFA-HFIP disaggregation, the presence of small oligomers were seen by DLS **(Figure 4-4 A, red curves**) and confirmed by EM (**Figure 4-4 B, i**). The sizes of these oligomers were determined to be ~ 7 nm. No such aggregates were seen in the monomer pool coming out of SEC (**Figure 4-4 A, blue curves; B,ii**).

4.3.4 FTIR shows differences in peptide films dried from HFIP

We investigated whether there might be some measureable property of Aβ peptides, in their response to exposure to HFIP, that might correlate with our experience using the TFA-HFIP disaggregation method on $A\beta_{40}$ and $A\beta_{42}$ described in this chapter. It has been shown previously that HFIP does induce self-assembly of Aβ peptides leading to the formation of oligomeric structure in HFIP [214]. We were particularly interested in the state of the peptides in our disaggregation protocol after HFIP had been removed to leave a thin film. We generated such films for both $A\beta_{40}$ and $A\beta_{42}$ and looked at their structures by FTIR, conducting secondary structural analysis on the spectra with Peakfit software (**2.4.2**). FTIR spectra recorded for $A\beta_{40}$ and $A\beta_{42}$ peptides in the dried form (**Figure 4-5**) suggest that both peptides, which are random coils as monomers in solution, adopt considerable α-helical structure after exposure to HFIP, based on a predominant peak at the 1659 cm^{-1}. This is not surprising, since other fluorinated alcohols, like trifluoroethanol, have this property. We also observed some degree of β-structure formation in both peptide films, based on the Amide I band at 1627 cm^{-1}. Interestingly, the

amount of β-structure is significantly more in the case of $A\beta_{42}$ (45%) compared to $A\beta_{40}$ (24%). The presence of β-structure suggests that both peptides, perhaps due to being present in the films at very high concentrations, have already begun to aggregate even before they are dissolved in water in our protocol. It is not clear why $A\beta_{42}$ has higher β-content, but the presence of aggregates at the stage of the HFIP film may provide an explanation for the considerable aggregation that occurs during the centrifugation step. It could also provide an explanation for the ability of the Gdn-HCl SEC method to provide higher quality monomer, since the peptide is never present in such a highly concentrated state as it is in the HFIP film.

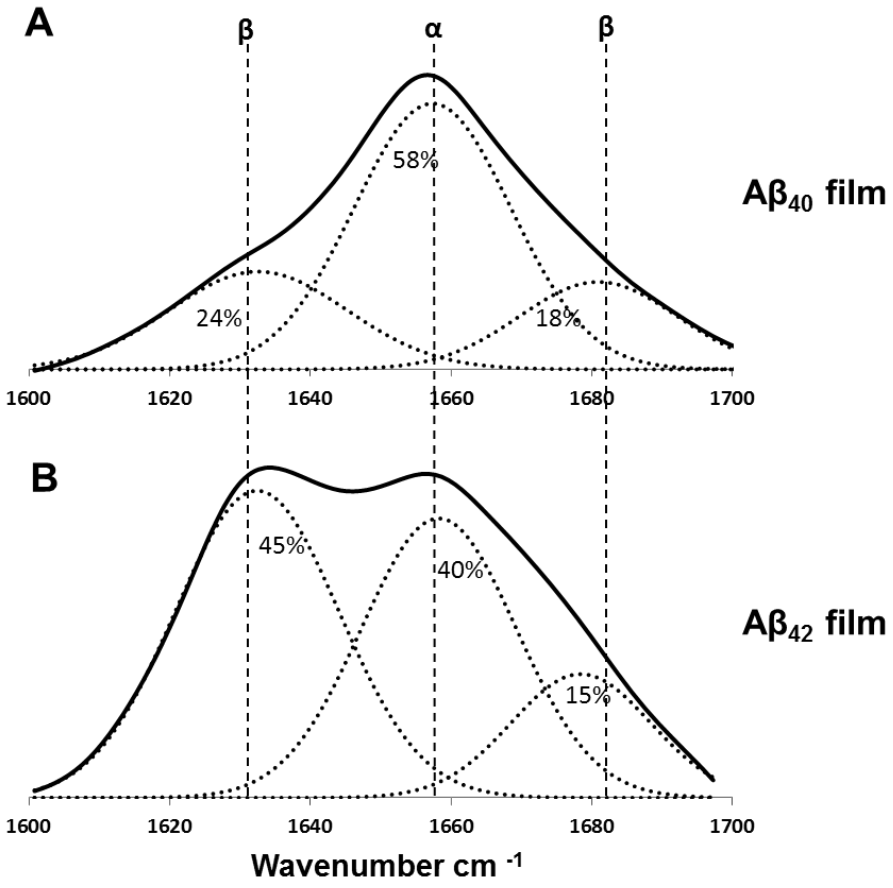

Figure 4-5: FTIR spectra of the freshly dissolved films in HFIP solution

Both $A\beta_{40}$ (A) and $A\beta_{42}$ (B) peptide are treated via TFA-HFIP disaggregation protocol till the lyophilization step and then resuspended in HFIP and evaporated. FTIR spectra of these films are shown here. The various % secondary structures present are depicted with the help of Peakfit algorithm.

4.3.5 Oligomers obtained from SEC also produce heterogeneous populations of aggregates

When Aβ peptides are dissolved in Gdn.HCl solution and injected into SEC, a small percent of Aβ (typically no more than 10%) elutes as aggregates or oligomers which can be separated from the monomer pool. HFIP is known to induce ordered amyloid structures in Aβ molecules [214]. When we replaced Gdn-HCl with HFIP for dissolving $A\beta_{42}$ before loading the SEC column, almost 50% of $A\beta_{42}$ peptide elutes as oligomer (**Figure 4-6 A**). To analyze if these oligomers/protofibrils are similar to the aggregates seen during TFA-HFIP disaggregation method for $A\beta_{42}$ peptides, we pooled the fractions eluting as oligomers and monomers separately from SEC of HFIP-treated $A\beta_{42}$. These eluted fractions were incubated separately at 37 ºC in PBS buffer and also in a 1:1 mixed ratio. After the samples were incubated for 7 days, they were analyzed using TEM (**2.3.2**) and HX-MS (**2.4.1**).

The monomer pool incubated at 37 ºC aggregated to form amyloid fibrils as shown previously for Gdn-HCl SEC-disaggregated $A\beta_{42}$ (**Figure 4-6 C,i**). HX-MS analysis on these aggregates showed the presence of only two distinct amounts of deuterium incorporation peaks as was the case with the lower concentration aggregates formed from TFA-HFIP disaggregated material (**Figure 4-3 B,i and Figure 4-1 B**). The lower *m/z* peak corresponding to the secondary structure of the fibrils has similar deuterium incorporation value as was seen in the case of fibril peak obtained earlier from TFA-HFIP method (**Table 4-2**).

Surprisingly, the oligomers pooled from SEC were very stable and even after 7 days of incubation at 37 ºC in quiescent conditions did not mature to form fibrils and were predominantly a uniform population of oligomers/protofibrils in the EM (**Figure 4-6 C,ii**). HX-

MS experiment on these aggregates showed three distinct deuterium incorporation peaks corresponding to fibrils, protofibrils and the fully exchanged monomer as was obtained with the higher concentration aggregates formed from the TFA-HFIP (**Figure 4-3 B,ii and Figure 4-1 A)**. The 1:1 mixed reaction of oligomer-monomer, showed a mixed population of fibrils and oligomers after 7 days of incubation (**Figure 4-6 C, iii**) very similar to the aggregates seen at 10 μM TFA-HFIP disaggregated $A\beta_{42}$ peptide (**Figure 4-2 B, 10 μM**). HX-MS analysis on these aggregates also show three distinct deuterium incorporation peaks with values similar to higher concentration aggregates formed from TFA-HFIP (**Table 4-2**).

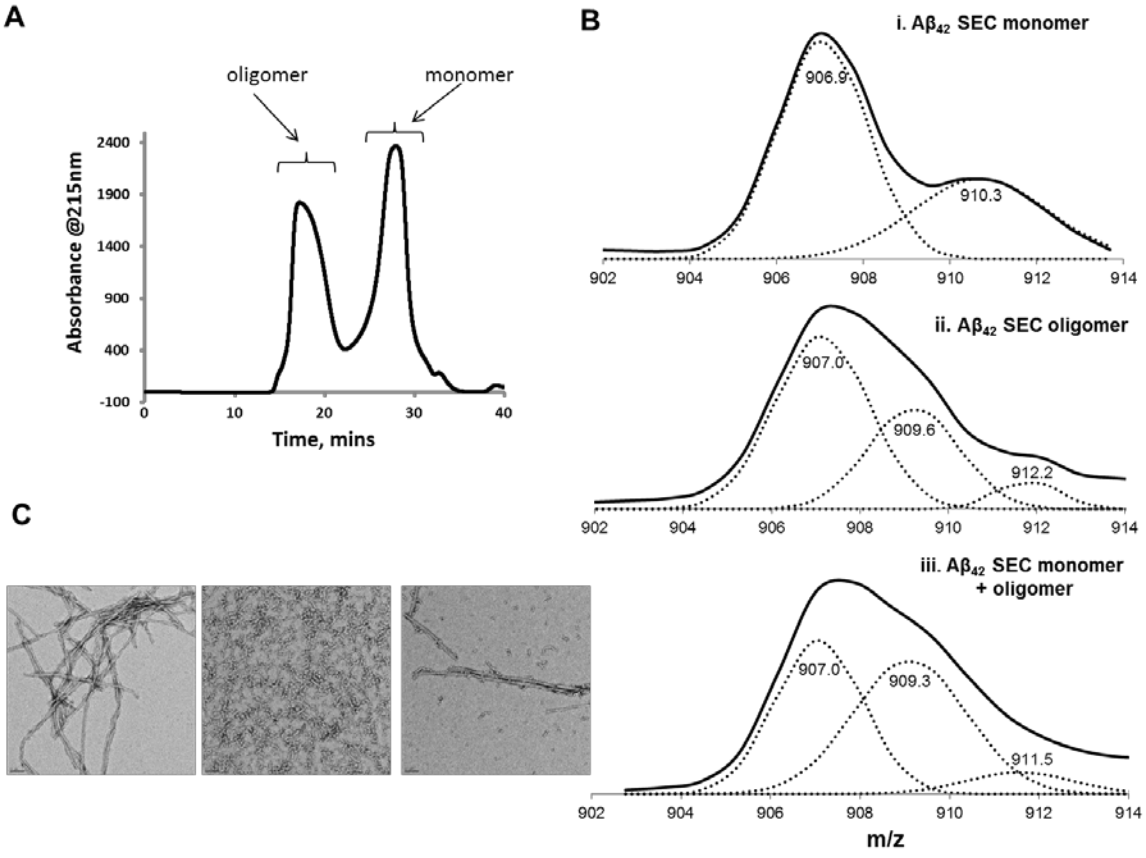

Figure 4-6: SEC generated $A\beta_{42}$ monomer-oligomer mixing experiment

$A\beta_{42}$ peptide was dissolved in HFIP, sonicated and injected into the SEC column. A. $A\beta_{42}$ fractionation by SEC showing the oligomer and the monomer peaks. The peaks were pooled separately and incubated separately or at a 1:1 ratio at 37 ºC for 7 days. B. HX-MS analysis done on the 7 day reaction. ESI-MS spectra of +5 charge state is shown here. C. TEM images of the aggregates formed after 7 days of incubation.

4.4 CONCLUSIONS

Although it has many excellent qualities, the Gdn.HCl-SEC method of peptide disaggregation has at least one major disadvantage in that it cannot easily be scaled down because of the dilution that occurs during chromatography. In contrast, methods relying on dissolution in volatile solvents like TFA and HFIP can be scaled down to adapt to situations where very small amounts of peptide are available. Since such uses of the TFA-HFIP method will always exist, it is important to try to understand what goes wrong when it does not work.

Organic solvents, particularly TFA and HFIP, have been used intensively to dissolve peptides that tend to aggregate. These solvents have been used in order to have stock solutions in which peptides are monomeric. Dissolution of Aβ peptides in HFIP followed by immediate drying has been one of the methods to make monomeric preparations of Aβ. The ability of these solvents to break β-sheet structures and induce helical conformations is presumed to be one of the reasons for their excellent solubilizing properties. In spite of this, extensive aggregation of Aβ in HFIP has been observed. The transition between α-helical to β-sheet structures is a key step in Aβ aggregation and could be induced in the presence of HFIP [214]. It has been shown previously that dissolution of amyloid-forming peptides in TFA and HFIP can result in the formation of ring-like annular structures in addition to self-assembled linear structures [215, 216].

When we analyzed the structure of Aβ in HFIP by looking at their FTIR spectra (**Figure 4-5**), HFIP seems to be inducing some kind of ordered β-structure, especially in $A\beta_{42}$, at least in the dry film stage of the disaggregation protocol. This presumably indicates some kind of aggregate formation in HFIP. These aggregates are likely initially small oligomers, as shown by the experiments summarized in **Figure 4-6**, and these are given the opportunity to grow and

accumulate during the centrifugation step of the TFA-HFIP protocol, as was shown by DLS (**Figure 4-4**) and by the high losses of peptide at long centrifugation times (~50% loss). The resulting aggregates might act as precursors to the oligomers that are observed at the end of the fibril assembly reactions. Thus, we conclude that formation of stable intermediate species at higher concentrations from peptides disaggregated by the TFA-HFIP method could be due to a combination of HFIP effects and ultra-centrifugation. It is not clear why this competing protofibril formation should depend on the starting concentration of peptide. One possibility is that the small oligomers present in the centrifugation supernatant might have the opportunity to dissociate back to monomers when present at low concentrations, but at higher concentrations in PBS are driven irreversibly to form larger oligomers and protofibrils that persist throughout the experiment.

In contrast, while small oligomers are also formed during the Gdn-HCl/SEC disaggregation step (**Figure 4-6**), the SEC component of this protocol allows us to separate these 'higher-sized' species from the 'lower-sized' monomer pool. Thus, the monomer pool is initially devoid of any higher order aggregates.

5.0 BIOPHYSICAL INVESTIGATIONS OF $A\beta_{43}$ PEPTIDE AGGREGATION

[This chapter has text, figures and tables reprinted/adapted with permission from the following submitted manuscript: **Chemuru, S**., Kodali, R. and Wetzel, R. "C-terminal threonine reduces $A\beta_{43}$ amyloidogenicity compared with $A\beta_{42}$". manuscript submitted. I had help from R.K. in the collection of TEM, FTIR and HX-MS data]

5.1 OVERVIEW

$A\beta_{43}$ peptide is a proteolytic processing product of the breakdown of APP by γ-secretase enzyme that is related to $A\beta_{42}$ by an additional Thr residue at the C-terminus. Although $A\beta_{43}$ is typically generated at low levels (~1 %) compared with the predominant $A\beta_{42}$ and $A\beta_{40}$ forms, it has been proposed that the longer peptide could have an impact on Aβ aggregation out of proportion to its brain content. In this Chapter, we carry out in vitro comparative analysis of the aggregation of $A\beta_{42}$, $A\beta_{43}$ and their mixtures. We found that $A\beta_{42}$ and $A\beta_{43}$ both spontaneously aggregate into mature amyloid fibrils *via* the sequential appearance of similar oligomeric and protofibrillar intermediates as detected by TEM, but also that $A\beta_{43}$ passes through these intermediates considerably more slowly than $A\beta_{42}$. The earliest of these transient assemblies appears to lack significant β-structure, based on its very low ThT fluorescence. We also found, contrary to expectations, that $A\beta_{43}$ fibrils are very inefficient in seeding $A\beta_{42}$ amyloid formation, even

though $A\beta_{42}$ fibrils seed fibril formation by $A\beta_{42}$ and $A\beta_{43}$ monomers equally well. Finally, mixtures of $A\beta_{42}$ and $A\beta_{43}$ aggregate into a single co-assembled fibril structure, but do so more slowly than $A\beta_{42}$ alone. Interestingly, the C-terminus of $A\beta_{43}$, while partially disordered in homogeneous fibrils, becomes fully integrated into the amyloid β-sheet when co-assembled with $A\beta_{42}$ into these fibrils. The results together suggest that low levels of $A\beta_{43}$ in the brain are unlikely to stimulate the aggregation of $A\beta_{42}$.

5.2 BACKGROUND

Aβ peptides are generated from the transmembrane APP through sequential cleavage by β-secretase and γ-secretase enzymes (Figure 1-1) [217]. Depending on the site of cleavage by γ-secretase, Aβ peptides of varying lengths in the C-terminus are generated [218]. The varying Aβ C-terminus has been attributed to the γ-secretase processing pathway that generates Aβ peptides by sequential cleavage of every three to four residues starting from $A\beta_{48}$/$A\beta_{49}$ which are obtained from APP [219]. Two major alloforms of Aβ exist in AD brain, $A\beta_{40}$ and $A\beta_{42}$, but there has been evidence for the presence of longer Aβ species, including $A\beta_{43}$, $A\beta_{46}$, $A\beta_{48}$, $A\beta_{49}$, that also co-exist in the brains of individuals with AD [220]. Especially, the presence of $A\beta_{43}$ is seen in plaque cores obtained from occipital and frontal cortex in both sporadic and familial AD cases [221, 222] and also in the case of diffuse plaques [220]. Longer Aβ species have also been detected in the case of transgenic mice models [223, 224] and in cell cultures expressing APP [219]. Generally, longer Aβ peptides are considered to be more hydrophobic and aggregation-prone as they are part of the transmembrane segment of APP [218].

There has been no comprehensive study so far conducted on Aβ variants which are longer than 42-amino acids although it has been seen that some FAD associated mutations in the presenilin genes increase the generation of longer Aβ species. The exact amount of longer Aβ species in brain plaques, especially $A\beta_{43}$, has not been determined in all the cases because of the lack of suitable antibodies to distinguish it from $A\beta_{42}$. Longer Aβ peptides tend to be more hydrophobic than shorter versions and, being rich in β-structure favoring β-branched amino acids, might be expected to be even more prone to make β-sheet rich aggregates [205]. $A\beta_{46}$ has been reported to spontaneously aggregate much more rapidly than $A\beta_{42}$ and $A\beta_{40}$ [157], and mature fibrils of $A\beta_{46}$ are able to seed elongation of $A\beta_{42}$ and $A\beta_{40}$ [225]. $A\beta_{43}$ in isolation has been reported to aggregate at similar [226] or faster [227, 228] rates compared with $A\beta_{42}$, and, when present in 10% the molar amount of $A\beta_{42}$, has been reported to not affect aggregation kinetics but rather to considerably alter the final ThT fluorescence amplitude of the reaction mixture [226].

Recently, Saito and colleagues produced transgenic mice models with elevated levels of $A\beta_{43}$ and they showed impairment of short-term memory and acceleration of disease pathology [227]. The data indicated that $A\beta_{43}$ showed higher propensity to aggregate and showed higher levels of neurotoxicity than $A\beta_{42}$. Recent data also suggest that the differences in the toxicity could be due to the fact that Thr43 residue favors direct contact with the protofibril surface more so than the C-terminus of $A\beta_{40}$ or $A\beta_{42}$ [228]. These recent findings indicate that $A\beta_{43}$ has been a neglected species in AD research and shows the potential importance of studying the aggregation properties of $A\beta_{43}$ peptide in vitro and also in association with other Aβ species.

Here, we studied the in vitro aggregation properties of $A\beta_{43}$ peptide alone and characterized the oligomers and the final aggregates obtained and compared to those obtained

from the wildtype $A\beta_{42}$ reaction. We further probed the hypothesized enhancement of $A\beta_{42}$ aggregation by $A\beta_{43}$. Mature fibrils are also formed at different rates, but with $A\beta_{43}$ mature fibrils forming more slowly than $A\beta_{42}$ fibrils in isolation. In addition, we found that small amounts of $A\beta_{43}$ in mixture with $A\beta_{42}$ in a ratio of 1:9, slow amyloid assembly compared with $A\beta_{42}$ alone, leading to mature fibrils co-assembled from both molecules. Consistent with all these rate effects, the added Thr residue at position 43 also impairs the protective β-sheet structure at the C-terminus residues of $A\beta_{43}$ in mature fibrils. We also describe an unusual lack of reciprocity in amyloid fibril cross-seeding with $A\beta_{43}$ amyloid being highly inefficient in seeding elongation of $A\beta_{42}$ monomers. The results provide new insights into some general features of Aβ aggregate assembly, and cast doubt on any stimulatory role of small amounts of $A\beta_{43}$ on $A\beta_{42}$ amyloid assembly in vivo as shown by others.

5.3 RESULTS

The focus of this work is on a detailed characterization of the in vitro aggregation of $A\beta_{43}$ alone and in mixture with $A\beta_{42}$ at approximate physiological ratios. We chose the Gdn-HCl/SEC disaggregation protocol given its superior performance with longer Aβ molecules (**see 4.0**). In addition, the mixing experiments actually required the use of Gdn-HCl/SEC disaggregation protocol (**see 2.0 and 4.0**). Doing this allowed us to eliminate any possible experimental bias by preassembly of the disaggregated peptides before mixing, such that they might not truly reflect the behavior of mixed monomers. By premixing $A\beta_{42}$ and $A\beta_{43}$ before disaggregation, and having the disaggregated monomers elute together in PBS from the SEC column, we have our best chance of focusing on assembly beginning with monomer-monomer interactions.

5.3.1 Aggregation kinetics comparison of $A\beta_{42}$ and $A\beta_{43}$ peptides

We assayed the aggregation kinetics of $A\beta_{42}$ and $A\beta_{43}$ peptides at starting monomer concentrations of 10 μM by following the reactions both by the loss of monomer from solution by sedimentation assay and also by the accumulation of amyloid-related aggregates through ThT fluorescence assay (**refer to 2.2.2**) (**Figure 5-1**). The drop in monomer concentration is a measure of total sedimentable aggregates produced, regardless of their morphology. Further, monomer concentrations at different time points allow estimation of the aggregate concentration, which can then be used to normalize the ThT readings (**see 2.2.2 for Method**). In addition, the monomer concentration at the end of the reaction, if it can be demonstrated to represent a true equilibrium position of the fibril formation reaction, is an important parameter, since we showed previously that these equilibrium concentrations – equivalent to the critical concentration (C_r) that controls aggregation initiation - are characteristic of particular aggregate morphologies and are also associated with fibril stability. The ThT values, when normalized for fibril mass using values obtained from the monomer concentrations at each time point, indicate the accumulation of amyloid-related aggregates. The weight concentration normalized values are characteristic of particular aggregate morphologies. For example, the ThT response of the oligomers formed in the early stages of $A\beta_{40}$ aggregation is minimal, and the responses of different amyloid polymorphs of $A\beta_{40}$ are all significantly different from each other.

For the $A\beta_{42}$ aggregation reaction at a starting concentration of 10 μM, the monomer concentration drops rapidly within the first several hours to about 50 % and continues to drop steadily until 100 hrs, after which no further changes occur (**Figure 5-1, ●**). This final concentration of monomer (the apparent C_r value) was 0.105 ± 0.01 μM (**Table 5-1**). The ThT signal produced by aliquots of this reaction correspondingly rose rapidly in the initial 24 hours,

reaching a plateau within 60 hrs to a relatively high yield of ThT fluorescence of ~2.2 * 10^5 fluorescence units per µg (**Figure 5-1, ●**). The steady increase in weight normalized ThT signal over the first 24 hrs suggests a transition through one or more intermediates with steadily increasing levels of ThT-positive β aggregates.

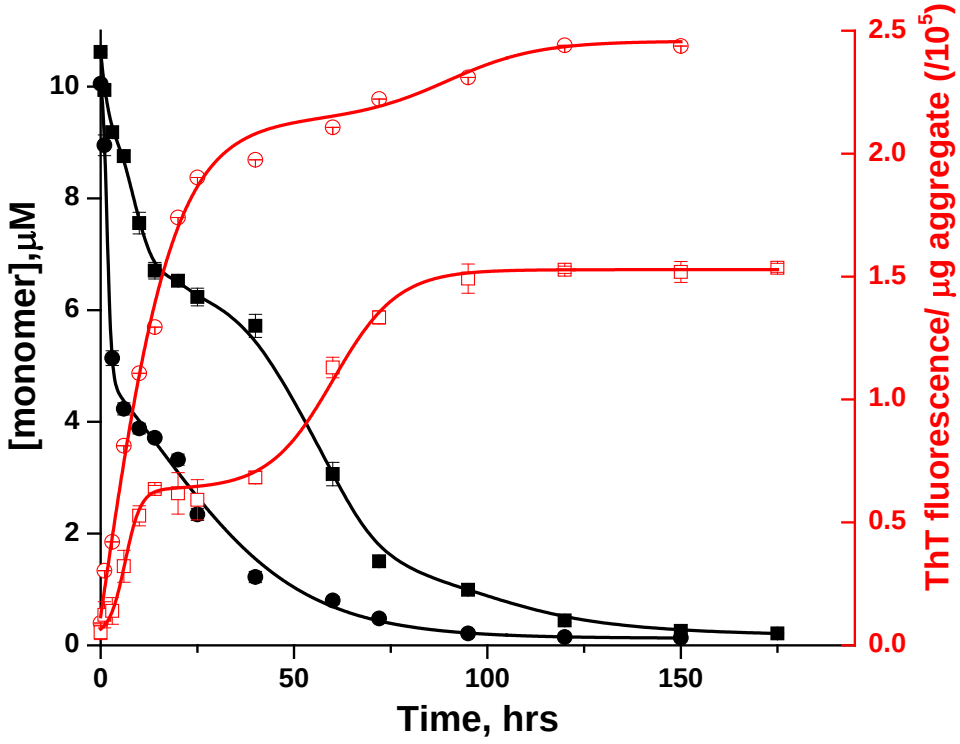

Figure 5-1: Amyloid assembly kinetics of Aβ$_{42}$ and Aβ$_{43}$ spontaneous aggregation.
10 µM reactions of Aβ$_{42}$ (●,○) and Aβ$_{43}$ (■,□) were initiated after disaggregating the monomers via SEC protocol. HPLC sedimentation assay to check for kinetics for monomer decay (●,■) and weight-normalized ThT fluorescence (○,□) are depicted here. The curves represent fits of the data points and are plotted for visualization purposes only.

This interpretation is supported by EM (**Figure 5-2**) and DLS (**Figure 5-3**) analyses of reaction time points. After 1 hr, when 10 % of the Aβ$_{42}$ molecules have already been converted to sedimentable aggregates (**Figure 5-1, ●**), DLS reveals a broad distribution of particles centered at ~ 10 nm in hydrodynamic radius (**Figure 5-3 B**), and this is consistent with EM images showing lightly staining particles in the same size range (**Figure 5-2 1hr**). After 2 hrs, when

about 30 % of the $A\beta_{42}$ molecules have been converted to aggregates (**Figure 5-1, ●**), most particles take up slightly more stain (**Figure 5-2 2hr**) and many have more clearly defined boundaries (**Figure 5-2 2hr**). By 8 hrs, when about of 60 % of $A\beta_{42}$ molecules are aggregated, EM analysis shows two types of oligomeric intermediate: narrow, positively stained filaments (**Figure 5-2 8hr**) and globular and wormlike negatively stained aggregates (**Figure 5-2 8hr**). At this point light scattering is high and the DLS data can no longer be deconvoluted. Between 8 and 12 hrs, while the total amount of sedimentable Aβ remains at ~ 60 % and the aggregate population remains mostly negatively stained globules and worms, an occasional negatively stained fibril can also be detected (**Figure 5-2 12 hr**). By 24 hrs, when ~ 75 % of the starting $A\beta_{42}$ is aggregated (**Figure 5-1, ●**), the reaction mixture is dominated by mature, negative-stained amyloid fibrils (**Figure 5-2 24hr**). By this point the weight-normalized ThT signal has risen to near maximum (**Figure 5-1, ○**).

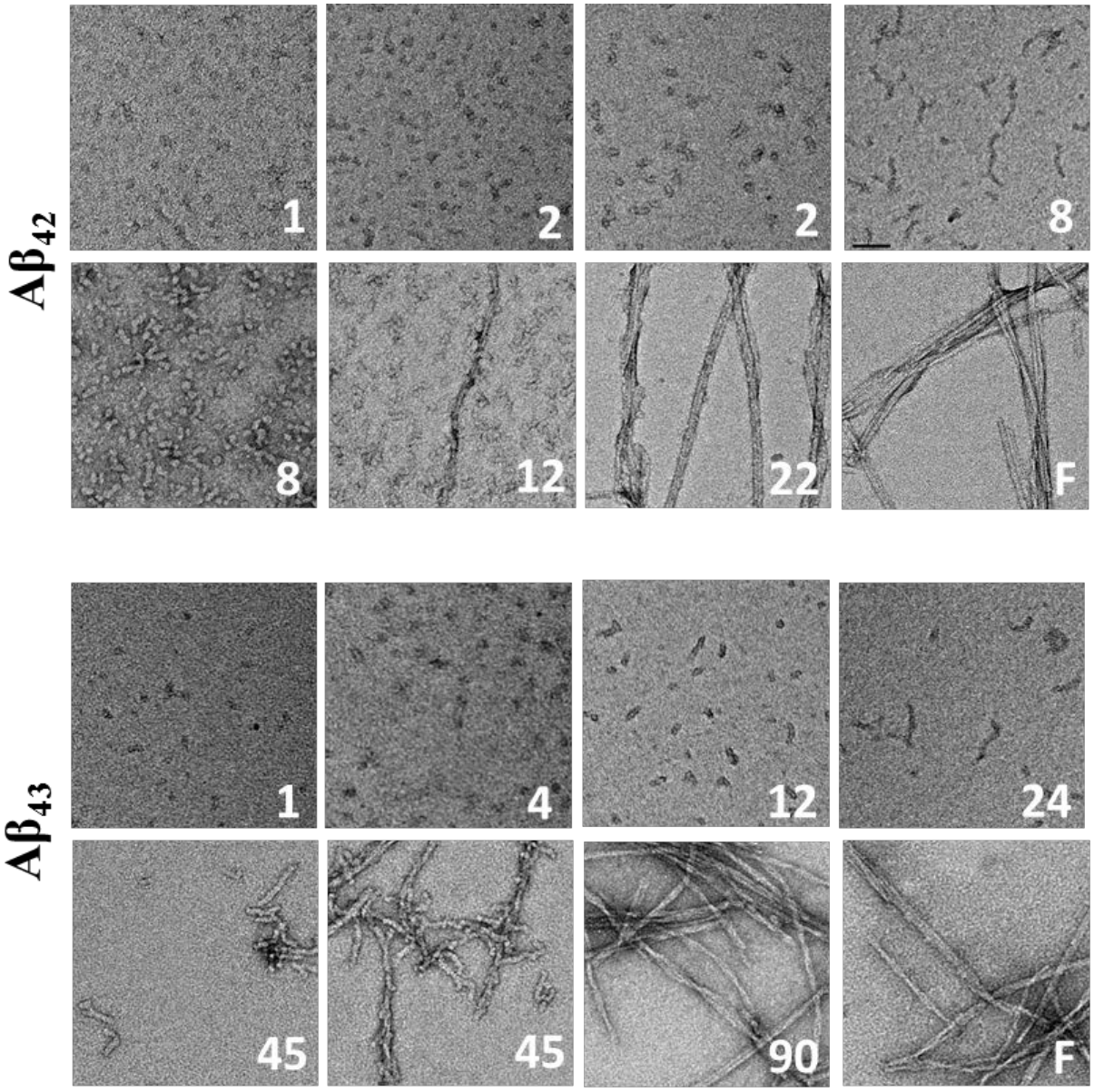

Figure 5-2: Time course Electron micrograph images of $A\beta_{42}$ and $A\beta_{43}$ reactions. Number inserts represent hours of incubation. Scale bars are 50 nm.

In contrast to the $A\beta_{42}$ data, $A\beta_{43}$ at 10.6 μM shows a slower drop in monomer concentration in the first 20-40 hrs to an intermediate concentration of about 5-6 μM. The monomer concentration drops about 30% within the first 10 hours, then continues to decline more slowly over the next 4 days, finally reaching apparent equilibrium at about 600 hrs (**Figure**

5-1, ■). The weight-normalized ThT signals rise steadily over the first 10 hrs to a plateau value that persists for the duration of the first 24 hrs, before again beginning to climb to a final plateau

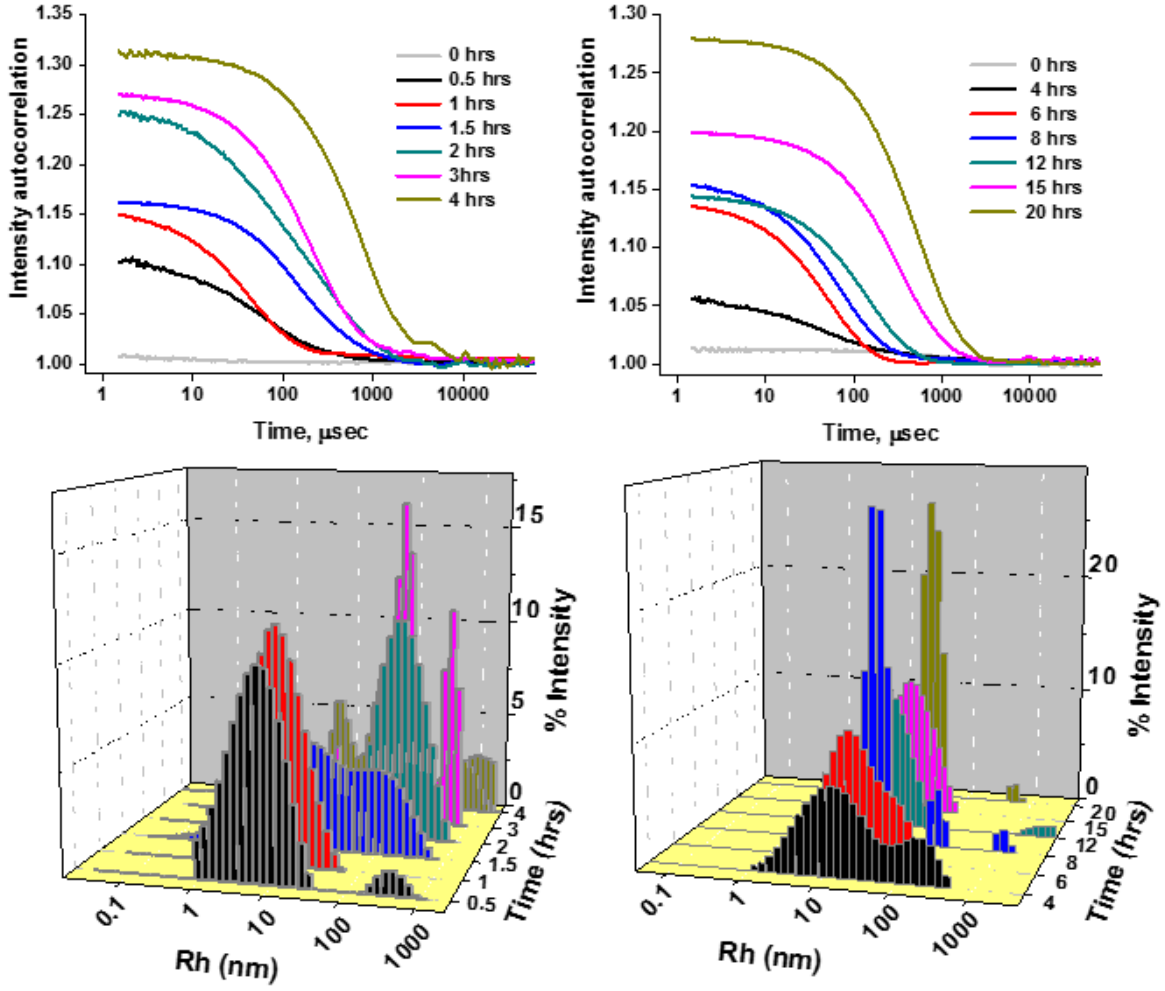

Figure 5-3: DLS analysis of amyloid assembly time points of $A\beta_{42}$ (left) and $A\beta_{43}$ (right) reactions

value of ~ 1.5 x 10^5 fluorescence units per µg reached at ~ 100 hrs (Figure 5-1, □; Figure 5-4, ■). After ~50 hrs, the monomer concentration drops further, to an apparent final equilibrium concentration of 0.202 ± 0.02 µM over the next 60-75 hrs (Figure 5-1, ■). That this value reflects a true equilibrium position was shown by setting up a fibril dissociation reaction (2.2.3). We found that the final aggregates dissociate over a period of ~ 600 hrs to a value of 0.167 ±

0.015 μM, very similar to the value obtained from the fibril association value (Figure 5-1, ■). The very slow (weeks) dissociation kinetics of these aggregates also shows the validity of our ThT protocol, in which aliquots of the ongoing reaction are diluted into buffer containing ThT and fluorescence read only over a few mins.

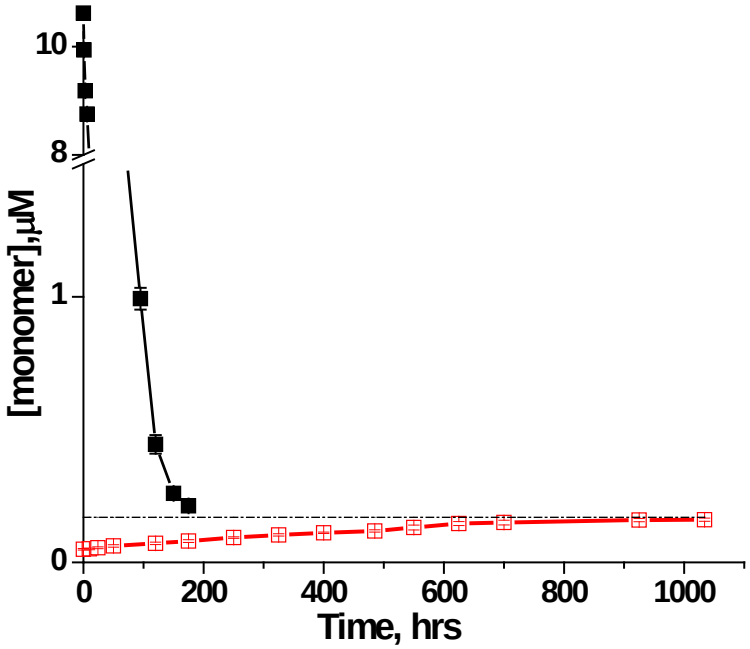

Figure 5-4: Fibril dissociation reaction to monitor equilibrium Cr value for $A\beta_{43}$
Fibrils from $A\beta_{43}$ taken at the end of the forward reaction (■) (~200 hrs) were diluted in 1x PBS four-fold and this diluted reaction is incubated at 37 ºC and the rise in monomer concentration measured (□) with the help of HPLC. The fits of the data points are for visualization purposes only.

The $A\beta_{43}$ assembly reaction proceeds through very similar structures to $A\beta_{42}$ intermediates, but with an extended time course consistent with the slower kinetics. After 1 hr, when ~ 7% of the $A\beta_{43}$ molecules are aggregated, EM shows poorly staining oligomers (**Figure 5-2 1hr**) similar to those seen at 1 hr for $A\beta_{42}$ assembly (**Figure 5-2 1hr**). After 4 hrs, when ~ 14 % of $A\beta_{43}$ molecules are aggregated (**Figure 5-1, ■**), aggregates remain relatively poorly resolved but take up somewhat more stain (**Figure 5-2 4hr**) in analogy to those seen at 2 hrs in

the $A\beta_{42}$ assembly reaction. By 12 hrs, when about 30% of $A\beta_{43}$ molecules are aggregated (**Figure 5-1, ■**), oligomers have more highly resolved boundaries **(Figure 5-2 12hr**) in analogy to aggregates seen at 2 hrs for $A\beta_{42}$. Beginning at 16 hrs, when ~ 40 % of $A\beta_{43}$ molecules are aggregated, and extending to 24 hrs, when about 46 % are aggregated (**Figure 5-1, ■**), the reaction mixture is composed entirely of thin, positively stained filaments (**Figure 5-2 24hr**) identical to those seen at 8 hrs in the $A\beta_{42}$ reaction. These filaments have average particle sizes in DLS at 20 hrs of ~ 75 nm in hydrodynamic radius (**Figure 5-3**). Between 25 hrs and 40 hrs, neither the percentage of aggregated $A\beta_{43}$ nor the weight normalized ThT signal has changed very much (**Figure 5-1**), but aggregate morphology changes dramatically, now being dominated by a mix of negatively stained worm-like aggregates either in isolation (**Figure 5-2 45hr**) or coating newly observed amyloid fibrils. From 45 hrs to 90 hrs, the amount of aggregated $A\beta_{43}$ increases from ~ 46 % to ~ 91 %, the weight normalized ThT increases from the intermediate plateau value of 0.6×10^5 to a final value of 1.5×10^5 fluorescence units per µg (**Figure 5-1**), and the reaction mixture transforms to uniform mature amyloid by EM (**Figure 5-2 90hr, F**).

The EM and weight normalized ThT data for the $A\beta_{43}$ reaction reveal a number of important trends that are also present, but are less obvious, in the faster-moving $A\beta_{42}$ assembly reaction. First, the steady rise in weight-normalized ThT signal during the first 10 hrs of the $A\beta_{43}$ assembly reaction is associated with a change in aggregate morphology from lightly staining, poorly resolved oligomers (**Figure 5-2 1,4 hr**) with no ThT signal to better-resolved oligomers (**Figure 5-2 12hr**) and narrow, positively stained filaments (**Figure 5-2 24hr**) that exhibit consistent weight-normalized ThT values. A similar set of transitions occurs in the early part of $A\beta_{42}$ assembly ending at about 8 hrs. Interestingly, the rates of increase and final

magnitudes of weight normalized ThT signals for this part of the assembly process are essentially identical for $A\beta_{42}$ and $A\beta_{43}$ (**Figure 5-5**).

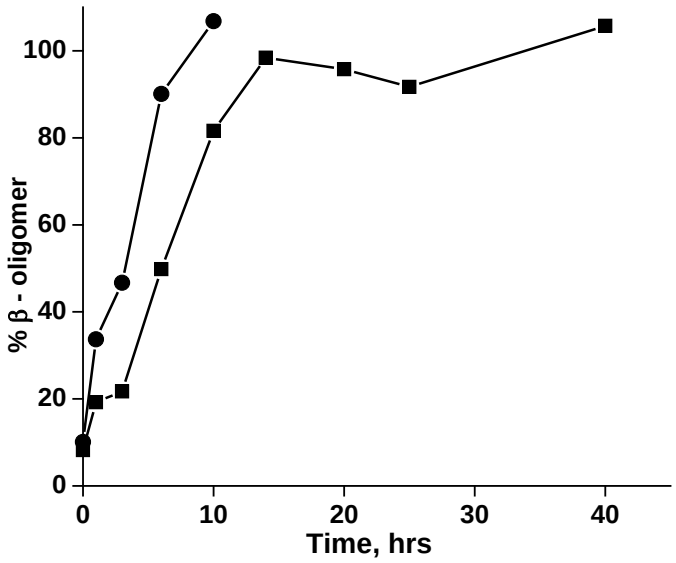

Figure 5-5: Kinetics of formation of ThT-positive oligomers for $A\beta_{42}$ (●) and $A\beta_{43}$ (■) reactions. ThT values at 10 hr for $A\beta_{42}$ (●) and 45 hr for $A\beta_{43}$ (■) were taken to be 100% (Figure 5-1) and the other values were plotted accordingly. These time points were chosen as these represent the last time point before the presence of fibrils were seen in EM analysis.

Second, the point where amyloid structure is nucleated, as defined by the time of first appearance of amyloid fibrils (~ 40 hrs), occurs when about 50% of $A\beta_{43}$ remains monomeric (**Figure 5-1, ■**). Similarly, nucleation of amyloid structure occurs at ~ 12 hrs in the $A\beta_{42}$ assembly reaction, when about 35% of the $A\beta_{42}$ molecules are monomeric (**Figure 5-1, ●**). The ThT signals at these points of nucleation are already substantial, since at least some of the intermediates present when amyloid is nucleated exhibit ThT signals and therefore presumably have some β-sheet structural elements.

Third, the direct precursor to the nucleus for amyloid elongation is not discernable from these data. In the $A\beta_{43}$ assembly reaction, there is a lag phase of constant ThT signal, from about

12 hrs to sometime between 25 and 40 hrs, that is occupied by narrow filaments (**Figure 5-2 24hr**) leading up to the point of nucleation (**Figure 5-1, ■**). Nucleation might involve the rearrangement of some of these filaments, or it might be driven by the conversion of some other species present in low amounts and/or at low visibility in EM. In the $A\beta_{42}$ reaction, nucleation of amyloid structure occurs at a time (~ 8 hrs) when both thin filaments and negatively stained oligomers are present. As noted above, substantial amounts of monomers and/or very small oligomers are also present in both reactions when nucleation occurs, and so cannot be excluded as possible sources of amyloid nuclei.

Fourth, nucleation of amyloid does not necessarily equate to a rapid increase in aggregation kinetics, as pointed out previously. Here, for both $A\beta_{42}$ (**Figure 5-1, ●**) and $A\beta_{43}$ (**Figure 5-1, ■**), the early steps of assembly are more rapid, in terms of mass of peptide converted over time into sedimentable particles, than the amyloid formation portions of the assembly reactions. These early aggregation steps appear to be non-nucleated assembly reactions, based on the absence of either a lag phase or marked curvature in the time courses of monomer loss.

According to these data, the two Aβ peptides assemble into amyloid fibrils by similar mechanistic pathways involving similar intermediates. The chief reason for the slower development of mature amyloid by $A\beta_{43}$ is the difference in approximate times of amyloid nucleation between $A\beta_{42}$ (~12 hrs) and $A\beta_{43}$ (~45 hrs). In contrast, post-nucleation events leading to essentially homogeneous suspensions of amyloid take place with similar kinetics.

5.3.2 Structural properties of aggregation reaction products

We discussed in great detail about the intermediate oligomer species present in both the reactions. Next, we looked at the structures of the final fibrils by EM, FTIR, HX-MS, C_r value, and weight-normalized ThT signals. As noted above, the major aggregated species observable in the EM in the 25-40 hr range in $A\beta_{43}$ amyloid assembly are positively stained, thin filaments that co-exist with monomeric peptides and are present over a long time period suggesting that they are in a quasi-equilibrium with monomer.

The final amyloid product of $A\beta_{42}$ incubation consists of typical unbranched, straight fibrils that appear to be composed of fibrils about 8-12 nm in diameter (**Figure 5-2 Final**). The C_r value of these fibrils, a measure of stability equal to the concentration of monomer after the reaction has reached equilibrium, is 0.105 ± 0.01 μM (**Table 5-1**). The weight-normalized ThT value for $A\beta_{42}$ fibrils is 2.5 x 10^5 fluorescence units per μg (**Table 5-1**).

Table 5-1: C_r parameters from spontaneous and seeded growth reactions

Monomer	$A\beta_{42}$ seeds	$A\beta_{43}$ seeds	$A\beta_{42}/A\beta_{43}$ seeds	unseeded
$A\beta_{42}$	0.09 ± 0.01	0.114 ± 0.007	0.10 ± 0.01	0.11 ± 0.01
$A\beta_{43}$	0.115 ± 0.007	0.20 ± 0.02	0.125 ± 0.006	0.20 ± 0.02
$A\beta_{42}/A\beta_{43}$	n.d.	n.d.	n.d.	0.067 ± 0.005 0.075 ± 0.007

The final amyloid product of $A\beta_{43}$ incubation is similar in gross appearance to $A\beta_{42}$ fibrils, exhibiting structures consisting of bundles of two or more filaments (**Figure 5-2 Final**).

The $A\beta_{43}$ filaments appear to be somewhat narrower, measuring 4-5 nm in diameter. The C_r value of $A\beta_{43}$ fibrils is slightly higher (i.e., less stable) than $A\beta_{42}$ fibrils, at 0.20 ± 0.02 μM (**Table 5-1**), and the weight-normalized ThT value is 1.5×10^5 (**Table 5-1**).

FTIR is well suited for analyzing the secondary structures of aggregates. Second derivative FTIR spectra show that the final aggregates of the 10 μM $A\beta_{42}$ and $A\beta_{43}$ reactions both exhibit a major, high intensity band in the β-sheet region between 1625-1640 cm^{-1} (**Figure 5-6**). These aggregates also exhibit one or more smaller bands of varying intensity in the 1640-1660 cm^{-1} region, which is typically assigned to α-helix or random coil structures, and in the 1660-1685 cm^{-1} region, which is normally associated with 3_{10} helix, and turns. The $A\beta_{43}$ aggregate also exhibits a small band at 1695 cm^{-1}, which is normally assigned to the anti-parallel β-sheet conformation. Since amyloid fibrils of point mutants of $A\beta_{40}$ can exhibit significant anti-parallel sheet, we cannot rule out a component of this structure in the $A\beta_{43}$ fibrils. Moreover, recently a similar band for anti-parallel β-sheet has also been seen in the case of $A\beta_{43}$ oligomers [229]. Except for this small deviation, FTIR shows no clear differences between $A\beta_{42}$ and $A\beta_{43}$ aggregates.

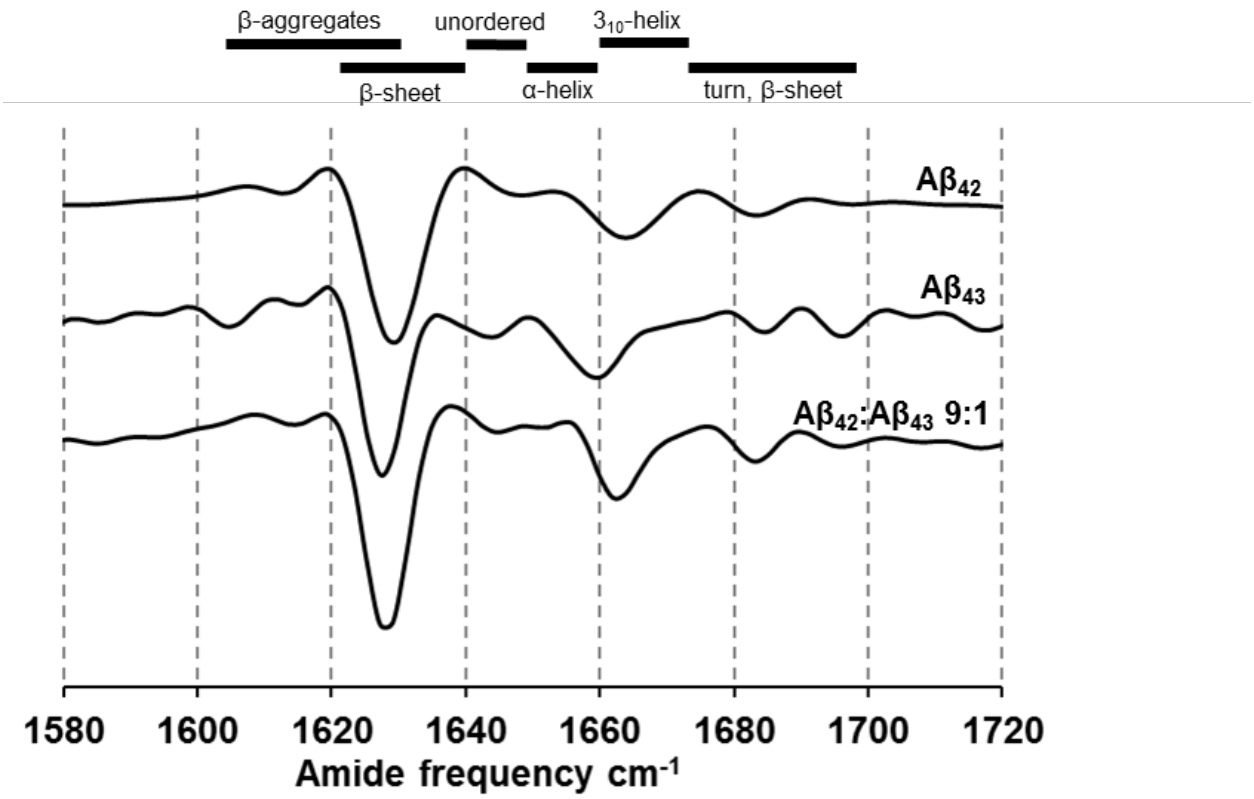

Figure 5-6: Second derivative FTIR spectra of various aggregates

HX protection experiments have proved an invaluable method for mapping amyloid fibril secondary structure providing information on the structural significance of H-bonding in addition to the implicit spatial relationships associated with H-bonding. The number of exchangeable backbone amide hydrogens that are protected by stable secondary structure after an overnight exposure to D_2O is characteristic of a particular Aβ polymorph, and using a rapid quench of exchange followed by mass spectrometric examination of re-dissolved Aβ monomers this information can be obtained easily on small amounts of sample. To obtain absolute values corresponding to the number of protected hydrogens, the raw data must be corrected for side chain exchange and backbone amide back exchange during sample workup. However,

uncorrected values can also be compared directly to obtain qualitative differences. Here we report uncorrected data.

The various aggregates described here display different degrees of exchange protection. In the case of the final $A\beta_{42}$ aggregates from the 10 μM reaction, we obtained a net incorporation of ≈15 deuteriums into each monomer in the fibril (**Table 5-2**); this corresponds to about half of the number that is obtained in an uncorrected exchange of the monomer's 41 backbone amide hydrogens under these conditions (not shown). In contrast, the 10 μM $A\beta_{43}$ product exhibits a net incorporation of ≈18 deuteriums (**Table 5-2**). The difference between these values is small but significant, indicating that there are approximately three fewer backbone amides involved in β-structure in $A\beta_{43}$ fibrils compared to $A\beta_{42}$ fibrils. $A\beta_{43}$ has an additional backbone amide group, which may or may not be responsible for one of these exchanged hydrogens, depending on its disposition in fibril structure ($A\beta_{42}$ fibrils generally exhibit β-structure to the end of the C-terminus).

Table 5-2: Fibril structural parameters from HX-MS studies
Number of backbone hydrogens exchanged with deuterium, uncorrected values

Monomer	$A\beta_{42}$ seeds	$A\beta_{43}$ seeds	$A\beta_{42}/A\beta_{43}$ seeds	unseeded
$A\beta_{42}$	14.7 ± 0.3	15.1 ± 0.3	15.0 ± 0.3	14.9 ± 0.3
$A\beta_{43}$	15.9 ± 0.4	18.3 ± 0.3	15.8 ± 0.2	18.2 ± 0.2
$A\beta_{42}/A\beta_{43}$	n.d.	n.d.	n.d.	15.3 ± 0.2 16.5 ± 0.3

We also examined the exchange protection specifically in the C-termini of Aβ peptides assembled into fibrils, using a protocol involving dissolution of fibrils from the exchange

reaction under quenched conditions, rapid pepsin digestion, and LC-MS analysis of the C-terminal fragment generated by cleavage after residue 34 (**2.4.1).**

The extent of deuterium incorporation in the C-terminal peptic fragments derived from $A\beta_{40}$, $A\beta_{42}$ and $A\beta_{43}$ aggregates is summarized in Figure 5-7. ESI-MS spectra of the 35-40 fragment obtained from $A\beta_{40}$ aggregates shows complete lack of protection as the spectra overlapped perfectly with that obtained from fully deuterated $A\beta_{40}$ monomer (**Figure 5-7 A**). This is consistent with the previous data obtained for all $A\beta_{40}$ polymorphs where we showed that the 35-40 segment in these $A\beta_{40}$ aggregates were devoid of any protection. In contrast, 35-42 segment in $A\beta_{42}$ aggregates showed complete protection, overlapping with the protonated monomer, indicating that β-sheet region in these aggregates extends till the extreme C-terminal amino acid, again a result consistent with previous studies (**Figure 5-7 B**). But more importantly, in the case of $A\beta_{43}$ aggregates, ESI-MS spectra display an intermediate result to that of $A\beta_{40}$ and $A\beta_{42}$. Here, the ESI-MS spectrum of $A\beta_{35-43}$ released from $A\beta_{43}$ amyloid exposed to exchange is substantially shifted to higher mass from the spectrum from protonated monomers, but at the same time is not shifted as much as the spectrum from deuterated monomers. This is consistent with partial protection of the $A\beta_{35-43}$ fragment within the amyloid fibril structure, suggesting that in spite of its β-branched structure, the C-terminal Thr residue in $A\beta_{43}$ to some extent compromises the integrity of the amyloid β-sheet at the C-terminus (**Figure 5-7 C**).

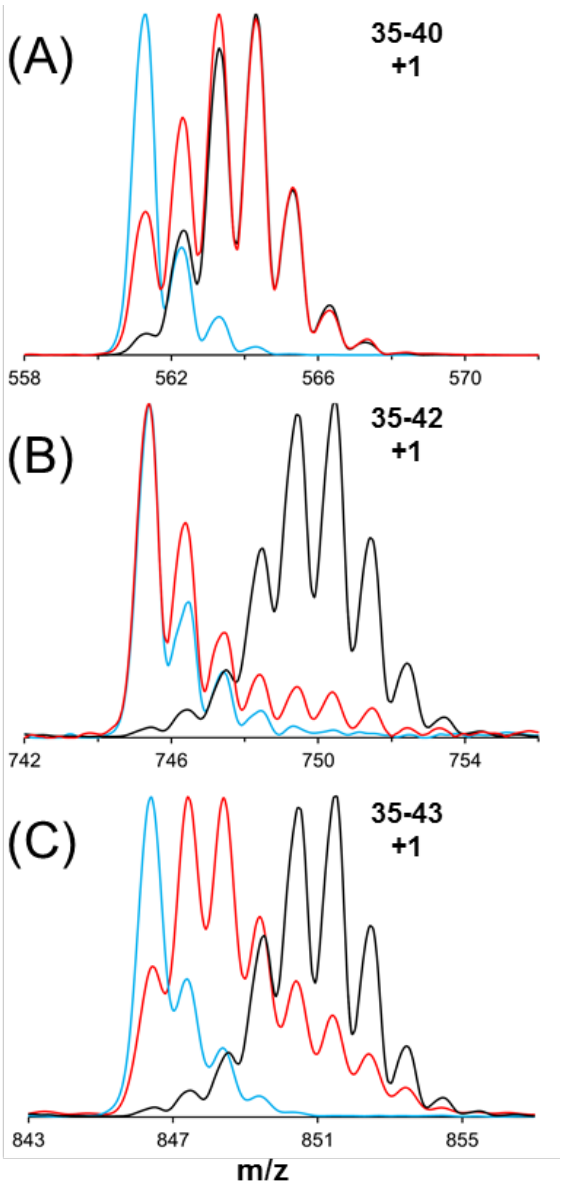

Figure 5-7: H-bonding status of Aβ C-terminus residues in fibrils
ESI-MS spectra of the pepsin-digested fragments of (A) $A\beta_{40}$ (B) $A\beta_{42}$ (C) $A\beta_{43}$. HX-MS protection of protonated monomer (cyan); deuterated monomer (black) and deuterated fibrils (red) are depicted.

Thus, the analysis of deuterium incorporation into the C-terminus qualitatively agrees with the analysis of exchange into the entire Aβ molecule (above), which in turn suggests that at least part of the difference in protective structure in these three homologous fibrils can be accounted for by differences in the status of the C-terminus. .

5.3.3 Effect of mixing on Aβ aggregation kinetics

Since, at least in some AD brains, the ratio of $A\beta_{42}$ to $A\beta_{43}$ is in the sub-stoichiometric range, we investigated the reaction kinetics and the properties of the aggregated product of a mixed reaction of these two peptides with a total Aβ concentration in the 10 μM range. To compare the effects of mixed incubation, we also reassessed the aggregation kinetics of homogeneous reactions of 10 μM $A\beta_{42}$ and 1.25 μM $A\beta_{43}$, and plotted the results in terms of % loss of monomer in order to normalize the different reactions to a common scale (**Figure 5-8)**. Interestingly, we found that the kinetics of monomer loss for both $A\beta_{42}$ and $A\beta_{43}$ are significantly slower in the mixed reaction than in the homogeneous reaction of $A\beta_{42}$ at 10 μM. Thus, in the mixed reaction, the $A\beta_{42}$ (●) and $A\beta_{43}$ (■) monomer concentrations both decay to less than 20% of the starting concentration after 10 hrs (**Figure 5-8)**. In contrast, after 10 hrs incubation of the homogeneous peptides, the $A\beta_{42}$ monomer concentration (○) has dropped to almost ~ 50%, and the $A\beta_{43}$ monomer concentration (□) is unchanged (**Figure 5-8**). This is a strong indication that these highly sequence related peptides are interacting, and probably co-aggregating into a common fibril, in the mixed reaction. A particularly strong indication of this in our case is the final concentration of $A\beta_{43}$ of 0.076 ± 0.007 μM in the mixed reaction, compared to the previously determined values of 0.205 μM in homogenous reactions (**Table 5-1**). In contrast, the C_r of $A\beta_{42}$ in the mixed reaction is essentially unchanged from the values of 0.105 μM found in homogeneous reaction. This suggests that the conformations of both peptides in the mixed fibril are dominated by the major component of the mixture and are essentially equivalent. HX-MS also tells a similar story. While the number of deuteriums exchanged into $A\beta_{42}$ in the fibril product from the mixed reaction, at 15.3 ± 0.2, is identical to the value found for homogeneous $A\beta_{42}$ fibrils, the value of 16.5 ± 0.3 for $A\beta_{43}$ in the mixed fibrils corresponds to

2-3 lesser deuteriums exchanged into $A\beta_{43}$ in the mixed reaction product (**Table 5-2**). Thus, $A\beta_{43}$ appears to make β-sheet H-bonds to a higher extent in this apparently mixed composition fibril. The ThT signal for the mixed fibrils, however, is not much different from that of homogeneous $A\beta_{42}$ fibrils. Likewise, the FTIR spectrum of the mixed fibrils is similar to spectra of the homogeneous fibrils from both peptides, but perhaps more closely resembles the spectrum of $A\beta_{42}$ amyloid with the 1695 cm^{-1} band missing (**Figure 5-6**).

Thus, in contrast to the original hypothesis, the presence of a small amount of $A\beta_{43}$ actually retards spontaneous amyloid assembly by $A\beta_{42}$, rather than enhance it. Although it is not clear why a small percentage of $A\beta_{43}$ should slow down spontaneous aggregation of $A\beta_{42}$, the data are a strong suggestion that these highly sequence-related peptides are interacting, and probably co-aggregating into a common fibril, in the mixed reaction.

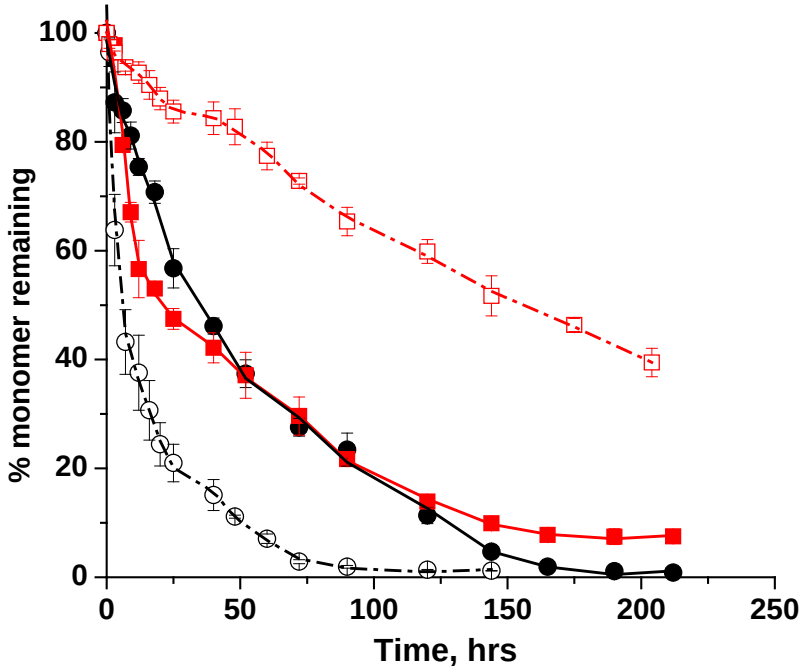

Figure 5-8: Amyloid assembly kinetics of a mixed reaction of Aβ$_{42}$ and Aβ$_{43}$ peptides
Aggregation kinetics of a 9:1 mixed of 10 μM Aβ$_{42}$ (●) and 1.25 μM Aβ$_{43}$ (■). Homogenous assembly of 10 μM Aβ$_{42}$ (○) and 1.25 μM Aβ$_{43}$ (□) is also shown.

5.3.4 Cross seeding reactions

As a further means of comparing fibril structures, we conducted cross-seeding experiments between these related peptides. The relative ability of an amyloid fibril from one peptide to seed amyloid formation in another peptide can be a sensitive, discriminating measure that is presumably linked to structural features of how polypeptides fold into the amyloid motif. In conducting cross-seeding reactions, one can monitor the effect of added seed on elongation kinetics or on the lag phase associated with the initial nucleation of aggregation. Very rapid aggregation reactions preclude the second approach, but also can compromise the first approach, since there has to be a window of lag time variation within which to observe seed-dependence of

the kinetics. Thus, it is necessary to arrange reaction conditions to allow differences to emerge. To facilitate this, we minimized the concentration of monomer, to slow down the spontaneous, nucleation-dependent reaction. There is a lower limit to the allowed starting concentration, however, and that is the C_r; near the C_r, even well-seeded reactions proceed slowly because of the significant back reaction of fibril dissociation. After the monomer concentration is optimized, the amount of seed, on a weight percentage basis, can be elevated in order to significantly stimulate the rate compared to the unseeded control.

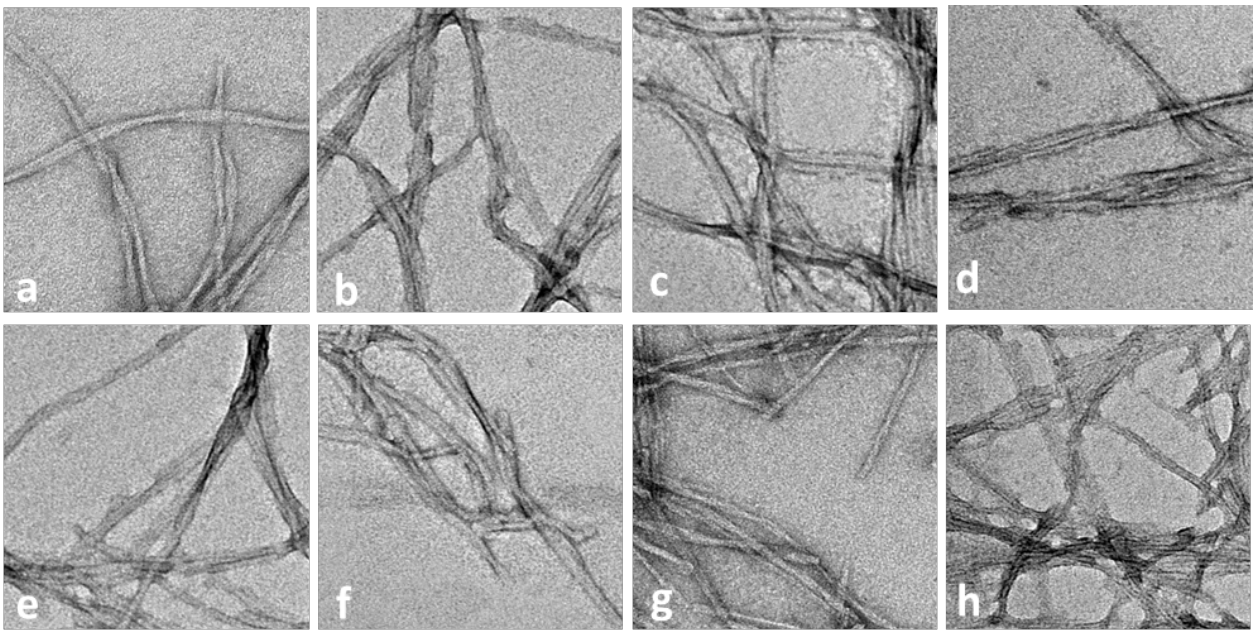

Figure 5-9: EM images of mature fibrils from various spontaneous and seeded growth reactions

We thus seeded reactions of freshly disaggregated $A\beta_{42}$ and $A\beta_{43}$ monomers at relatively low concentrations (5 μM) with high weight ratios of various seeds (10 %), isolated from the reactions described above, and measured the aggregation kinetics and some properties of the product fibrils. We found that 10 % by weight of $A\beta_{42}$ fibrils greatly stimulates the initial

aggregation kinetics of 5 μM monomeric $A\beta_{42}$ (**Figure 5-10 A**). In contrast, 10 % by weight of $A\beta_{43}$ fibrils has no discernable impact on the aggregation kinetics of 5 μM $A\beta_{42}$ (**Figure 5-10 A**). Interestingly, 10 % by weight of the fibril product from the 9:1 $A\beta_{42}$:$A\beta_{43}$ reaction stimulates the aggregation of 5 μM $A\beta_{42}$ to the same extent as homogeneous $A\beta_{42}$ fibrils. This data further supports the above structural data that suggests that the 9:1 fibrils resemble $A\beta_{42}$ fibrils. One very interesting additional outcome of this experiment is that, while $A\beta_{43}$ has enough structural compatibility with $A\beta_{42}$ that it can co-assemble into an $A\beta_{42}$-like amyloid fibril, the homogeneous fibrils made by $A\beta_{43}$ are nonetheless not able to seed $A\beta_{42}$ monomer.

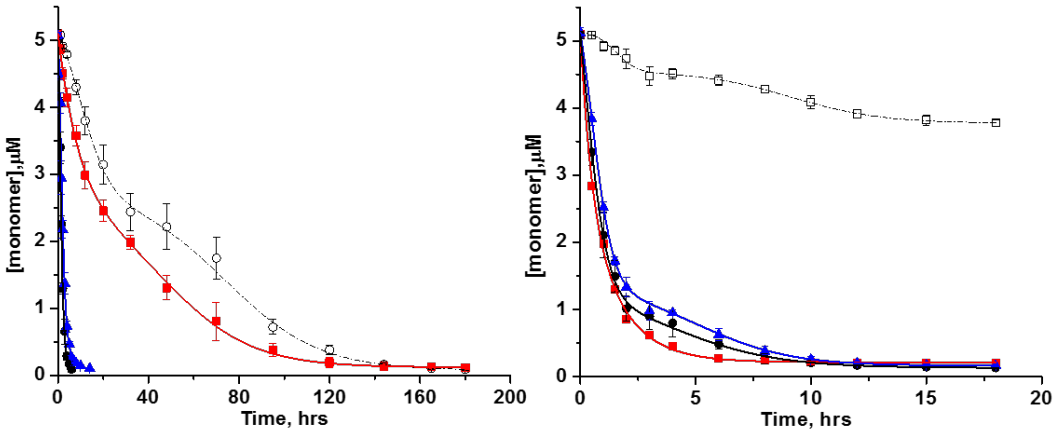

Figure 5-10: Cross seeding reaction kinetics
Aggregation kinetics of 5 μM monomer of A. $A\beta_{42}$ and B. 5 μM $A\beta_{43}$ seeded with 10 % w/w of $A\beta_{43}$ seeds (■), $A\beta_{42}$ seeds (●) and 9:1 $A\beta_{42}$:$A\beta_{43}$ mixed seeds (▲). Fits are for visualization purposes only.

In the mirror image experiment, while there is little aggregation of 5 μM homogeneous monomeric $A\beta_{43}$ in the first 5 hrs of incubation, all three possible amyloid seeds, at 10% by weight, are seen to produce significant enhancement of aggregation, so that all three seeded reactions go essentially to completion (i.e., to equilibrium) within 5-7 hrs (**Figure 5-10 B)**. Both $A\beta_{42}$ and 8:1 fibrils produce rapid aggregation kinetics tending to relatively low final monomer

concentrations. These rates and apparent C_r values are essentially identical, again pointing to a structural similarity of the 9:1 fibrils to $A\beta_{42}$ fibrils. Thus, all three fibrils appear to be equally capable of seeding $A\beta_{43}$ elongation, but, interestingly, they appear to dictate different final structures, with the $A\beta_{42}$ and 8:1 fibrils making a more $A\beta_{42}$-like elongation product with a C_r of ~ 0.1 μM.

Further analysis of the fibril products of these seeded elongation reactions reveals some interesting subtleties. In HX-MS analysis (**Table 5-2**), all product aggregates, with the exception of the $A\beta_{42}$ monomer seeded with $A\beta_{43}$ aggregates, have similar N-H exchange to that of the parent seed (**Table 5-2**). This exception is, of course, due to the fact that, since the $A\beta_{43}$ fibrils do not seed $A\beta_{42}$ elongation, the $A\beta_{42}$ monomers have to undergo spontaneous aggregation, and as a consequence make the typical $A\beta_{42}$ fibril product. This is also shown in the EM, where the product of ineffective seeding of $A\beta_{42}$ monomers by $A\beta_{43}$ fibrils generates fibrils (**Figure 5-10 D**) that faithfully resemble normal fibrils from spontaneous aggregation of $A\beta_{42}$ under these conditions (**Figure 5-2 F**). Thus, while in some respects the low percentage of $A\beta_{43}$ in the 8:1 fibrils seems to adapt to the $A\beta_{42}$ fibril structure features, the 8:1 fibrils nonetheless have a unique, surprisingly robust morphology that propagates with high fidelity with either $A\beta_{42}$ or $A\beta_{43}$ monomers.

EM also reveals an apparently subtle uniqueness in the morphology of the fibrils produced from seeding $A\beta_{43}$ monomers with $A\beta_{42}$ fibrils. Other parameters such as HX-MS (**Table 5-2**) and C_r (**Table 5-1**) suggest that $A\beta_{43}$ adopts an $A\beta_{42}$-like conformation in the cross-seeding product. HX-MS values show that the protection in the case of $A\beta_{43}$ monomers with $A\beta_{42}$ seeds seem to indicate an $A\beta_{42}$ –like structure for the final aggregates with lower stability as indicated by C_r.

5.4 DISCUSSION

Recent studies have shown that even small amounts of the less abundant Aβ species can alter the structure and toxicity of the more abundant $A\beta_{40}$ and $A\beta_{42}$ aggregates [229]. Recently we had monitored the aggregation of one of the 'minor' species of Aβ present in the brain, $A\beta_{46}$ peptide, and showed that it aggregates much faster than $A\beta_{42}$ and $A\beta_{40}$ peptides suggesting that even smaller amounts of $A\beta_{46}$ in the brain could seed $A\beta_{42}$ or $A\beta_{40}$ and potentially alter the course of their reactions [157]. Among the other 'minor' species of Aβ, $A\beta_{43}$ is of particular interest because of its enriched presence in plaque cores of AD disease brains [222]. Production of $A\beta_{43}$ is also enhanced in the case of few familial AD causing mutations associated with the presenilin genes [230].

Hence, we characterized the in vitro aggregation properties of $A\beta_{43}$ peptide present alone and also in a biologically relevant mixture along with $A\beta_{42}$. $A\beta_{43}$ amyloid is clearly structurally different from $A\beta_{42}$ amyloid, displaying a lower ThT response and a slightly higher elongation C_r value (0.202 μM) compared to $A\beta_{42}$ amyloid (0.105 μM). Previously it was shown in the case of $A\beta_{40}$ polymorphs that C_r is a property of the final amyloid structure and has a strong correlation with the number of strongly protected backbone amide hydrogens [125]. An $A\beta_{40}$ polymorph prepared under standard quiescent conditions in PBS at 37 °C similar to the aggregates studied here, had an equilibrium C_r of ~ 1 μM and an NH-exchange value of 16.7 Da (number of protected backbone hydrogens ~ 22.3). $A\beta_{42}$ aggregates studied under similar conditions displayed a much lower Cr of ~0.105 μM and higher number of protected amide hydrogens

(~26) which correlates to the fact that aggregates with much stronger β-sheet protection are more stable. The difference in the parameters between $A\beta_{42}$ and $A\beta_{40}$ aggregates is not surprising and is predominantly due to the C-terminal amino-acid sequence. The presence of additional two hydrophobic residues, Ile and Ala, contributes to a higher number of backbone protected hydrogens and hence the lower C_r value; in the case of $A\beta_{42}$, the backbone protection extends all the way till the end of C-terminus. Even though higher Aβ length peptides are expected to be more hydrophobic, the presence of the side chain hydroxyl group on the threonine (Thr43) in the case of $A\beta_{43}$ could slightly reverse the hydrophobic effect of $A\beta_{42}$ peptide and could make it behave similar to $A\beta_{40}$ aggregates. The fact that $A\beta_{43}$ aggregates have a slightly higher C_r (0.2 μM) and lesser backbone amide hydrogen protection (~23.5 protons) confirms the fact that the C-terminal Thr residue alters the secondary structure of the resulting fibrils.

The role of C-terminal residues in Aβ aggregation and fibril structure has received significant attention [87, 231, 232]. We have showed previously that, in the case of $A\beta_{40}$, all the polymorphs characterized had a low level of strong H-bonded structure in its extreme C-terminal residues (amino acids 35-40) [125]. Whereas in the case of $A\beta_{42}$ aggregates characterized under quiescent conditions in PBS buffer at 37 °C, HX-MS indicate the presence of a highly protective structure in the C-terminus all the way till the last residue. It is interesting to note that, in the case of $A\beta_{43}$ aggregates under similar conditions, there is only a partial protection in the C-terminal residues 35-43 presumably because the β-sheet does not extend till the end. But when the peptide is incubated either in the presence of excess $A\beta_{42}$ or in a seeded elongation process with $A\beta_{42}$ seeds, the structure seems to resemble that of $A\beta_{42}$ aggregates and have increased protection values.

Amyloid growth by monomer addition or seeded elongation is highly structurally discriminating and could be a good measure to compare structural similarities between two different aggregates [233, 234]. Cyclic amplification through seeding has been used to amplify brain fibrils for physical studies [121, 128, 235, 236]. In a surprising result, even though $A\beta_{43}$ aggregates look morphologically very similar to their $A\beta_{42}$ counterparts, they fail to act as competent seeds for $A\beta_{42}$ monomers. In a reaction where $A\beta_{42}$ monomers are normally incubated in the presence of $A\beta_{43}$ seeds, there was no acceleration of aggregation and the resulting product resembled that of the $A\beta_{42}$ aggregates alone. It is not clear as to why $A\beta_{43}$ aggregates do not behave as efficient seeds, but a similar result was previously seen for one of the polymorphs of $A\beta_{40}$ which had lesser β-sheet protection and also failed to act as efficient seeds to propagate its structure under different conditions [125].

The various Aβ peptides co-exist in an AD brain in a complex fashion. We report here that under a biologically relevant mixture of Aβ peptides (in a ratio of 9:1 of $A\beta_{42}$:$A\beta_{43}$), small amounts of $A\beta_{43}$ can modulate the behavior of $A\beta_{42}$ peptide and can form an altered morphology of the mixed aggregates. In the mixed reaction, $A\beta_{42}$ aggregates more slowly and $A\beta_{43}$ more quickly than comparable concentrations in isolation, suggesting co-aggrergation. The structure of $A\beta_{43}$ within this mixed fibril is an intriguing blend of $A\beta_{42}$–like and $A\beta_{43}$-like structural features. Overall, our results indicate that $A\beta_{43}$ has a unique aggregation behavior that is, however, not what was expected, since it actually slows down aggregation of $A\beta_{42}$ rather than speeding it up. Nonetheless the result shows the potential importance of tracking it as a separate molecule in studies of Aβ profiles in AD brains.

It is surprising that an additional amino acid, threonine, alters the β-sheet nature at the extreme C-terminus. Threonine, like valine and isoleucine, is branched at the β-carbon – a

feature that is normally associated with enhanced β-sheet propensity [237]. In spite of this, the addition of Thr appears to reduce the ability of the Aβ C-terminus to fully engage in β-sheet formation within the fibril. But threonine has an additional structural feature, a hydroxyl group – also on the β-carbon – and this is expected to enhance the tendency of Thr43 in fibrils to be disordered and interact with solvent water. This hypothesis could be tested in future studies. One of the interesting study would be the effect of crowding agents, like dextran or polyethylene glycols (PEG) on $A\beta_{43}$ C-terminal structure in fibrils. Such macromolecular crowding has been shown previously to alter fibril morphologies presumably by changing solvent properties [238]. Changing growth conditions, like agitation, salt concentrations, can also be explored to try and understand the effect of addition of threonine to Aβ structure.

Another experimental approach might be to alter the 43^{rd} residue in subtle ways and inquire whether the altered amino acid is included in or excluded from fibril structure. Our lab has previously studied positional effects of amino acids on fibril structure and stability by studying single point mutations in Aβ background [239, 240]. In addition, other studies have shown the effect of systematic amino-acid replacement at a single residue position on seed-dependent amyoid fibril formation [241]. Thus, similar experiments can be done by mutating the Thr43 residue and monitoring the fibril structure changes. Amino acids like valine or isoleucine, are also β-branched but lack the reactive hydroxyl group. So mutating to these residues would be interesting to see if the β-sheet extends to the end of C-termini or not. On the other hand, serine, which retains the Thr hydroxyl group but which is lacking the methyl group on the β-carbon, would be expected – according to our hypothesis – to discourage β-sheet formation at the C-terminus even more than Thr. It is also worth noting that there are many non-standard amino

acids available for peptide synthesis, and some of these might offer further comparative analyses of fibril formation.

We also hypothesize that the unusual seeding properties of $A\beta_{43}$ described earlier owe to the above-discussed structural variation at the Aβ C-terminus. To test this one might use the fibrils obtained from the mutational analyses proposed above to explore cross-seeding behaviors between mutant fibrils and $A\beta_{42}$ fibrils. Will the mutant Aβ fibrils be capable of seeding $A\beta_{42}$ monomer, in a way that $A\beta_{43}$ fibrils are not? If $A\beta_{42}$ fibrils can seed amyloid formation by the mutant Aβ monomer, will the peculiar amyloid structural properties we found in $A\beta_{43}$ fibrils also be present in the mutant Aβ fibrils?

6.0 ROLE OF CHIRALITY IN Aβ SEED PROPAGATION

[In this chapter, I had help from R.K. in the collection of TEM, FTIR data]

6.1 OVERVIEW

One of the key features of amyloid assembly is seeded elongation process which occurs in the case of most amyloid systems. The propagation of distinct Aβ fibril conformation over multiple rounds of seeded elongation demonstrates the basic ability of Aβ to form amyloid "strains" with the potential to correspond to distinct phenotypes in AD. The fidelity of this process has been studied to look at structural polymorphs and also as a model for prion propagation. Here, to probe the specificity of amyloid formation and growth, we synthesized and examined the self-assembly of the D-enantiomer of $A\beta_{40}$ in vitro. Early studies on the role of chirality suggested that "cross-seeding" (that is, using one species as amyloid seed and a different species as monomer) is not feasible between two opposite enantiomers. But our lab recently reported that D- and L-polyglutamine (polyQ) can engage in efficient cross-seeding, presumably via a "rippled β-sheet" interface between seed and incoming monomer in the anti-parallel β-sheet core of polyQ amyloid. To examine if this cross-seeding is a general phenomenon common to other amyloid systems, we examined it in the Aβ background. Previous literature has reported that L-$A\beta_{40}$ fibrils cannot seed fibril formation by D-$A\beta_{40}$. But surprisingly, we found cross-seeding

efficiency similar to what our group reported previously for polyQ amyloid. This suggests that cross-seeding can also occur through a similar 'rippled' β-sheet interface in the parallel, in-register structure of the Aβ amyloid core.

6.2 INTRODUCTION

Seeded elongation is a critically important aspect of amyloid fibril formation, a process that is the basis of biological propagation of prions [242-244]. The recruitment of cellular amyloid into growing amyloid assemblies is expected to be a highly structurally specific mechanism which depends on many factors like the sensitivity of amyloid seeding to fibril structure [245], the primary amino acid sequence [233, 234] and also the amino acid chirality [246, 247]. Spontaneous growth of amyloid fibrils is often considered as a nucleated growth polymerization pathway [248] in which the overall rate of amyloid formation is limited predominantly by the slow generation of nuclei (Introduction). These nuclei once formed can quickly grow via monomer addition (elongation phase) which is thermodynamically favorable, resulting in rapid extension of amyloid structure [124]. The elongation mechanism can be individually studied with the help of seeded fibril growth reactions using exogenous seeds. This is particularly useful in the case of Aβ research because of the complexity involved in the nucleation step. Seeded elongation is also important as a mechanism for eliminating the need for nucleation to happen [124]. This is particularly useful in eliminating lag times and promoting rapid fibril growth even at very low peptide concentrations. Seeded elongation reactions have also been studied to explore amyloid fibril structure, by looking at the compatibility of one peptide with another in a 'cross-seeding' reaction [125]. The efficiency of cross-seeding could be an estimate of the fit

between the amyloid folding unit of the seed molecule and the incoming monomer. Seeded elongation has also been used in efforts to prepare, for later analysis, large amounts of fibrils whose conformations are assumed to replicate the conformation of a small amount of brain-derived amyloid used as the seed [121, 245]. The specificity of the cross-seeding reaction for Aβ peptides has been studied previously. The amyloid fibrils from a number of proteins have been shown to seed fibril formation by Aβ peptides, but not nearly as efficiently as self-seeding by Aβ fibrils [233, 249, 250].

Given the fact that there is strong D,L-chiral specificity in protein folding and in most protein activities [251], previous results suggesting that amyloid cross-seeding has stringent chiral specificity [246, 247] were not surprising. In particular, a study by the Maggio group on the ability of soluble radiolabeled Aβ monomers to be deposited onto existing amyloid plaques in brain slices showed that iodinated L-$A\beta_{40}$ is efficiently taken up by the natural (and therefore composed of L-$A\beta_{40}$) amyloid templates, while D-$A\beta_{40}$ monomer is not [246]. In contrast, our lab described previously that highly efficient cross-seeding of amyloid fibril growth happens between L- and D-polyQ [252] (**Figure 6-1 A, B**). K.K. and co-workers showed that this cross-seeding is also observed when D -polyQ amyloid prepared in vitro is taken up by cells expressing an L-polyQ sequence. The stereochemical compatibility of chiral cross-seeding in such an anti-parallel arrangement is consistent with theoretical studies by Pauling and Corey showing that mixed β-sheets of alternating L- and D-peptides, producing "rippled" β-sheets, are stereochemically feasible [253]. Recently, such soluble stable mixed D,L-β-sheets have been obtained in experiments [254, 255]. A schematic visualization of a modeled structural compatibility between a D-polyQ and a L-polyQ assembly aligned in an anti-parallel fashion was shown in the paper taking a known x-ray diffraction based structural model for L-fibril end

(**Figure 6-1 C**) [252, 256]. This model was consistent with the idea of the presence of a "rippled" β-sheet interface with no steric clashes. This provided an explanation for efficient cross-seeding in the polyQ background.

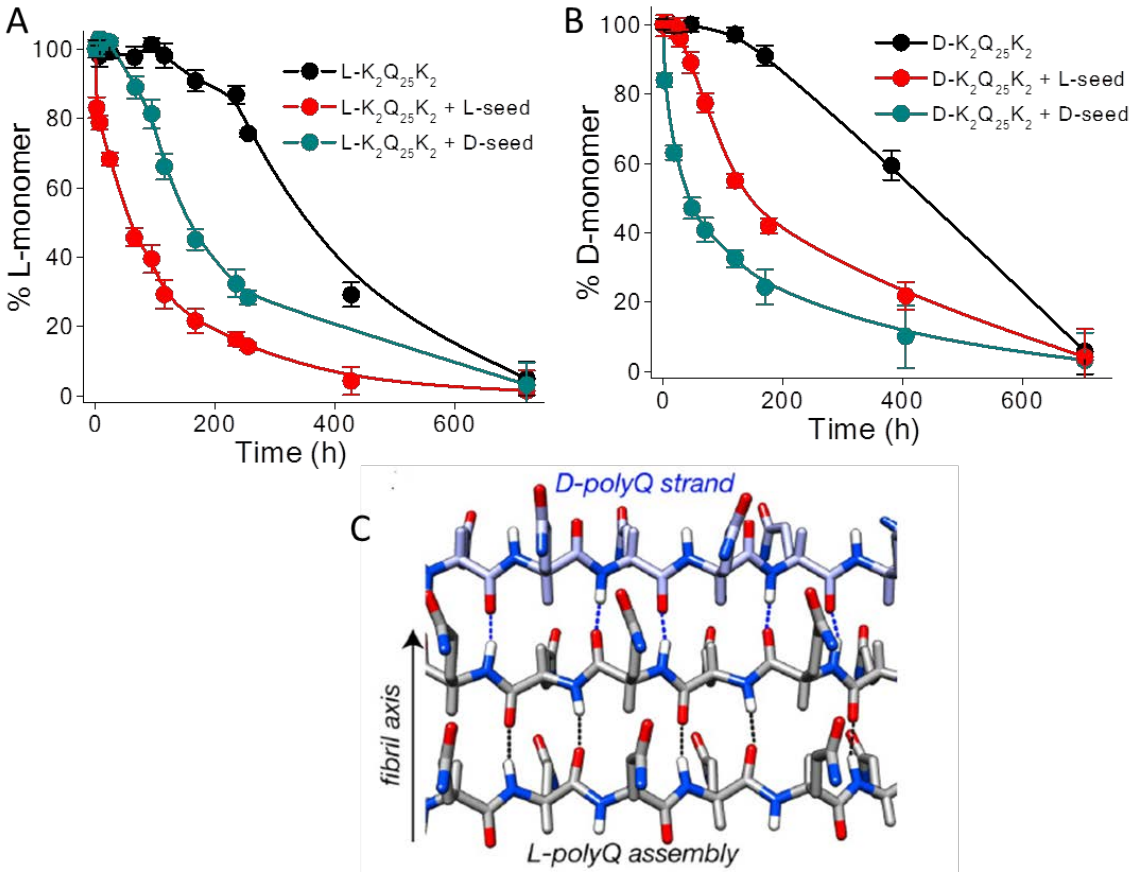

Figure 6-1: Seeding reactions between D,L-polyQ amyloids
Interactions between polyQ amyloid (PKKKRKVGGQ$_{25}$KK) and monomers ($K_2Q_{25}K_2$) at 37 ºC in PBS [252]. A. L-polyQ monomers and B. D-polyQ monomers (30 μM) seeded with 12% (w/w) seeds. C. Schematic D-polyQ strand aligned in anti-parallel fashion with an anti-parallel L-polyQ amyloid assembly model [252].

We wanted to explore the notion that chiral cross-seeding could be a more generic phenomenon and in particular whether it could occur with more typical amyloid fibrils whose core consists of parallel, in-register β-sheet [257, 258], which contrast with the anti-parallel structure of polyQ amyloid [259, 260]. PolyQ system is also comparatively simple and possibly better suited for D,L- cross seeding, because there is no bulky side chains in polyQ, the way there

are in most amyloidogenic peptides, and it might be more difficult to accommodate a number of different, bulky side chains at the rippled interface. Hence, we wanted to explore if a peptide assembling into parallel, in-register β-sheet amyloid, such as Aβ, could support sterically acceptable D-/L-interactions and exhibit D,L-interactions.

In this Chapter, we test whether chemically synthesized D- and L-$A\beta_{40}$ peptides are capable of efficient cross-seeding in amyloid fibril growth, in in vitro experiments similar in design to those previously described with polyQ. The results obtained here suggest that chiral cross seeding of amyloid may not be confined to polyQ or to anti-parallel β-sheet amyloid, but rather may be a more general phenomenon.

6.3 RESULTS

6.3.1 D-$A\beta_{40}$ peptide synthesis

Initially, D-$A\beta_{40}$ peptide was synthesized in a general fashion from Keck Biotechnology Center at Yale University just like all the other Aβ peptides synthesized in a crude fashion by Fmoc synthesis strategy. We found, however, that this peptide synthesis gave an inferior product that, in spite of its acceptable purity by LC-MS analysis, aggregated extremely poorly and could not be used for our experiments (**Appendix A**). (Just as all-D synthetic proteins can fold as efficiently as all-L, we expect that Aβ of opposite chirality should undergo spontaneous amyloid formation identically to all-L. This was the case with polyQ amyloid [252]) One of the reasons why the product might be impure is the presence of epimerization during synthesis resulting in peptide with higher % of L-amino acids present [173]. In fact, the coupling agent used during the

initial synthesis by the Keck Center, HBTU, is known to be less effective in reducing epimerization during synthesis. Hence, we worked in consultation with the Keck Center to explore the use of other coupling agents which would react faster with less epimerization during coupling. Two of the coupling reagents explored were COMU and HATU, and we found that HATU provided a better quality product (as defined by amyloid formation kinetics) with higher yields of the pure peptide (**Appendix A**). The peptide from HATU synthesis was used in our experiments here. We also purchased D-Aβ_{40} peptide from Sigma Aldrich (Catalog No: A5973), and this peptide had a similar aggregation profile to that of L-Aβ_{40} peptide and similar cross-seeding behavior to the Keck D-Aβ_{40} F-moc product using HATU. Sigma Aldrich, like other peptide suppliers, does not reveal details of their source or synthetic methods, so we don't know how they successfully produced their product. The Keck synthesis was required because of the cost of the Sigma-Aldrich material.

6.3.2 Spontaneous aggregation reactions

In an achiral solvent, we expect D-Aβ_{40} of good quality to undergo spontaneous aggregation to make amyloid fibrils with similar kinetics of formation and basic morphology as L-Aβ_{40}. This was confirmed by experiment. The aggregation kinetics of L- and D-Aβ40 under quiescent conditions was monitored with the help of HPLC sedimentation assay (**2.2.1**) (**Figure 6-2**). Both L- and D-Aβ_{40} peptides were incubated at a starting monomer concentration of ~50 μM. The aggregation kinetics for both the peptides was identical, with the reactions reaching equilibrium around 250 hrs. The D-Aβ_{40} aggregated at a slightly reduced rate with $t_{½}$ of 72 hrs when compared to the L-Aβ_{40} with a $t_{½}$ ~58 hrs. ($t_{½}$ is a simple measure of time taken for 50% drop in monomer concentration and is useful to use as a crude way to quantify amyloid formation

kinetics.) The slight difference in half-lives is probably real and may reflect some small degree of poorer quality in the D-peptide.

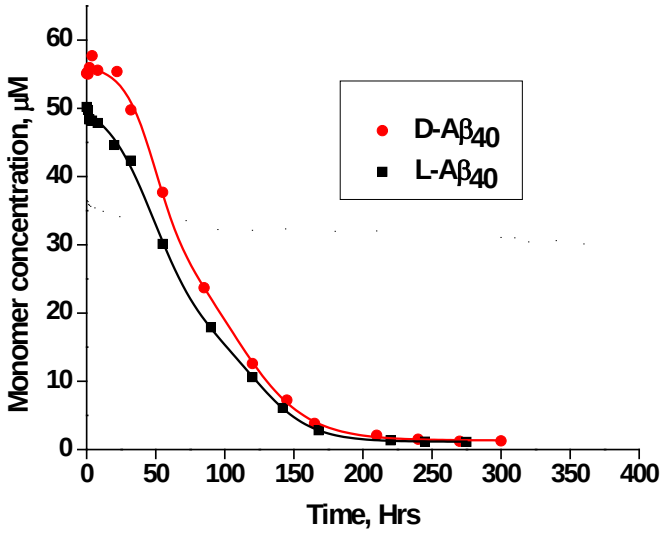

Figure 6-2: Aggregation kinetics comparison of D- and L-Aβ40 peptides

The fibril products of spontaneous amyloid formation by the D- and L-peptides are essentially identical in EM morphology (**Figure 6-3 C, no seed**). In addition, the secondary structures of the fibrils are identical, as seen both in the FTIR spectra of the isolated aggregates (**Figure 6-3 B**) and in the CD spectra of suspensions of aggregates (**Figure 6-3 A**). Both the techniques indicated a high level of β-sheet structure as expected. In the case of CD measurements, as expected with ordered structures of opposite chirality, the CD spectrum of D-Aβ40 amyloid is of opposite sign to that of L-Aβ40 fibrils (**Figure 6-3 A**). The fact that we observe this mirror image CD spectrum confirms that the peptide in the "D-Aβ40" amyloid fibrils is that of opposite chirality to that of L-Aβ40.

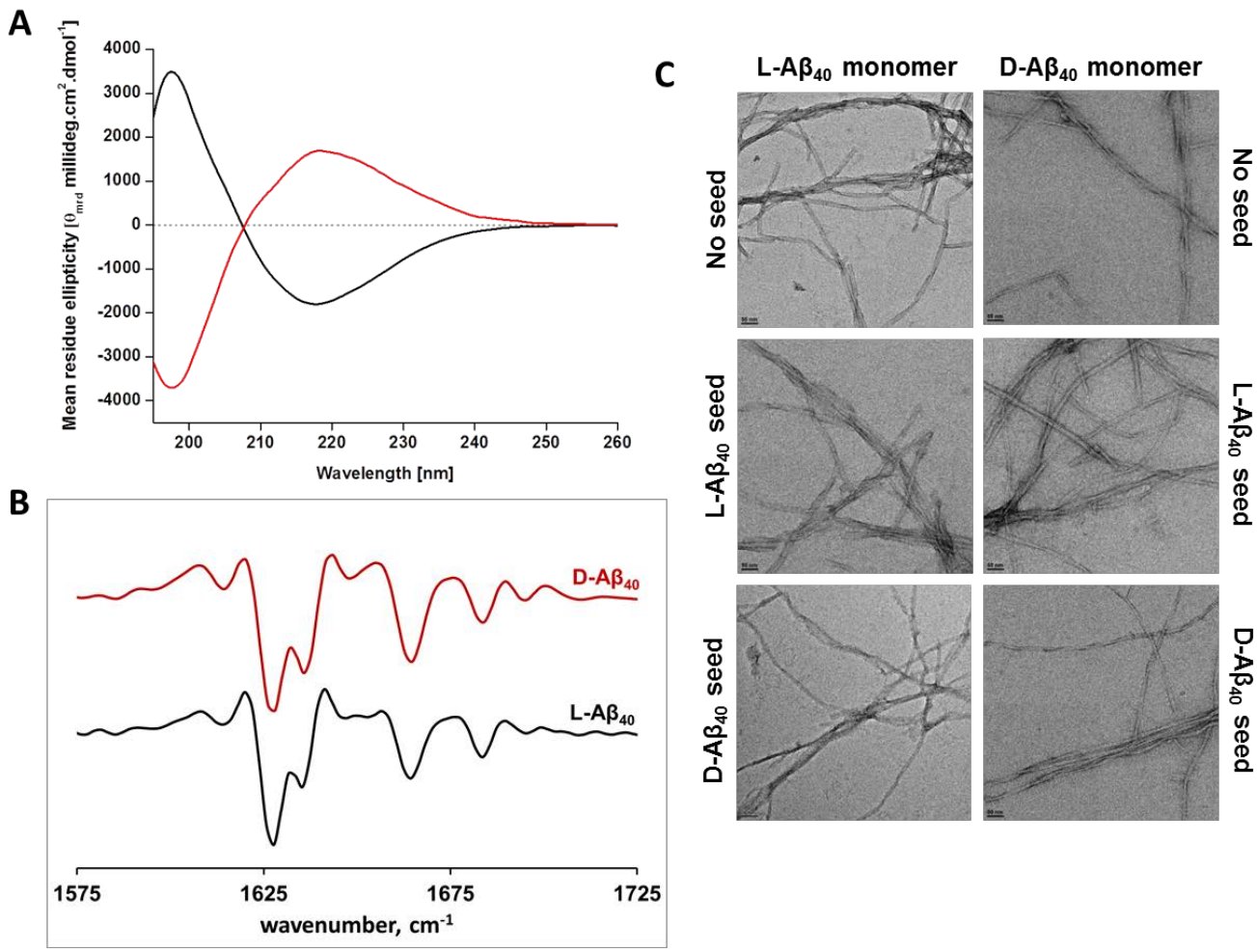

Figure 6-3: Physical characterization of D-and L-Aβ40 amyloids
A. CD and B. Second derivative FTIR spectra of D- and L-Aβ40 amyloid fibrils C. Negative stain EM images of the various seeded reactions.

The C_r values for both the spontaneous growth reactions were also essentially identical (Table 6-1). We obtained a C_r value of 1.07 ± 0.03 μM for the spontaneous aggregation of L-Aβ40 when compared to the value of 1.22 ± 0.04 μM for the D-Aβ40. Thus, by all of the criteria measured, D-Aβ40 behaves identically to L-Aβ40 in fibril assembly and forms fibrils with similar properties.

6.3.3 Cross-seeding experiments

To look at the in vitro seeding specificities of L- and D-$A\beta_{40}$ fibrils towards monomers of matched and opposite chirality, we initiated the aggregation reactions with 10% by weight of fibril seeds to monomer (**Figure 6-4**). We found that, as was the case with polyQ system, L-$A\beta_{40}$ fibrils greatly stimulated the aggregation of L-monomers (**Figure 6-4 A, ●**) compared with the unseeded reaction, with a $t_{½}$ increase of 100 fold (**Figure 6-4 A, ■**) (**Table 6-1**). The $t_{½}$ value reduced from ~58 hrs in the case of spontaneous growth kinetics to ~0.5 hrs in the case of seeded growth reactions (**Table 6-1)**. More importantly, we found out that the reaction of L-monomers with D-fibrils (**Figure 6-4 A, ▲**) also proceeds at a rate much faster than the unseeded reaction (**Table 6-1**) with a $t_{½}$ of ~ 9 hrs. The morphologies of the fibrils produced at the end of the reaction are essentially identical by EM analysis (**Figure 6-3 C**) and are similar in appearance to those of the spontaneous growth reactions. Identical results were obtained in the opposite reaction where D-monomers were seeded with L and D-aggregates (**Figure 6-4 B**). The C_r values of all the reactions are reported in **Table 6-1.**

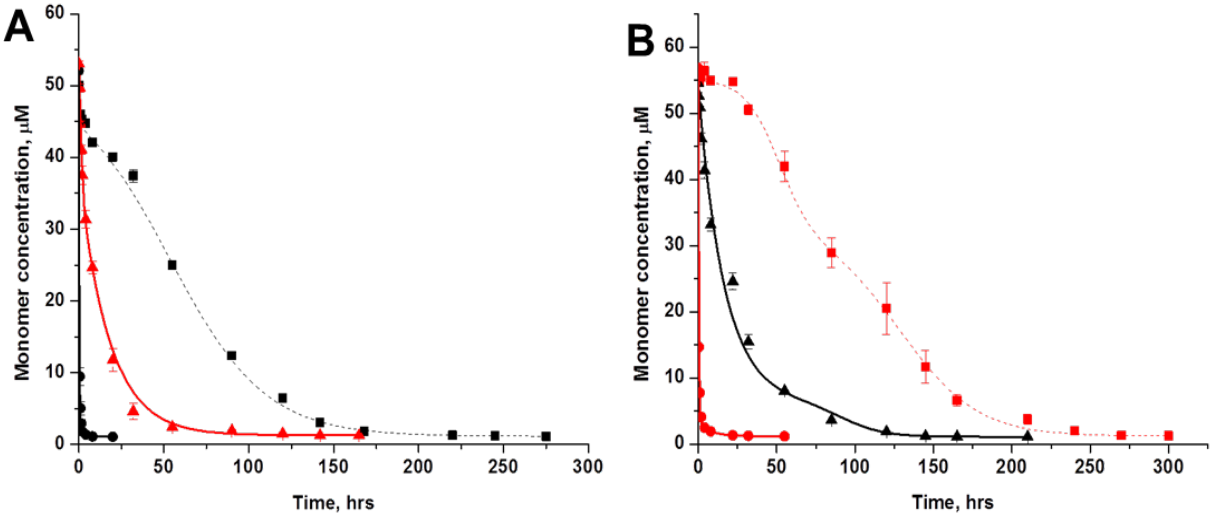

Figure 6-4: Seeded elongation of L-Aβ40 and D-Aβ40 monomers with various aggregates
A.Aggregation kinetics of 30 μM reaction of L-Aβ40 monomer with no seed (■) and seeded with 10% (w/w) of L-Aβ40 (●) and D-Aβ40 (▲) aggregates. B. Aggregation kinetics of 30 μM reaction of D-Aβ40 monomer with no seed (■) and seeded with 10% (w/w) of D-Aβ40 (●) and L-Aβ40 (▲) aggregates. Fits of the data points are done for visualization purposes only.

Table 6-1: Summary of results

	L-Aβ40 monomer	D-Aβ40 monomer
C_r, spontaneous growth[a]	1.07 ± 0.03 μM	1.22 ± 0.04 μM
$t_{½}$, spontaneous growth[a]	58 hrs	72 hrs
C_r, seeded growth, L-Aβ40 seed	1.02 ± 0.04 μM	1.131 ± 0.02 μM
C_r, seeded growth, D-Aβ40 seed	1.12 ± 0.03 μM	1.205 ± 0.012 μM
$t_{½}$, seeded growth, L-Aβ40 seed	0.5 hrs	22 hrs
$t_{½}$, seeded growth, D-Aβ40 seed	9 hrs	0.75 hrs
C_r, spontaneous growth, agitated[b]	0.22 ± 0.06 μM	0.49 ± 0.02 μM
$t_{½}$, spontaneous growth, agitated[b]	n.d.	8 hrs

[a] Peptides kept at 37 ºC PBS buffer under quiescent conditions [125]
[b] Peptides kept at 37 ºC PBS buffer under agitation conditions [125]

6.3.4 Presence of polymorphism in the D-Aβ40 system

Previous results from the lab has shown that in the case of L-Aβ40 peptide, varying structures of aggregates can be obtained under unique sets of spontaneous growth conditions [125]. The existence of these multiple amyloid forms is the basis of strain effects in yeast prion biology and might contribute to the variations in AD pathology as well. We reported 5 distinct structures of fibrillar aggregates of L-Aβ40 peptide as well as a non-fibrillar aggregate induced in the presence of zinc ions [125]. These varying polymorphs also differ in parameters like Cr, ThT binding, EM morphology and HX-MS protection.

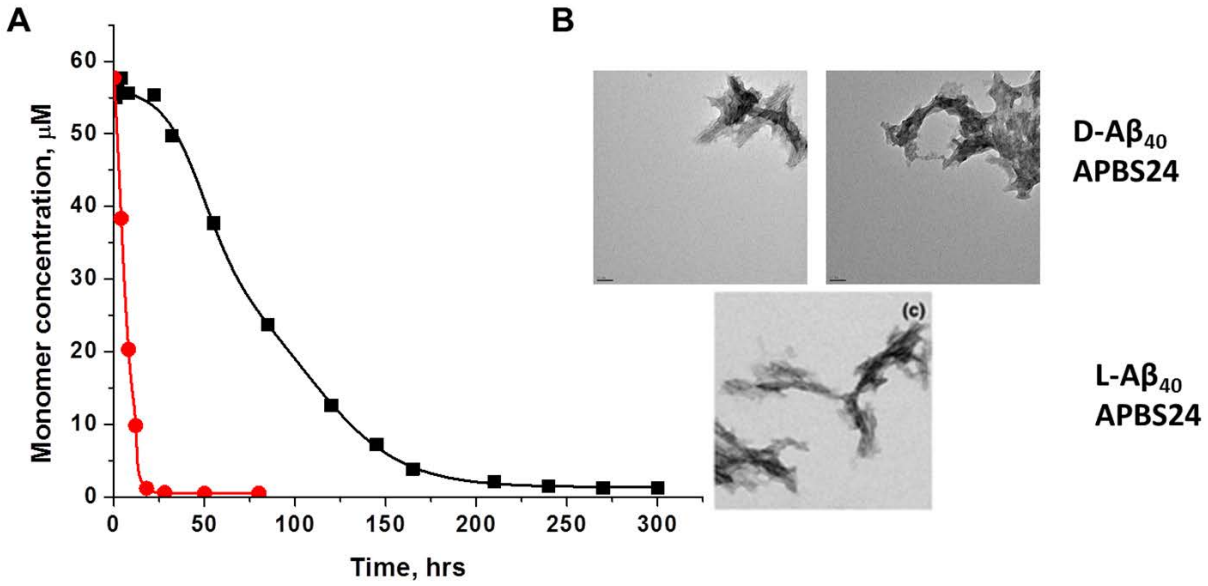

Figure 6-5: Presence of polymorphic form of D-Aβ40 aggegates
A.D-Aβ40 and L-Aβ40 peptides kept under quiescent conditions at 37 ºC (■) and agitating conditions at 24 ºC (●) [125]. The representative EM images are shown in B.

We wanted to see if such polymorphism is present in the D-$A\beta_{40}$ peptide enantiomer as well. We kept a reaction of D-$A\beta_{40}$ under agitation conditions at room temperature as was done previously for L-$A\beta_{40}$ peptide [125]. This polymorph was called L-$A\beta_{40}$ APBS24. We found that as in the case of L-$A\beta_{40}$ peptide, D-$A\beta_{40}$ aggregation was also greatly influenced by agitation. The aggregation proceeded faster with a $t_{1/2}$ of 8 hrs when compared to that of 72 hrs for quiescent conditions (**Figure 6-5 A**). The C_r was also much lower for the agitated fibrils (0.49 ± 0.02 μM) when compared to the quiescent D-$A\beta_{40}$ at 37 ºC (**Table 6-1**). EM morphology of the final fibrils was short, straight and they appear to be composed of laterally associated filaments lacking any twist (**Figure 6-5** B). Similar structures were seen previously for L-$A\beta_{40}$ peptide at agitated conditions (**Figure 6-5 B**).

6.4 DISCUSSION

The ability of amyloid fibrils to seed the elongation of protein monomers has been shown to be highly sequence specific. Previous results showed stringent chiral specificity in amyloid seeding reactions. In one study with radiolabeled Aβ enantiomers, Aβ deposition onto authentic brain amyloid was highly stereospecific [246]. This assay was done by studying deposition of a very low concentration of radio-iodinated, monomeric Aβ onto a synthetic template of immobilized fibrillar L-$A\beta_{40}$ aggregates on a polymer matrix. There are several possible explanations for why cross-seeding was not seen previously. One possibility is that the chemical synthesis of the D-$A\beta_{40}$ suffered from the same problems as some of our attempted syntheses, as outlined earlier (**Chapter 3**) and in the **Appendix A**. Another, probably more significant, possibility is that the effort to observe cross-seeding was doomed to fail due to the very low

concentration of labelled Aβ monomers used. In our previous paper on achiral cross-seeding of polyQ fibrils, we reported that the difference between homologous and heterologous seeding efficiencies increased as concentration decreased [252]. This is probably due to the different stereochemical requirements of the critical first step of cross-seeded elongation in what has been termed the "dock-and-lock" mechanism of amyloid fibril elongation. In the polyQ experiments, our group was able to show that the docking of a monomer to a fibril of opposite chirality has an especially restrictive concentration dependence compared to chiral self-seeding. That means that the barrier to cross-seeding can be overcome by raising the monomer concentration to effectively "saturate" the fibril growth surface. It is important to note that in the Aβ experiments described here, our monomer concentrations were substantially higher than those used by the Maggio group [246].

Previously, our lab has showed that in the case of PolyQ aggregates, there is stereochemical compatability between D-monomers and L-aggregates (and vice-versa) in an anti-parallel arrangement [252]. The cross-seeding seen between D-monomers and L-aggregates is not as efficient as self-seeding but is much greater than spontaneous aggregation. This model of chiral cross-seeding was anticipated previously by Pauling and Corey and they proposed the anti-parallel 'rippled' β-sheet model [253]. We show here that this cross-seeding is equally efficient in a much more complex system like Aβ which has a typical complex sequence and also a parallel, in-register β-sheet arrangement. It is important to emphasize, however, that in contrast to mixed D- and L-peptide β-sheets, D- and L-peptide amyloid cross-seeding only requires a single "rippled β-sheet" interface to form, and then only long enough for the elongation of the new fibrils to be established.

As expected D-Aβ$_{40}$ behaves just like a mirror-image of the L-peptide and forms aggregates in spontaneous growth which are similar to the L-aggregates in all the properties measured. This confirms the previous in vitro studies on D-Aβ$_{40}$ aggregates where they show similar biophysical properties to the aggregates like that of the corresponding L-aggregates [246]. When aggregation reactions are initiated with 10% by weight of cross-seeded fibrils, we found a significant amount of stimulation when compared to the unseeded reactions (3-6 fold). The amount of enhancement is similar to what was seen in the case of polyQ cross-seeded reactions which shows that the reactions are not influenced by the complexity of the Aβ sequence and the parallel β-sheet nature of its amyloid fibrils. In fact, like the rippled anti-parallel β-sheet, rippled parallel β-sheets between L- and D-polypeptides were also proposed by Pauling and Corey, featuring a structure that has no steric clashes and acceptable values of H-bond distances and bond angles (**Figure 6-6**) [253].

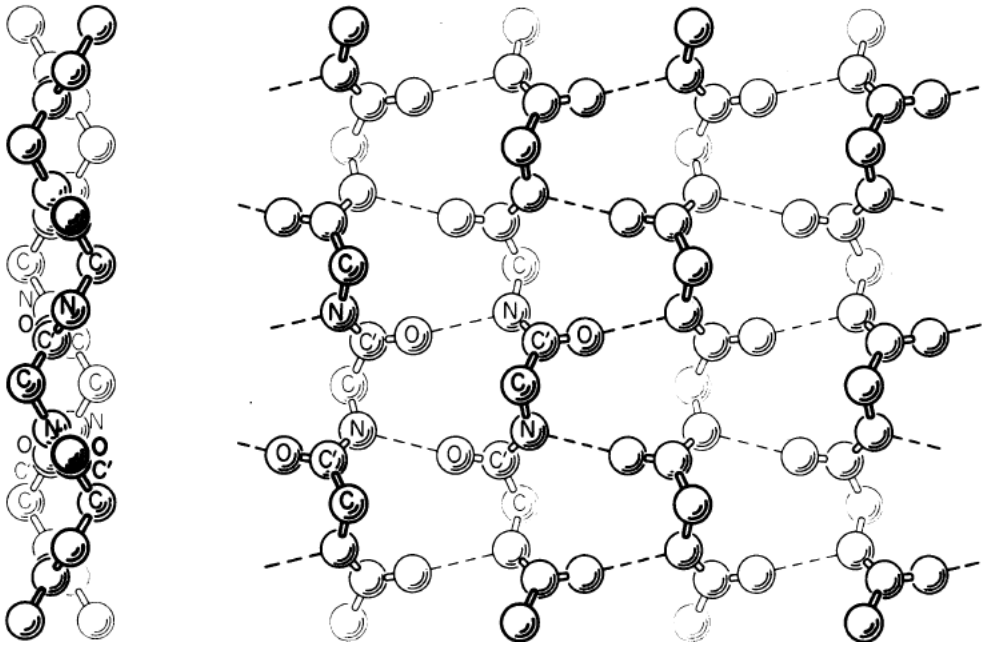

Figure 6-6: Parallel chain 'rippled' β-sheet model of hydrogen bonded polypeptide chains ([253])

One interesting aspect of achiral cross-seeding is that, at least in a highly unusual way, it breaks the paradigm often observed and more often assumed in amyloid studies, which holds that if seeding enhances amyloid formation kinetics, the structure of the product fibrils will necessarily adopt structural features of the seed fibrils. In the D, L cross-seeding described here and in the case of polyQ [252], we observe quite good acceleration of assembly kinetics in a situation where it is physically impossible for the product fibrils to take on, at the atomic level, the structure of the seed fibrils. This is of course due to the adventitious alignment of H-bond donor and acceptor groups in the extended conformations of both the fibril growth edge and the incoming monomer, in spite of their opposing chiralities at their α-carbons. Based on unpublished data from our laboratory, it seems likely that there are other, less trivial, examples of seeded reaction products that, although formed by rapid kinetics, do not replicate the structure of the seed. Such results will require the field to reexamine this basic assumption and how it underpins some structural arguments and analyses.

7.0 CONCLUSIONS

Previous work from the lab on Aβ focused predominantly on the in vitro characterization of aggregates formed in $A\beta_{40}$ background. Structural features of $A\beta_{40}$ fibrils were elucidated by limited proteolysis [153], hydrogen-deuterium exchange [108, 115, 150, 156, 261, 262], thioflavin binding [233], stability measurements [123, 124], and mutational analysis [261]. Seeded fibril elongation studies on single point mutants of $A\beta_{40}$ also provide descriptions on the structure of the fibrils. The kinetics and the thermodynamic parameters involved in the in vitro aggregation of $A\beta_{40}$, including the steps involved in nucleation and elongation have been studied by employing a variety of methods. It was shown that aggregation proceeds to a reversible equilibrium position exhibiting a characteristic equilibrium constant and associated free energy of elongation ([124]). The lab has also previously shown the polymorphic structures, ability of a single polypeptide chain to grow into more than one stable structure, exist in the case of $A\beta_{40}$ molecule each of which can propagate with retention of its structure [125]. The experiments done previously show that external factors, like conditions of amyloid growth, could lead to variations in details of H-bonding in the structures which can differ significantly between the polymorphs.

We were interested in extending the $A\beta_{40}$ work in understanding the fibril formation mechanism in the $A\beta_{42}$ background based on its stronger association to AD pathology. Historically, our source for obtaining these biologically relevant molecules has primarily been

solid phase peptide synthesis. This offers us the ease to work with these peptides and also gives us a much cheaper way to study them when compared to the recombinant synthesis, provided we get a pure starting material to work with. Based on the inherent nature of the technique, however, chemically synthesized peptides often have other impurities which are mostly deletion fragments of the desired peptide. These impurities need to be avoided during synthesis and separated after synthesis to obtain the pure material. Chemical synthesis and subsequent purification of $A\beta_{40}$ peptides are not very challenging and result in pure peptides with high yields and > 95% purity. But addition of C-terminal hydrophobic residues to generate Aβ molecules of longer lengths create a much more difficult synthesis resulting in lower yields and purities of the resulting peptides. This is because of the inherent hydrophobicity of these longer Aβ sequences which results in aggregation during synthesis. In **Chapter 3**, we describe a new method of reversible addition of C-terminal flanking charged residues to Aβ peptides to significantly improve their synthetic quality, yield and purity [157]. We linked 2-6 Lys residues to the Aβ peptide's C-terminus through peptide bonds during the synthesis. These extra charged residues are then removed post-purification using an immobilized CPB column. With this method, we obtained both longer Aβ sequences, such as $A\beta_{42}$ and $A\beta_{46}$ peptides, of much higher yields and purities than those obtained without Lys addition. This method is robust and can be applicable as a general useful method for making other difficult-to-synthesize hydrophobic peptides which are otherwise problematic to synthesize using conventional chemical synthesis.

Previous work in the lab on $A\beta_{42}$ peptides, looked at the structures of their aggregates by HX-MS methodology, which has been developed with great precision to study $A\beta_{40}$ peptides. Studies of $A\beta_{42}$, obtained using the lab's standard protocols for disaggregating Aβ peptides, suggested that the final aggregation product sometimes represents an incomplete aggregation

reaction, resulting in a mixed population of fibrils and unusually stable intermediates with lower HX-MS protection values. In **Chapter 4**, we confirmed the previous findings that the standard disaggregation method that is consistently successful for $A\beta_{40}$ peptides leads to incomplete fibril formation reaction with $A\beta_{42}$ peptides. We confirmed that the behavior of $A\beta_{42}$ is not related to intrinsic properties of the peptide by following $A\beta_{42}$ aggregation of peptide disaggregated by a different method - dissolution of peptide in a strong denaturing agent (Gdn-HCl) followed by monomer isolation *via* SEC [143]. This technique indeed solved the problem of incomplete aggregation and gave a homogenous fibril population for $A\beta_{42}$ peptide, even when incubated at relatively high concentrations, which is comparable to those obtained with $A\beta_{40}$. Investigations into why the two methods differ were inconclusive, and further studies need to be done to fully explain the source of the problem with the TFA-HFIP method. Nonetheless, from a practical point of view, the results obtained clearly show that choosing the right disaggregation method can play a significant role in determining the course and products of an aggregation reaction. Each disaggregation method has strengths and weaknesses which sometimes dictate the choice of method, but the weaknesses even of the chosen method must always be kept in mind.

In **Chapter 5**, we shifted our focus to a fundamental analysis of another variant of Aβ, $A\beta_{43}$, which is typically present at low levels (1% of $A\beta_{40}$; 10% of $A\beta_{42}$) compared with the predominant Aβ forms. It has been earlier proposed that the longer C-terminal variants of Aβ would tend to be more hydrophobic and hence could have an impact on Aβ aggregation out of proportion to its brain content [227]. We carried out in vitro comparative analysis of the aggregation of $A\beta_{42}$, $A\beta_{43}$ and their mixtures. We found out that $A\beta_{43}$ passes through the oligomeric intermediate stage considerably more slowly than $A\beta_{42}$ before eventually arriving at mature amyloid fibrils. The presence of prolonged oligomers could be the reason for its proposed

potent neurotoxicity [52]. We also found, contrary to expectations, that $A\beta_{43}$ fibrils are very inefficient in seeding $A\beta_{42}$ amyloid formation, even though $A\beta_{42}$ fibrils seed fibril formation by $A\beta_{42}$ and $A\beta_{43}$ monomers equally well. The results together suggest that low levels of $A\beta_{43}$ in the brain are unlikely to favorably impact the aggregation of $A\beta_{42}$ which is contrary to previous data on $A\beta_{43}$.

In **Chapter 6**, in another fundamental study, we probed one of the key features of amyloid assembly, seeded elongation, with respect to its stereochemical specificity. The fidelity of this process has been previously studied to look at various structural polymorphs of Aβ and also as a model for prion propagation. Early studies on the role of chirality suggested that chiral cross-seeding is not feasible between two opposite enantiomers [246]. But our lab recently reported that D- and L-polyglutamine can engage in efficient cross-seeding, presumably through a "rippled β-sheet" interface between the seed and incoming monomer in the anti-parallel β-sheet core of polyQ amyloid [252]. To examine if this cross-seeding is a general phenomenon common to other amyloid systems, we extended this study in the Aβ background, by probing the self-assembly and chiral cross-seeding of the D-and L-enantiomers of $A\beta_{40}$ in vitro. In contrast to an old literature report, we found cross-seeding efficiency similar to what we reported previously for polyQ amyloid. This suggests that cross-seeding, surprisingly, is not chirally discriminating and can also occur through a similar 'rippled' β-sheet interface in the parallel, in-register structure of the Aβ amyloid core. The possibility that a rippled β-sheet can be assembled from alternating strands of L- and D-peptides organized in parallel β-sheet was proposed by Linus Pauling in a theoretical analysis in the 1950s, long before the nature of amyloid was known [253]. Our results suggest some interesting contradictions or caveats to the general impression

that seeded elongation consistently propagates the structure of the seed, and thus raises issues of potential importance to prion biology.

APPENDIX A

IMPORTANCE OF COUPLING AGENT IN Aβ SYNTHESIS

A.1 PROBLEMS WITH D-Aβ$_{40}$ SYNTHESIS

D-Aβ$_{40}$ peptide synthesized using the regular Fmoc synthesis protocol from Keck Biotechnology Center at Yale University was defective and did not aggregate efficiently (**Figure A-1, Table A-1**). It aggregated from a starting monomer concentration of 37 μM to about a final concentration of 30.3 μM. We tried exploring the reason for this defect by synthesizing D-Aβ$_{40}$ peptide with other coupling agents. Two other coupling agents were employed: COMU and HATU. During solid phase synthesis, peptides are synthesized by coupling the carboxyl group of the incoming monomeric amino acid to the amino group at the N-terminus of the growing peptide chain. For coupling, the carboxyl group is usually activated. This is important for speeding up the reaction. One of the popular groups of activating agents are triazoles. HBTU, COMU and HATU fall under this group of activating agents. HATU and COMU are newly developed activating agents which have been proven to be very efficient in difficult sterically hindered couplings and usually give a minimal levels of racemization.

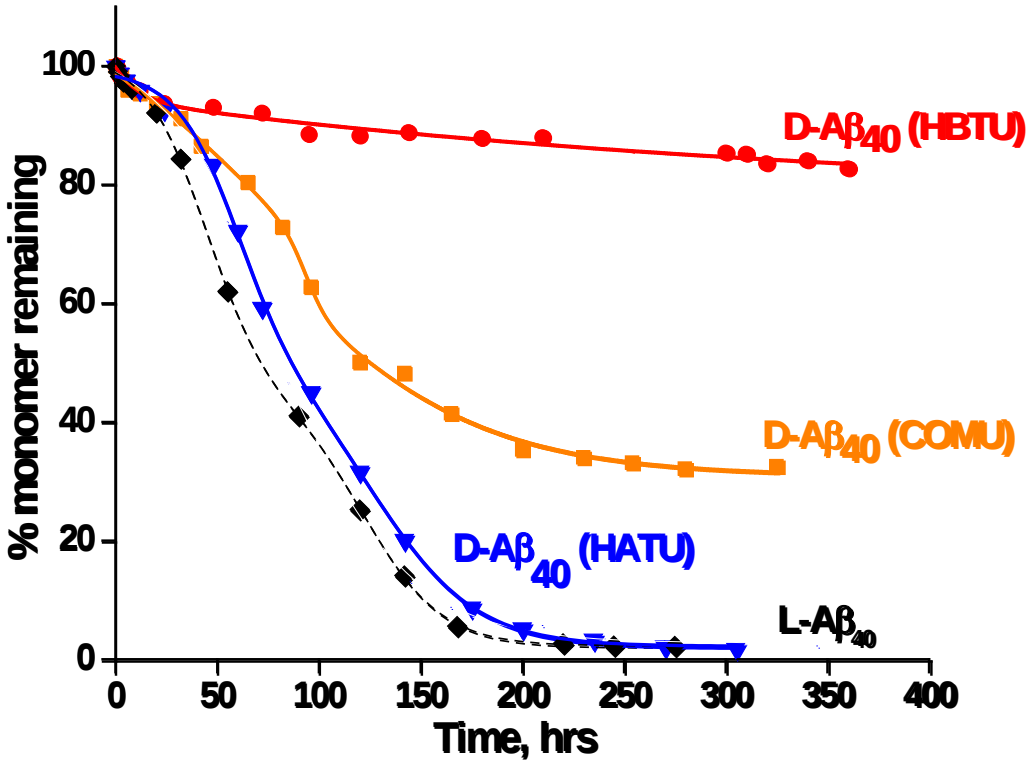

Figure A-1: Aggregation kinetics of D-Aβ40 peptides synthesized with different activating agents
The peptides were purified (2.1.1) and disaggregated using the Gdn-HCl method (2.1.4). The starting monomer concentrations of these peptides are: 37 μM (D-Aβ40 HBTU), 30 μM (D-Aβ40 HATU), 7 μM (D-Aβ40 COMU) (2.1.5). By comparison, a 32 μM reaction of L-Aβ40 is shown.

From **Figure** A-1, it is clear that D-Aβ40 peptide synthesized via COMU and HATU activating agent behaves much better than the peptide synthesized with HBTU as activating agent. The figure is somewhat misleading as to the relative efficiencies of these reactions since it is plotted as percent monomer rather than concentration, and the starting concentrations, out of necessity, were quite different. The graph suggests that the COMU product was not as good as aggregating as the HATU product, but this is not the case: the peptides from these 2 activating agents actually aggregate to essentially the same final equilibrium concentrations of 1.5 μM and 1.15 μM respectively, which are comparable to the equilibrium concentrations obtained from L-

$A\beta_{40}$ peptide synthesized with HATU as activating agent 1.07 μM (Table A-1). The problem with COMU turned out to be that it gave very poor yields of ~2% of the pure peptide from the crude when compared to ~17% for HATU product. The low COMU yield was probably due to a previously unreported high degree of instability of the COMU agent, which meant that it decomposed during the prolonged automated synthesis of the $A\beta_{40}$ and hence was less effective, especially in the last coupling steps. Hence we chose to focus on HATU as a potentially improved coupling agent.

Table A-1: D-$A\beta_{40}$ final equilibrium concentration values

Peptide	Final concentrations (μM)
D-$A\beta_{40}$ (HBTU)	30.3
D-$A\beta_{40}$ (COMU)	1.5
D-$A\beta_{40}$ (HATU)	1.15
L-$A\beta_{40}$ (HATU)	1.07

A.2 ENANTIOMETRIC PURITY ANALYSIS

One of the reasons for this big difference in the aggregation propensity of these peptides could arise from impurities in the peptide. It has been previously shown that even small amounts of impurities in the form of racemized peptides in synthetic Aβ, prevent or slow Aβ incorporation into amyloid fibrils [173]. Hence we were interested in seeing if the differences in the aggregation of various D-peptides are due to the differences in the amounts of impure L-enantiomer content. For this D-enantiomer analysis, we sent the samples to C.A.T. GmBH &

Co, Tubingen, Germany (www.cat-online.com), who used gas chromatography on a chiral matrix to separate L- and D-enantiomers of amino acids. Given the cost of the analysis, we asked them to focus only on those amino acids considered to be more susceptible to racemization during peptide synthesis. The results of the analysis done on D-$A\beta_{40}$ (HBTU) and D-$A\beta_{40}$ (HBTU) are shown in Table A-2.

Table A-2: Racemate Analysis of synthetic D-$A\beta_{40}$ (HBTU)

Amino acid	**L-enantiomer content (%)[a]**
alanine	0.20 %
valine	< 0.10 %
isoleucine	< 0.10 % (L-isoleucine) 0.12 % L-allo-isoleucine
serine	1.15 %
aspartate and asparagine	1.11 %
methionine	7.78 %
phenylalanine	0.39 %
glutamate and glutamine	0.68 %
tyrosine	0.33 %
lysine	0.49 %
arginine	0.22 %
histidine	1.02 %

[a] % L -enantiomer content analysis in D-$A\beta_{40}$ molecules was carried out by GC-MS methodology

As can be seen from **Table A-2**, most of the amino acids have a significant % of L-enantiomer impurity. The impure D-Aβ_{40} molecules containing these L-enantiomers cannot be separated from the pure all-D form of the peptide by conventional RP-HPLC alone. These impurities have similar masses and similar covalent structures to the pure authentic D-Aβ_{40} molecule. Hence, these impurities could contribute to the lack of aggregation in this peptide. This finding agrees well with a previous study showing that synthetic L-Aβ variants containing racemic impurities exhibit altered aggregation kinetics ([173]).

However, upon racemate analysis of the D-Aβ_{40} (HATU) molecule which aggregates as well as the L-Aβ_{40}, it was found that this peptide also contains significant amount of racemic impurities (**Table A-3)**.

Table A-3: Racemate Analysis of synthetic D-Aβ_{40} (HATU)

Amino acid	**D-enantiomer content (%)**
leucine	0.38 %
aspartic acid	2.45 %
methionine	6.88 %
histidine	2.26 %

Hence, the differences in the peptide aggregation properties of the various D-Aβ_{40} peptides cannot be just explained with the amount of racemate impurities present in one sample when compared to the other. Furthermore, in subsequent studies we found variable results in aggregation ability even with peptides synthesized with HATU. Thus, our findings that some synthetic D-Aβ peptides with similar degrees of purity exhibit widely different abilities to aggregate remains unexplained and quite mysterious.

BIBLIOGRAPHY

1. Brookmeyer, R., et al., *Forecasting the global burden of Alzheimer's disease.* Alzheimers Dement, 2007. **3**(3): p. 186-91.

2. Berrios, G., *Dementia: historical overview*, in *Dementia: Second edition*, D. Ames, A. Burns, and J. O'Brien, Editors. 2000, A Hodder Arnold Publication. p. 1-12.

3. Kidd, M., *Paired helical filaments in electron microscopy of Alzheimer's disease.* Nature, 1963. **197**: p. 192-3.

4. Kidd, M., *Alzheimer's Disease--an Electron Microscopical Study.* Brain, 1964. **87**: p. 307-20.

5. Terry, R.D., *The Fine Structure of Neurofibrillary Tangles in Alzheimer's Disease.* J Neuropathol Exp Neurol, 1963. **22**: p. 629-42.

6. Terry, R.D., N.K. Gonatas, and M. Weiss, *Ultrastructural Studies in Alzheimer's Presenile Dementia.* Am J Pathol, 1964. **44**: p. 269-97.

7. Glenner, G.G. and C.W. Wong, *Alzheimer's disease: initial report of the purification and characterization of a novel cerebrovascular amyloid protein.* Biochem Biophys Res Commun, 1984. **120**(3): p. 885-90.

8. Gorevic, P.D., et al., *Isolation and partial characterization of neurofibrillary tangles and amyloid plaque core in Alzheimer's disease: immunohistological studies.* J Neuropathol Exp Neurol, 1986. **45**(6): p. 647-64.

9. Masters, C.L., et al., *Amyloid plaque core protein in Alzheimer disease and Down syndrome.* Proc Natl Acad Sci U S A, 1985. **82**(12): p. 4245-9.

10. Selkoe, D.J., et al., *Isolation of low-molecular-weight proteins from amyloid plaque fibers in Alzheimer's disease.* J Neurochem, 1986. **46**(6): p. 1820-34.

11. Grundke-Iqbal, I., et al., *Abnormal phosphorylation of the microtubule-associated protein tau (tau) in Alzheimer cytoskeletal pathology.* Proc Natl Acad Sci U S A, 1986. **83**(13): p. 4913-7.

12. Kosik, K.S., C.L. Joachim, and D.J. Selkoe, *Microtubule-associated protein tau (tau) is a major antigenic component of paired helical filaments in Alzheimer disease.* Proc Natl Acad Sci U S A, 1986. **83**(11): p. 4044-8.

13. Nukina, N. and Y. Ihara, *One of the antigenic determinants of paired helical filaments is related to tau protein.* J Biochem, 1986. **99**(5): p. 1541-4.

14. Wood, J.G., et al., *Neurofibrillary tangles of Alzheimer disease share antigenic determinants with the axonal microtubule-associated protein tau (tau).* Proc Natl Acad Sci U S A, 1986. **83**(11): p. 4040-3.

15. Weingarten, M.D., et al., *A protein factor essential for microtubule assembly.* Proc Natl Acad Sci U S A, 1975. **72**(5): p. 1858-62.

16. Kosik, K.S., *Tau protein and neurodegeneration.* Mol Neurobiol, 1990. **4**(3-4): p. 171-9.

17. Ballatore, C., V.M. Lee, and J.Q. Trojanowski, *Tau-mediated neurodegeneration in Alzheimer's disease and related disorders.* Nat Rev Neurosci, 2007. **8**(9): p. 663-72.

18. Lee, V.M., M. Goedert, and J.Q. Trojanowski, *Neurodegenerative tauopathies.* Annu Rev Neurosci, 2001. **24**: p. 1121-59.

19. Terry, R.D., et al., *Senile dementia of the Alzheimer type without neocortical neurofibrillary tangles.* J Neuropathol Exp Neurol, 1987. **46**(3): p. 262-8.

20. Selkoe, D.J., *Alzheimer's disease: genes, proteins, and therapy.* Physiol Rev, 2001. **81**(2): p. 741-66.

21. Lai, F. and R.S. Williams, *A prospective study of Alzheimer disease in Down syndrome.* Arch Neurol, 1989. **46**(8): p. 849-53.

22. Rumble, B., et al., *Amyloid A4 protein and its precursor in Down's syndrome and Alzheimer's disease.* N Engl J Med, 1989. **320**(22): p. 1446-52.

23. Nilsberth, C., et al., *The 'Arctic' APP mutation (E693G) causes Alzheimer's disease by enhanced Abeta protofibril formation.* Nat Neurosci, 2001. **4**(9): p. 887-93.

24. Hendriks, L., et al., *Presenile dementia and cerebral haemorrhage linked to a mutation at codon 692 of the beta-amyloid precursor protein gene.* Nat Genet, 1992. **1**(3): p. 218-21.

25. Grabowski, T.J., et al., *Novel amyloid precursor protein mutation in an Iowa family with dementia and severe cerebral amyloid angiopathy.* Ann Neurol, 2001. **49**(6): p. 697-705.

26. Van Nostrand, W.E., et al., *Pathogenic effects of cerebral amyloid angiopathy mutations in the amyloid beta-protein precursor.* Ann N Y Acad Sci, 2002. **977**: p. 258-65.

27. Levy, E., et al., *Mutation of the Alzheimer's disease amyloid gene in hereditary cerebral hemorrhage, Dutch type.* Science, 1990. **248**(4959): p. 1124-6.

28. Tycko, R., et al., *Evidence for novel beta-sheet structures in Iowa mutant beta-amyloid fibrils.* Biochemistry, 2009. **48**(26): p. 6072-84.

29. Bitan, G., S.S. Vollers, and D.B. Teplow, *Elucidation of primary structure elements controlling early amyloid beta-protein oligomerization.* J Biol Chem, 2003. **278**(37): p. 34882-9.

30. Gessel, M.M., et al., *Familial Alzheimer's disease mutations differentially alter amyloid beta-protein oligomerization.* ACS Chem Neurosci. **3**(11): p. 909-18.

31. De Jonghe, C., et al., *Pathogenic APP mutations near the gamma-secretase cleavage site differentially affect Abeta secretion and APP C-terminal fragment stability.* Hum Mol Genet, 2001. **10**(16): p. 1665-71.

32. Guo, Q., et al., *Alzheimer's presenilin mutation sensitizes neural cells to apoptosis induced by trophic factor withdrawal and amyloid beta-peptide: involvement of calcium and oxyradicals.* J Neurosci, 1997. **17**(11): p. 4212-22.

33. Chan, S.L., et al., *Presenilin-1 mutations increase levels of ryanodine receptors and calcium release in PC12 cells and cortical neurons.* J Biol Chem, 2000. **275**(24): p. 18195-200.

34. Harper, J.D. and P.T. Lansbury, Jr., *Models of amyloid seeding in Alzheimer's disease and scrapie: mechanistic truths and physiological consequences of the time-dependent solubility of amyloid proteins.* Annu Rev Biochem, 1997. **66**: p. 385-407.

35. Selkoe, D.J., *The molecular pathology of Alzheimer's disease.* Neuron, 1991. **6**(4): p. 487-98.

36. LaFerla, F.M. and S. Oddo, *Alzheimer's disease: Abeta, tau and synaptic dysfunction.* Trends Mol Med, 2005. **11**(4): p. 170-6.

37. Chauhan, N.B. and G.J. Siegel, *Reversal of amyloid beta toxicity in Alzheimer's disease model Tg2576 by intraventricular antiamyloid beta antibody.* J Neurosci Res, 2002. **69**(1): p. 10-23.

38. Banks, W.A., et al., *Anti-amyloid beta protein antibody passage across the blood-brain barrier in the SAMP8 mouse model of Alzheimer's disease: an age-related selective uptake with reversal of learning impairment.* Exp Neurol, 2007. **206**(2): p. 248-56.

39. Selkoe, D.J., *Physiological production of the beta-amyloid protein and the mechanism of Alzheimer's disease.* Trends Neurosci, 1993. **16**(10): p. 403-9.

40. Selkoe, D.J., et al., *The role of APP processing and trafficking pathways in the formation of amyloid beta-protein.* Ann N Y Acad Sci, 1996. **777**: p. 57-64.

41. Haass, C., *Take five--BACE and the gamma-secretase quartet conduct Alzheimer's amyloid beta-peptide generation.* EMBO J, 2004. **23**(3): p. 483-8.

42. Haass, C., et al., *Trafficking and proteolytic processing of APP.* Cold Spring Harb Perspect Med. **2**(5): p. a006270.

43. Sastre, M., et al., *Presenilin-dependent gamma-secretase processing of beta-amyloid precursor protein at a site corresponding to the S3 cleavage of Notch.* EMBO Rep, 2001. **2**(9): p. 835-41.

44. Qi-Takahara, Y., et al., *Longer forms of amyloid beta protein: implications for the mechanism of intramembrane cleavage by gamma-secretase.* J Neurosci, 2005. **25**(2): p. 436-45.

45. Takami, M., et al., *gamma-Secretase: successive tripeptide and tetrapeptide release from the transmembrane domain of beta-carboxyl terminal fragment.* J Neurosci, 2009. **29**(41): p. 13042-52.

46. Yagishita, S., et al., *DAPT-induced intracellular accumulations of longer amyloid beta-proteins: further implications for the mechanism of intramembrane cleavage by gamma-secretase.* Biochemistry, 2006. **45**(12): p. 3952-60.

47. Zhao, G., et al., *gamma-Cleavage is dependent on zeta-cleavage during the proteolytic processing of amyloid precursor protein within its transmembrane domain.* J Biol Chem, 2005. **280**(45): p. 37689-97.

48. Selkoe, D.J., *Normal and abnormal biology of the beta-amyloid precursor protein.* Annu Rev Neurosci, 1994. **17**: p. 489-517.

49. Dahlgren, K.N., et al., *Oligomeric and fibrillar species of amyloid-beta peptides differentially affect neuronal viability.* J Biol Chem, 2002. **277**(35): p. 32046-32053.

50. Shankar, G.M., et al., *Amyloid-beta protein dimers isolated directly from Alzheimer's brains impair synaptic plasticity and memory.* Nat Med, 2008. **14**(8): p. 837-42.

51. Sandebring, A., et al., *The pathogenic abeta43 is enriched in familial and sporadic Alzheimer disease.* PLoS One. **8**(2): p. e55847.

52. Saito, T., et al., *Potent amyloidogenicity and pathogenicity of Abeta43.* Nat Neurosci. **14**(8): p. 1023-32.

53. Hardy, J. and D. Allsop, *Amyloid deposition as the central event in the aetiology of Alzheimer's disease.* Trends Pharmacol Sci, 1991. **12**(10): p. 383-8.

54. Mudher, A. and S. Lovestone, *Alzheimer's disease-do tauists and baptists finally shake hands?* Trends Neurosci, 2002. **25**(1): p. 22-6.

55. Lesne, S., et al., *A specific amyloid-beta protein assembly in the brain impairs memory.* Nature, 2006. **440**(7082): p. 352-7.

56. Townsend, M., et al., *Effects of secreted oligomers of amyloid beta-protein on hippocampal synaptic plasticity: a potent role for trimers.* J Physiol, 2006. **572**(Pt 2): p. 477-92.

57. Haass, C. and D.J. Selkoe, *Soluble protein oligomers in neurodegeneration: lessons from the Alzheimer's amyloid beta-peptide.* Nat Rev Mol Cell Biol, 2007. **8**(2): p. 101-12.

58. Klein, W.L., G.A. Krafft, and C.E. Finch, *Targeting small Abeta oligomers: the solution to an Alzheimer's disease conundrum?* Trends Neurosci, 2001. **24**(4): p. 219-24.

59. Mucke, L., et al., *High-level neuronal expression of abeta 1-42 in wild-type human amyloid protein precursor transgenic mice: synaptotoxicity without plaque formation.* J Neurosci, 2000. **20**(11): p. 4050-8.

60. Nelson, P.T., H. Braak, and W.R. Markesbery, *Neuropathology and cognitive impairment in Alzheimer disease: a complex but coherent relationship.* J Neuropathol Exp Neurol, 2009. **68**(1): p. 1-14.

61. Lambert, M.P., et al., *Diffusible, nonfibrillar ligands derived from Abeta1-42 are potent central nervous system neurotoxins.* Proc Natl Acad Sci U S A, 1998. **95**(11): p. 6448-53.

62. Campioni, S., et al., *A causative link between the structure of aberrant protein oligomers and their toxicity.* Nat Chem Biol. **6**(2): p. 140-7.

63. Demuro, A., et al., *Calcium dysregulation and membrane disruption as a ubiquitous neurotoxic mechanism of soluble amyloid oligomers.* J Biol Chem, 2005. **280**(17): p. 17294-300.

64. Kourie, J.I., et al., *Heterogeneous amyloid-formed ion channels as a common cytotoxic mechanism: implications for therapeutic strategies against amyloidosis.* Cell Biochem Biophys, 2002. **36**(2-3): p. 191-207.

65. Kayed, R., et al., *Permeabilization of lipid bilayers is a common conformation-dependent activity of soluble amyloid oligomers in protein misfolding diseases.* J Biol Chem, 2004. **279**(45): p. 46363-6.

66. Fagan, T., et al., *Alzheimer Research Forum Live Discussion: Now you see them, now you don't: The amyloid channel hypothesis.* J Alzheimers Dis, 2006. **9**(2): p. 219-24.

67. Lashuel, H.A. and P.T. Lansbury, Jr., *Are amyloid diseases caused by protein aggregates that mimic bacterial pore-forming toxins?* Q Rev Biophys, 2006. **39**(2): p. 167-201.

68. Dong, Z., et al., *Calcium in cell injury and death.* Annu Rev Pathol, 2006. **1**: p. 405-34.

69. Lauren, J., et al., *Cellular prion protein mediates impairment of synaptic plasticity by amyloid-beta oligomers.* Nature, 2009. **457**(7233): p. 1128-32.

70. Anfinsen, C.B., *Principles that govern the folding of protein chains.* Science, 1973. **181**(4096): p. 223-30.

71. Westermark, G.T., K.H. Johnson, and P. Westermark, *Staining methods for identification of amyloid in tissue.* Methods Enzymol, 1999. **309**: p. 3-25.

72. Lin, C.Y., et al., *Toxic human islet amyloid polypeptide (h-IAPP) oligomers are intracellular, and vaccination to induce anti-toxic oligomer antibodies does not prevent h-IAPP-induced beta-cell apoptosis in h-IAPP transgenic mice.* Diabetes, 2007. **56**(5): p. 1324-32.

73. Fandrich, M., *On the structural definition of amyloid fibrils and other polypeptide aggregates.* Cell Mol Life Sci, 2007. **64**(16): p. 2066-78.

74. Qiang, W., et al., *Antiparallel beta-sheet architecture in Iowa-mutant beta-amyloid fibrils.* Proc Natl Acad Sci U S A. **109**(12): p. 4443-8.

75. Irvine, G.B., et al., *Protein aggregation in the brain: the molecular basis for Alzheimer's and Parkinson's diseases.* Mol Med, 2008. **14**(7-8): p. 451-64.

76. Ferreira, S.T., M.N. Vieira, and F.G. De Felice, *Soluble protein oligomers as emerging toxins in Alzheimer's and other amyloid diseases.* IUBMB Life, 2007. **59**(4-5): p. 332-45.

77. Chiang, P.K., M.A. Lam, and Y. Luo, *The many faces of amyloid beta in Alzheimer's disease.* Curr Mol Med, 2008. **8**(6): p. 580-4.

78. Truant, R., et al., *Huntington's disease: revisiting the aggregation hypothesis in polyglutamine neurodegenerative diseases.* FEBS J, 2008. **275**(17): p. 4252-62.

79. Prusiner, S.B., *Molecular biology of prion diseases.* Science, 1991. **252**(5012): p. 1515-22.

80. Yankner, B.A., L.K. Duffy, and D.A. Kirschner, *Neurotrophic and neurotoxic effects of amyloid beta protein: reversal by tachykinin neuropeptides.* Science, 1990. **250**(4978): p. 279-82.

81. Wirak, D.O., et al., *Deposits of amyloid beta protein in the central nervous system of transgenic mice.* Science, 1991. **253**(5017): p. 323-5.

82. Selkoe, D.J., *Alzheimer's disease. Missense on the membrane.* Nature, 1995. **375**(6534): p. 734-5.

83. Duff, K., et al., *Increased amyloid-beta42(43) in brains of mice expressing mutant presenilin 1.* Nature, 1996. **383**(6602): p. 710-3.

84. Walsh, D.M., et al., *Naturally secreted oligomers of amyloid beta protein potently inhibit hippocampal long-term potentiation in vivo.* Nature, 2002. **416**(6880): p. 535-9.

85. Kayed, R., et al., *Common structure of soluble amyloid oligomers implies common mechanism of pathogenesis.* Science, 2003. **300**(5618): p. 486-9.

86. Sanchez, I., C. Mahlke, and J. Yuan, *Pivotal role of oligomerization in expanded polyglutamine neurodegenerative disorders.* Nature, 2003. **421**(6921): p. 373-9.

87. Bitan, G., et al., *Amyloid beta -protein (Abeta) assembly: Abeta 40 and Abeta 42 oligomerize through distinct pathways.* Proc Natl Acad Sci U S A, 2003. **100**(1): p. 330-5.

88. Bernstein, S.L., et al., *Amyloid beta-protein: monomer structure and early aggregation states of Abeta42 and its Pro19 alloform.* J Am Chem Soc, 2005. **127**(7): p. 2075-84.

89. Sitkiewicz, E., et al., *Di-tyrosine cross-link decreases the collisional cross-section of abeta peptide dimers and trimers in the gas phase: an ion mobility study.* PLoS One. **9**(6): p. e100200.

90. Garzon-Rodriguez, W., et al., *Soluble amyloid Abeta-(1-40) exists as a stable dimer at low concentrations.* J Biol Chem, 1997. **272**(34): p. 21037-44.

91. Bitan, G., A. Lomakin, and D.B. Teplow, *Amyloid beta-protein oligomerization: prenucleation interactions revealed by photo-induced cross-linking of unmodified proteins.* J Biol Chem, 2001. **276**(37): p. 35176-84.

92. Garai, K., et al., *Selective destabilization of soluble amyloid beta oligomers by divalent metal ions.* Biochem Biophys Res Commun, 2006. **345**(1): p. 210-5.

93. Kumar, S. and J. Walter, *Phosphorylation of amyloid beta (A beta) peptides - A trigger for formation of toxic aggregates in Alzheimer's disease.* Aging-Us, 2011. **3**(8): p. 803-812.

94. Harper, J.D., et al., *Observation of metastable Abeta amyloid protofibrils by atomic force microscopy.* Chem Biol, 1997. **4**(2): p. 119-25.

95. Hartley, D.M., et al., *Protofibrillar intermediates of amyloid beta-protein induce acute electrophysiological changes and progressive neurotoxicity in cortical neurons.* J Neurosci, 1999. **19**(20): p. 8876-84.

96. Walsh, D.M., et al., *Amyloid beta-protein fibrillogenesis. Detection of a protofibrillar intermediate.* J Biol Chem, 1997. **272**(35): p. 22364-72.

97. Walsh, D.M., et al., *Amyloid beta-protein fibrillogenesis. Structure and biological activity of protofibrillar intermediates.* J Biol Chem, 1999. **274**(36): p. 25945-52.

98. Lashuel, H.A., et al., *Neurodegenerative disease: amyloid pores from pathogenic mutations.* Nature, 2002. **418**(6895): p. 291.

99. Gong, Y., et al., *Alzheimer's disease-affected brain: presence of oligomeric A beta ligands (ADDLs) suggests a molecular basis for reversible memory loss.* Proc Natl Acad Sci U S A, 2003. **100**(18): p. 10417-22.

100. Serra-Vidal, B., et al., *Hydrogen/Deuterium Exchange-Protected Oligomers Populated during Abeta Fibril Formation Correlate with Neuronal Cell Death.* ACS Chem Biol. **9**(11): p. 2678-85.

101. Lindgren, M. and P. Hammarstrom, *Amyloid oligomers: spectroscopic characterization of amyloidogenic protein states.* FEBS J. **277**(6): p. 1380-8.

102. Jayaraman, M., et al., *Slow amyloid nucleation via alpha-helix-rich oligomeric intermediates in short polyglutamine-containing huntingtin fragments.* J Mol Biol. **415**(5): p. 881-99.

103. Kirkitadze, M.D., M.M. Condron, and D.B. Teplow, *Identification and characterization of key kinetic intermediates in amyloid beta-protein fibrillogenesis.* J Mol Biol, 2001. **312**(5): p. 1103-19.

104. Goldsbury, C.S., et al., *Studies on the in vitro assembly of a beta 1-40: implications for the search for a beta fibril formation inhibitors.* J Struct Biol, 2000. **130**(2-3): p. 217-31.

105. Sengupta, P., et al., *The amyloid beta peptide (Abeta(1-40)) is thermodynamically soluble at physiological concentrations.* Biochemistry, 2003. **42**(35): p. 10506-13.

106. Garai, K., et al., *Quasihomogeneous nucleation of amyloid beta yields numerical bounds for the critical radius, the surface tension, and the free energy barrier for nucleus formation.* J Chem Phys, 2008. **128**(4): p. 045102.

107. Serio, T.R., et al., *Nucleated conformational conversion and the replication of conformational information by a prion determinant.* Science, 2000. **289**(5483): p. 1317-21.

108. Kheterpal, I., et al., *Abeta protofibrils possess a stable core structure resistant to hydrogen exchange.* Biochemistry, 2003. **42**(48): p. 14092-8.

109. Tay, W.M., et al., *The Alzheimer's amyloid-beta(1-42) peptide forms off-pathway oligomers and fibrils that are distinguished structurally by intermolecular organization.* J Mol Biol. **425**(14): p. 2494-508.

110. Chen, Y.R. and C.G. Glabe, *Distinct early folding and aggregation properties of Alzheimer amyloid-beta peptides Abeta40 and Abeta42: stable trimer or tetramer formation by Abeta42.* J Biol Chem, 2006. **281**(34): p. 24414-22.

111. Smith, A.M., et al., *Direct observation of oligomeric species formed in the early stages of amyloid fibril formation using electrospray ionisation mass spectrometry.* J Mol Biol, 2006. **364**(1): p. 9-19.

112. Williams, A.D., et al., *Structural properties of Abeta protofibrils stabilized by a small molecule.* Proc Natl Acad Sci U S A, 2005. **102**(20): p. 7115-20.

113. Nichols, M.R., et al., *Amyloid-beta protofibrils differ from amyloid-beta aggregates induced in dilute hexafluoroisopropanol in stability and morphology.* J Biol Chem, 2005. **280**(4): p. 2471-80.

114. Sandberg, A., et al., *Stabilization of neurotoxic Alzheimer amyloid-beta oligomers by protein engineering.* Proc Natl Acad Sci U S A. **107**(35): p. 15595-600.

115. Kheterpal, I., et al., *Structural differences in Abeta amyloid protofibrils and fibrils mapped by hydrogen exchange--mass spectrometry with on-line proteolytic fragmentation.* J Mol Biol, 2006. **361**(4): p. 785-95.

116. Scheidt, H.A., I. Morgado, and D. Huster, *Solid-state NMR reveals a close structural relationship between amyloid-beta protofibrils and oligomers.* J Biol Chem. **287**(27): p. 22822-6.

117. Lendel, C., et al., *A Hexameric Peptide Barrel as Building Block of Amyloid-beta Protofibrils.* Angew Chem Int Ed Engl. **53**(47): p. 12756-60.

118. Fandrich, M., J. Meinhardt, and N. Grigorieff, *Structural polymorphism of Alzheimer A beta and other amyloid fibrils.* Prion, 2009. **3**(2): p. 89-93.

119. Sachse, C., M. Fandrich, and N. Grigorieff, *Paired beta-sheet structure of an A beta(1-40) amyloid fibril revealed by electron microscopy.* Proc Natl Acad Sci U S A, 2008. **105**(21): p. 7462-7466.

120. Lu, J.X., et al., *Molecular Structure of beta-Amyloid Fibrils in Alzheimer's Disease Brain Tissue.* Cell, 2013. **154**(6): p. 1257-1268.

121. Paravastu, A.K., et al., *Seeded growth of beta-amyloid fibrils from Alzheimer's brain-derived fibrils produces a distinct fibril structure.* Proc Natl Acad Sci U S A, 2009. **106**(18): p. 7443-8.

122. Schmidt, M., et al., *Comparison of Alzheimer Abeta(1-40) and Abeta(1-42) amyloid fibrils reveals similar protofilament structures.* Proc Natl Acad Sci U S A, 2009. **106**(47): p. 19813-8.

123. O'Nuallain, B., et al., *Kinetics and thermodynamics of amyloid assembly using a high-performance liquid chromatography-based sedimentation assay.* Methods Enzymol, 2006. **413**: p. 34-74.

124. O'Nuallain, B., et al., *Thermodynamics of A beta(1-40) amyloid fibril elongation.* Biochemistry, 2005. **44**(38): p. 12709-18.

125. Kodali, R., et al., *A beta(1-40) Forms Five Distinct Amyloid Structures whose beta-Sheet Contents and Fibril Stabilities Are Correlated.* J Mol Biol, 2010. **401**(3): p. 503-517.

126. Jarrett, J.T., E.P. Berger, and P.T. Lansbury, *The Carboxy Terminus of the Beta-Amyloid Protein Is Critical for the Seeding of Amyloid Formation - Implications for the Pathogenesis of Alzheimers-Disease.* Biochemistry, 1993. **32**(18): p. 4693-4697.

127. Clark, P.L., *Protein folding in the cell: reshaping the folding funnel.* Trends Biochem Sci, 2004. **29**(10): p. 527-34.

128. Lu, J.X., et al., *Molecular structure of beta-amyloid fibrils in Alzheimer's disease brain tissue.* Cell. **154**(6): p. 1257-68.

129. Luhrs, T., et al., *3D structure of Alzheimer's amyloid-beta(1-42) fibrils.* Proc Natl Acad Sci U S A, 2005. **102**(48): p. 17342-7.

130. Kodali, R. and R. Wetzel, *Polymorphism in the intermediates and products of amyloid assembly.* Curr Opin Struct Biol, 2007. **17**(1): p. 48-57.

131. Chiti, F., et al., *Designing conditions for in vitro formation of amyloid protofilaments and fibrils.* Proc Natl Acad Sci U S A, 1999. **96**(7): p. 3590-4.

132. Chamberlain, A.K., et al., *Ultrastructural organization of amyloid fibrils by atomic force microscopy.* Biophys J, 2000. **79**(6): p. 3282-93.

133. Tycko, R., *Solid-state NMR as a probe of amyloid structure.* Prot Pept Lett, 2006. **13**(3): p. 229-234.

134. Goldsbury, C.S., et al., *Polymorphic fibrillar assembly of human amylin.* J Struct Biol, 1997. **119**(1): p. 17-27.

135. Pedersen, J.S., et al., *The changing face of glucagon fibrillation: Structural polymorphism and conformational imprinting.* J Mol Biol, 2006. **355**(3): p. 501-523.

136. Jimenez, J.L., et al., *Cryo-electron microscopy structure of an SH3 amyloid fibril and model of the molecular packing.* Embo Journal, 1999. **18**(4): p. 815-821.

137. Jimenez, J.L., et al., *The protofilament structure of insulin amyloid fibrils.* Proc Natl Acad Sci U S A, 2002. **99**(14): p. 9196-201.

138. Frost, B. and M.I. Diamond, *Prion-like mechanisms in neurodegenerative diseases.* Nat Rev Neurosci. **11**(3): p. 155-9.

139. Duyckaerts, C., *Neurodegenerative lesions: seeding and spreading.* Rev Neurol (Paris). **169**(10): p. 825-33.

140. Costanzo, M. and C. Zurzolo, *The cell biology of prion-like spread of protein aggregates: mechanisms and implication in neurodegeneration.* Biochem J. **452**(1): p. 1-17.

141. Evans, K.C., et al., *Apolipoprotein E is a kinetic but not a thermodynamic inhibitor of amyloid formation: implications for the pathogenesis and treatment of Alzheimer disease.* Proc Natl Acad Sci U S A, 1995. **92**(3): p. 763-7.

142. Wood, S.J., et al., *Physical, morphological and functional differences between ph 5.8 and 7.4 aggregates of the Alzheimer's amyloid peptide Abeta.* J Mol Biol, 1996. **256**(5): p. 870-7.

143. Jan, A., D.M. Hartley, and H.A. Lashuel, *Preparation and characterization of toxic Abeta aggregates for structural and functional studies in Alzheimer's disease research.* Nat Protoc. **5**(6): p. 1186-209.

144. Kuipers, B.J. and H. Gruppen, *Prediction of molar extinction coefficients of proteins and peptides using UV absorption of the constituent amino acids at 214 nm to enable quantitative reverse phase high-performance liquid chromatography-mass spectrometry analysis.* J Agric Food Chem, 2007. **55**(14): p. 5445-51.

145. Stsiapura, V.I., et al., *Computational study of thioflavin T torsional relaxation in the excited state.* J Phys Chem A, 2007. **111**(22): p. 4829-35.

146. Amdursky, N., Y. Erez, and D. Huppert, *Molecular rotors: what lies behind the high sensitivity of the thioflavin-T fluorescent marker.* Acc Chem Res. **45**(9): p. 1548-57.

147. Jayaraman, M., et al., *Assays for studying nucleated aggregation of polyglutamine proteins.* Methods. **53**(3): p. 246-54.

148. Wetzel, R., *Kinetics and thermodynamics of amyloid fibril assembly.* Acc Chem Res, 2006. **39**(9): p. 671-9.

149. O'Nuallain, B., et al., *Thermodynamics of A beta(1-40) amyloid fibril elongation.* Biochemistry, 2005. **44**(38): p. 12709-12718.

150. Kheterpal, I., et al., *Abeta amyloid fibrils possess a core structure highly resistant to hydrogen exchange.* Proc Natl Acad Sci U S A, 2000. **97**(25): p. 13597-601.

151. Hodkinson, J.P., S.E. Radford, and A.E. Ashcroft, *The role of conformational flexibility in beta2-microglobulin amyloid fibril formation at neutral pH.* Rapid Commun Mass Spectrom. **26**(16): p. 1783-92.

152. Liu, K., et al., *Deuterium-proton exchange on the native wild-type transthyretin tetramer identifies the stable core of the individual subunits and indicates mobility at the subunit interface.* J Mol Biol, 2000. **303**(4): p. 555-65.

153. Kheterpal, I., et al., *Structural features of the Abeta amyloid fibril elucidated by limited proteolysis.* Biochemistry, 2001. **40**(39): p. 11757-67.

154. Lu, X., P.L. Wintrode, and W.K. Surewicz, *Beta-sheet core of human prion protein amyloid fibrils as determined by hydrogen/deuterium exchange.* Proc Natl Acad Sci U S A, 2007. **104**(5): p. 1510-5.

155. Smirnovas, V., et al., *Distinct structures of scrapie prion protein (PrPSc)-seeded versus spontaneous recombinant prion protein fibrils revealed by hydrogen/deuterium exchange.* J Biol Chem, 2009. **284**(36): p. 24233-41.

156. Kheterpal, I., K.D. Cook, and R. Wetzel, *Hydrogen/deuterium exchange mass spectrometry analysis of protein aggregates.* Methods Enzymol, 2006. **413**: p. 140-66.

157. Chemuru, S., R. Kodali, and R. Wetzel, *Improved chemical synthesis of hydrophobic Abeta peptides using addition of C-terminal lysines later removed by carboxypeptidase B.* Biopolymers. **102**(2): p. 206-21.

158. Burdick, D., et al., *Assembly and aggregation properties of synthetic Alzheimer's A4/beta amyloid peptide analogs.* J Biol Chem, 1992. **267**(1): p. 546-54.

159. Zagorski, M.G., et al., *Methodological and chemical factors affecting amyloid beta peptide amyloidogenicity.* Methods Enzymol, 1999. **309**: p. 189-204.

160. Tickler, A.K., A.B. Clippingdale, and J.D. Wade, *Amyloid-beta as a "difficult sequence" in solid phase peptide synthesis.* Protein Pept Lett, 2004. **11**(4): p. 377-84.

161. Clippingdale, A.B., et al., *Synthesis and secondary structural studies of penta(acetyl-Hmb)A beta(1-40).* J Pept Res, 1999. **53**(6): p. 665-72.

162. Irie, K., et al., *Structure of beta-amyloid fibrils and its relevance to their neurotoxicity: implications for the pathogenesis of Alzheimer's disease.* J Biosci Bioeng, 2005. **99**(5): p. 437-47.

163. Tickler, A.K. and J.D. Wade, *Overview of solid phase synthesis of "difficult peptide" sequences.* Curr Protoc Protein Sci, 2007. **Chapter 18**: p. Unit 18 8.

164. Clippingdale, A.B., C.J. Barrow, and J.D. Wade, *Peptide thioester preparation by Fmoc solid phase peptide synthesis for use in native chemical ligation.* J Pept Sci, 2000. **6**(5): p. 225-34.

165. Fauvet, B., et al., *One-pot total chemical synthesis of human alpha-synuclein.* Chem Commun (Camb). **49**(81): p. 9254-6.

166. Cunningham, F. and C.M. Deber, *Optimizing synthesis and expression of transmembrane peptides and proteins.* Methods, 2007. **41**(4): p. 370-80.

167. Deber, C.M., et al., *Conformational origin of a difficult coupling in a human growth hormone releasing factor analog.* Pept Res, 1989. **2**(2): p. 184-8.

168. Pudelko, M., J. Kihlberg, and M. Elofsson, *Application of gel-phase 19F NMR spectroscopy for optimization of solid-phase synthesis of a hydrophobic peptide from the signal sequence of the mucin MUC1.* J Pept Sci, 2007. **13**(5): p. 354-61.

169. Larsen, B.D. and A. Holm, *Incomplete Fmoc deprotection in solid-phase synthesis of peptides.* Int J Pept Protein Res, 1994. **43**(1): p. 1-9.

170. Wang, S. and Y. Ishii, *Revealing protein structures in solid-phase peptide synthesis by 13C solid-state NMR: evidence of excessive misfolding for Alzheimer's beta.* J Am Chem Soc. **134**(6): p. 2848-51.

171. Narita, M., et al., *Syntheses and Properties of Resin-Bound Oligopeptides .3. Infrared Spectroscopic Conformational-Analysis of Polystyrene Resin-Bound Human Proinsulin-C-Peptide Fragments - Beta-Sheet Aggregation of Peptide Chains during Solid-Phase Peptide-Synthesis.* Bull Chem Soc Jpn, 1988. **61**(4): p. 1201-1206.

172. Larsen, B.D., et al., *The Merrifield Peptide-Synthesis Studied by near-Infrared Fourier-Transform Raman-Spectroscopy.* J Am Chem Soc, 1993. **115**(14): p. 6247-6253.

173. Finder, V.H., et al., *The Recombinant Amyloid-beta Peptide A beta 1-42 Aggregates Faster and Is More Neurotoxic than Synthetic A beta 1-42.* J Mol Biol, 2010. **396**(1): p. 9-18.

174. Fukuda, H., et al., *Synthesis, aggregation, and neurotoxicity of the Alzheimer's Abeta1-42 amyloid peptide and its isoaspartyl isomers.* Bioorg Med Chem Lett, 1999. **9**(7): p. 953-6.

175. El-Agnaf, O.M., et al., *Oligomerization and toxicity of beta-amyloid-42 implicated in Alzheimer's disease.* Biochem Biophys Res Commun, 2000. **273**(3): p. 1003-7.

176. Zarandi, M., et al., *Synthesis of Abeta[1-42] and its derivatives with improved efficiency.* J Pept Sci, 2007. **13**(2): p. 94-9.

177. Tickler, A.K., C.J. Barrow, and J.D. Wade, *Improved preparation of amyloid-beta peptides using DBU as Nalpha-Fmoc deprotection reagent.* J Pept Sci, 2001. **7**(9): p. 488-94.

178. Murakami, K., et al., *Neurotoxicity and physicochemical properties of A beta mutant peptides from cerebral amyloid angiopathy - Implication for the pathogenesis of cerebral amyloid angiopathy and Alzheimer's disease.* J Biol Chem, 2003. **278**(46): p. 46179-46187.

179. Bagley, C.J., et al., *Synthesis of insulin-like growth factor I using N-methyl pyrrolidinone as the coupling solvent and trifluoromethane sulphonic acid cleavage from the resin.* Int J Pept Protein Res, 1990. **36**(4): p. 356-61.

180. Hood, C.A., et al., *Fast conventional Fmoc solid-phase peptide synthesis with HCTU.* J Pept Sci, 2008. **14**(1): p. 97-101.

181. Bacsa, B., et al., *Solid-phase synthesis of difficult peptide sequences at elevated temperatures: a critical comparison of microwave and conventional heating technologies.* J Org Chem, 2008. **73**(19): p. 7532-42.

182. Bacsa, B., S. Bosze, and C.O. Kappe, *Direct solid-phase synthesis of the beta-amyloid (1-42) peptide using controlled microwave heating.* J Org Chem. **75**(6): p. 2103-6.

183. Grillo-Bosch, D., F. Rabanal, and E. Giralt, *Improved Fmoc-based solid-phase synthesis of homologous peptide fragments of human and mouse prion proteins.* J Pept Sci. **17**(1): p. 32-8.

184. Carpino, L.A., et al., *Synthesis of 'difficult' peptide sequences: application of a depsipeptide technique to the Jung-Redemann 10- and 26-mers and the amyloid peptide A beta(1-42).* Tetrahedron Lett, 2004. **45**(40): p. 7519-7523.

185. Mutter, M., et al., *Switch peptides in statu nascendi: Induction of conformational transitions relevant to degenerative diseases.* Angew Chem Int Ed, 2004. **43**(32): p. 4172-4178.

186. Sohma, Y., et al., *Novel and efficient synthesis of difficult sequence-containing peptides through O-N intramolecular acyl migration reaction of O-acyl E isopeptides.* Chem Commun, 2004(1): p. 124-125.

187. Guichou, J.F., L. Patiny, and M. Mutter, *Pseudo-prolines (Psi Pro): direct insertion of Psi Pro systems into cysteine containing peptides.* Tetrahedron Lett, 2002. **43**(24): p. 4389-4390.

188. Clippingdale, A.B., et al., *Secondary structural modifications of A beta(1-40) induced by multiple 2-acetoxy-4-methoxybenzyl (acetylHmb) protection.* Lett Pept Sci, 1999. **6**(5-6): p. 289-293.

189. Quibell, M., W.G. Turnell, and T. Johnson, *Improved Preparation of Beta-Amyloid(1-43) - Structural Insight Leading to Optimized Positioning of N-(2-Hydroxy-4-Methoxybenzyl) (Hmb) Backbone Amide Protection.* J Chem Soc, Perkin Trans 1, 1995(16): p. 2019-2024.

190. Kim, Y.S., J.A. Moss, and K.D. Janda, *Biological tuning of synthetic tactics in solid-phase synthesis: Application to A beta(1-42).* J Org Chem, 2004. **69**(22): p. 7776-7778.

191. Choma, C.T., G.T. Robillard, and D.R. Englebretsen, *Synthesis of hydrophobic peptides: An Fmoc "Solubilising Tail" method.* Tetrahedron Lett, 1998. **39**(16): p. 2417-2420.

192. Sato, T., Y. Saito, and S. Aimoto, *Synthesis of the C-terminal region of opioid receptor like 1 in an SDS micelle by the native chemical ligation: effect of thiol additive and SDS concentration on ligation efficiency.* J Pept Sci, 2005. **11**(7): p. 410-416.

193. Johnson, E.C.B. and S.B.H. Kent, *Towards the total chemical synthesis of integral membrane proteins: a general method for the synthesis of hydrophobic peptide-(alpha)thioester building blocks.* Tetrahedron Lett, 2007. **48**(10): p. 1795-1799.

194. Harris, P.W.R. and M.A. Brimble, *Toward the Total Chemical Synthesis of the Cancer Protein NY-ESO-1.* Biopolymers, 2010. **94**(4): p. 542-550.

195. Lahiri, S., et al., *Total Chemical Synthesis of an Integral Membrane Enzyme: Diacylglycerol Kinase from Escherichia coli.* Angew Chem Int Ed, 2011. **50**(17): p. 3988-3992.

196. Blanco, R.M. and J.M. Guisan, *Stabilization of Enzymes by Multipoint Covalent Attachment to Agarose Aldehyde Gels - Borohydride Reduction of Trypsin Agarose Derivatives.* Enzyme Microb Technol, 1989. **11**(6): p. 360-366.

197. Gold, A.M. and D.E. Fahrney, *The mechanism of reactivation of phenylmethanesulfonyl alpha-chymotrypsin.* Biochem Biophys Res Commun, 1963. **10**: p. 55-9.

198. Boyes, B.E. and J.J. Kirkland, *Rapid, High-Resolution Hplc Separation of Peptides Using Small Particles at Elevated-Temperatures.* Peptide Res, 1993. **6**(5): p. 249-258.

199. Thompson, A.J., T.K. Lim, and C.J. Barrow, *On-line high-performance liquid chromatography/mass spectrometric investigation of amyloid-beta peptide variants found in Alzheimer's disease.* Rapid Commun Mass Spectrom, 1999. **13**(23): p. 2348-2351.

200. Melnyk, R.A., et al., *Polar residue tagging of transmembrane peptides.* Biopolymers, 2003. **71**(6): p. 675-685.

201. Kemmler, W., J.D. Peterson, and D.F. Steiner, *Studies on Conversion of Proinsulin to Insulin .1. Conversion in-Vitro with Trypsin and Carboxypeptidase-B.* J Biol Chem, 1971. **246**(22): p. 6786-&.

202. Chance, R.E. and B.H. Frank, *Research, Development, Production, and Safety of Biosynthetic Human Insulin.* Diabetes Care, 1993. **16**: p. 133-142.

203. Wolfe, M.S., *Processive proteolysis by gamma-secretase and the mechanism of Alzheimer's disease.* Biol Chem, 2012. **393**(9): p. 899-905.

204. Zhao, G.J., et al., *Identification of a new presenilin-dependent zeta-cleavage site within the transmembrane domain of amyloid precursor protein.* J Biol Chem, 2004. **279**(49): p. 50647-50650.

205. Chou, P.Y. and G.D. Fasman, *Empirical Predictions of Protein Conformation.* Annu Rev Biochem, 1978. **47**: p. 251-276.

206. Wetzel, R., et al., *Production of Biologically-Active N-Alpha-Desacetylthymosin Alpha-1 in Escherichia-Coli through Expression of a Chemically Synthesized Gene.* Biochemistry, 1980. **19**(26): p. 6096-6104.

207. Wood, S.J., et al., *Selective inhibition of Abeta fibril formation.* J Biol Chem, 1996. **271**(8): p. 4086-92.

208. Chen, S. and R. Wetzel, *Solubilization and disaggregation of polyglutamine peptides.* Protein Sci, 2001. **10**(4): p. 887-91.

209. Fezoui, Y., et al., *An improved method of preparing the amyloid beta-protein for fibrillogenesis and neurotoxicity experiments.* Amyloid, 2000. **7**(3): p. 166-78.

210. Zhang, S., et al., *The Alzheimer's peptide a beta adopts a collapsed coil structure in water.* J Struct Biol, 2000. **130**(2-3): p. 130-41.

211. Bitan, G. and D.B. Teplow, *Preparation of aggregate-free, low molecular weight amyloid-beta for assembly and toxicity assays.* Methods Mol Biol, 2005. **299**: p. 3-9.

212. Ward, R.V., et al., *Fractionation and characterization of oligomeric, protofibrillar and fibrillar forms of beta-amyloid peptide.* Biochemical J, 2000. **348**: p. 137-144.

213. Shankar, G.M., et al., *Isolation of low-n amyloid beta-protein oligomers from cultured cells, CSF, and brain.* Methods Mol Biol. **670**: p. 33-44.

214. Pachahara, S.K., et al., *Hexafluoroisopropanol induces self-assembly of beta-amyloid peptides into highly ordered nanostructures.* J Pept Sci. **18**(4): p. 233-41.

215. Zhu, M., et al., *Annular oligomeric amyloid intermediates observed by in situ atomic force microscopy.* J Biol Chem, 2004. **279**(23): p. 24452-9.

216. Malisauskas, M., et al., *Amyloid protofilaments from the calcium-binding protein equine lysozyme: formation of ring and linear structures depends on pH and metal ion concentration.* J Mol Biol, 2003. **330**(4): p. 879-90.

217. Selkoe, D.J., *Alzheimer's Disease.* Cold Spring Harb Perspect Biol, 2011. **3**(7).

218. Selkoe, D.J., *Alzheimer's disease: Genes, proteins, and therapy.* Physiological Rev, 2001. **81**(2): p. 741-766.

219. Qi-Takahara, Y., et al., *Longer forms of amyloid beta protein: Implications for the mechanism of intramembrane cleavage by gamma-secretase.* J Neurosci, 2005. **25**(2): p. 436-445.

220. Iizuka, T., et al., *Amyloid Beta-Protein Ending at Thr43 Is a Minor Component of Some Diffuse Plaques in the Alzheimers-Disease Brain, but Is Not Found in Cerebrovascular Amyloid.* Brain Res, 1995. **702**(1-2): p. 275-278.

221. Mori, H., et al., *Mass-Spectrometry of Purified Amyloid-Beta Protein in Alzheimers-Disease.* J Biol Chem, 1992. **267**(24): p. 17082-17086.

222. Welander, H., et al., *A beta 43 is more frequent than Abeta 40 in amyloid plaque cores from Alzheimer disease brains.* J Neurochem, 2009. **110**(2): p. 697-706.

223. Esh, C., et al., *Altered APP processing in PDAPP (Va1717 -> Phe) transgenic mice yields extended-length A beta peptides.* Biochemistry, 2005. **44**(42): p. 13807-13819.

224. Shimojo, M., et al., *Enzymatic characteristics of I213T mutant presenilin-1/gamma-secretase in cell models and knock-in mouse brains: familial Alzheimer disease-linked mutation impairs gamma-site cleavage of amyloid precursor protein C-terminal fragment beta.* J Biol Chem, 2008. **283**(24): p. 16488-96.

225. Lambermon, M.H.L., R.V. Rappaport, and J. McLaurin, *Biophysical characterization of longer forms of amyloid beta peptides: possible contribution to flocculent plaque formation.* J Neurochem, 2005. **95**(6): p. 1667-1676.

226. Vandersteen, A., et al., *Molecular Plasticity Regulates Oligomerization and Cytotoxicity of the Multipeptide-length Amyloid-beta Peptide Pool.* J Biol Chem, 2012. **287**(44): p. 36732-36743.

227. Saito, T., et al., *Potent amyloidogenicity and pathogenicity of A beta 43.* Nature Neuroscience, 2011. **14**(8): p. 1023-U120.

228. Conicella, A.E. and N.L. Fawzi, *The C-Terminal Threonine of A beta 43 Nucleates Toxic Aggregation via Structural and Dynamical Changes in Monomers and Protofibrils.* Biochemistry, 2014. **53**(19): p. 3095-3105.

229. Vandersteen, A., et al., *Molecular plasticity regulates oligomerization and cytotoxicity of the multipeptide-length amyloid-beta peptide pool.* J Biol Chem. **287**(44): p. 36732-43.

230. Nakaya, Y., et al., *Random mutagenesis of presenilin-1 identifies novel mutants exclusively generating long amyloid beta-peptides.* J Biol Chem, 2005. **280**(19): p. 19070-7.

231. Jarrett, J.T., E.P. Berger, and P.T. Lansbury, Jr., *The carboxy terminus of the beta amyloid protein is critical for the seeding of amyloid formation: implications for the pathogenesis of Alzheimer's disease.* Biochemistry, 1993. **32**(18): p. 4693-7.

232. Yan, Y. and C. Wang, *Abeta42 is more rigid than Abeta40 at the C terminus: implications for Abeta aggregation and toxicity.* J Mol Biol, 2006. **364**(5): p. 853-62.

233. O'Nuallain, B., et al., *Seeding specificity in amyloid growth induced by heterologous fibrils.* J Biol Chem, 2004. **279**(17): p. 17490-9.

234. Krebs, M.R., et al., *Observation of sequence specificity in the seeding of protein amyloid fibrils.* Protein Sci, 2004. **13**(7): p. 1933-8.

235. Meyer, V., et al., *Amplification of Tau fibrils from minute quantities of seeds.* Biochemistry. **53**(36): p. 5804-9.

236. Salvadores, N., et al., *Detection of misfolded Abeta oligomers for sensitive biochemical diagnosis of Alzheimer's disease.* Cell Rep. **7**(1): p. 261-8.

237. Chou, P.Y. and G.D. Fasman, *Prediction of the secondary structure of proteins from their amino acid sequence.* Adv Enzymol Relat Areas Mol Biol, 1978. **47**: p. 45-148.

238. Ma, B., et al., *Macromolecular crowding modulates the kinetics and morphology of amyloid self-assembly by beta-lactoglobulin.* Int J Biol Macromol. **53**: p. 82-7.

239. Williams, A.D., S. Shivaprasad, and R. Wetzel, *Alanine scanning mutagenesis of Abeta(1-40) amyloid fibril stability.* J Mol Biol, 2006. **357**(4): p. 1283-94.

240. Shivaprasad, S. and R. Wetzel, *Scanning cysteine mutagenesis analysis of Abeta-(1-40) amyloid fibrils.* J Biol Chem, 2006. **281**(2): p. 993-1000.

241. Peim, A., et al., *Mutagenic exploration of the cross-seeding and fibrillation propensity of Alzheimer's beta-amyloid peptide variants.* Protein Sci, 2006. **15**(7): p. 1801-5.

242. Griffith, J.S., *Self-replication and scrapie.* Nature, 1967. **215**(5105): p. 1043-4.

243. Chien, P., et al., *Generation of prion transmission barriers by mutational control of amyloid conformations.* Nature, 2003. **424**(6951): p. 948-51.

244. Saborio, G.P., B. Permanne, and C. Soto, *Sensitive detection of pathological prion protein by cyclic amplification of protein misfolding.* Nature, 2001. **411**(6839): p. 810-3.

245. Petkova, A.T., et al., *Self-propagating, molecular-level polymorphism in Alzheimer's beta-amyloid fibrils.* Science, 2005. **307**(5707): p. 262-5.

246. Esler, W.P., et al., *Stereochemical specificity of Alzheimer's disease beta-peptide assembly.* Biopolymers, 1999. **49**(6): p. 505-14.

247. Wadai, H., et al., *Stereospecific amyloid-like fibril formation by a peptide fragment of beta2-microglobulin.* Biochemistry, 2005. **44**(1): p. 157-64.

248. Ferrone, F., *Analysis of protein aggregation kinetics.* Methods Enzymol, 1999. **309**: p. 256-74.

249. Ono, K., et al., *Cross-seeding effects of amyloid beta-protein and alpha-synuclein.* J Neurochem. **122**(5): p. 883-90.

250. Ono, K., et al., *Exogenous amyloidogenic proteins function as seeds in amyloid beta-protein aggregation.* Biochim Biophys Acta. **1842**(4): p. 646-53.

251. Milton, R.C., S.C. Milton, and S.B. Kent, *Total chemical synthesis of a D-enzyme: the enantiomers of HIV-1 protease show reciprocal chiral substrate specificity [corrected]*. Science, 1992. **256**(5062): p. 1445-8.

252. Kar, K., et al., *D-polyglutamine amyloid recruits L-polyglutamine monomers and kills cells.* J Mol Biol. **426**(4): p. 816-29.

253. Pauling, L. and R.B. Corey, *Two Rippled-Sheet Configurations of Polypeptide Chains, and a Note about the Pleated Sheets.* Proc Natl Acad Sci U S A, 1953. **39**(4): p. 253-6.

254. Swanekamp, R.J., et al., *Coassembly of enantiomeric amphipathic peptides into amyloid-inspired rippled beta-sheet fibrils.* J Am Chem Soc. **134**(12): p. 5556-9.

255. Dzwolak, W., et al., *The diastereomeric assembly of polylysine is the low-volume pathway for preferential formation of beta-sheet aggregates.* J Am Chem Soc, 2004. **126**(12): p. 3762-8.

256. Sikorski, P. and E. Atkins, *New model for crystalline polyglutamine assemblies and their connection with amyloid fibrils.* Biomacromolecules, 2005. **6**(1): p. 425-32.

257. Torok, M., et al., *Structural and dynamic features of Alzheimer's Abeta peptide in amyloid fibrils studied by site-directed spin labeling.* J Biol Chem, 2002. **277**(43): p. 40810-5.

258. Petkova, A.T., et al., *A structural model for Alzheimer's beta -amyloid fibrils based on experimental constraints from solid state NMR.* Proc Natl Acad Sci U S A, 2002. **99**(26): p. 16742-7.

259. Buchanan, L.E., et al., *Structural motif of polyglutamine amyloid fibrils discerned with mixed-isotope infrared spectroscopy.* Proc Natl Acad Sci U S A. **111**(16): p. 5796-801.

260. Schneider, R., et al., *Structural characterization of polyglutamine fibrils by solid-state NMR spectroscopy.* J Mol Biol. **412**(1): p. 121-36.

261. Williams, A.D., et al., *Mapping abeta amyloid fibril secondary structure using scanning proline mutagenesis.* J Mol Biol, 2004. **335**(3): p. 833-42.

262. Whittemore, N.A., et al., *Hydrogen-deuterium (H/D) exchange mapping of Abeta 1-40 amyloid fibril secondary structure using nuclear magnetic resonance spectroscopy.* Biochemistry, 2005. **44**(11): p. 4434-41.